GL01312

GEOPHYSICS, VOL. 47, NO. 6 (JUNE 1982); P. 938-945, 7 FIGS., 4 TABLES.

Inversion of self-potential data from the Cerro Prieto geothermal field, Mexico

David V. Fitterman* and Robert F. Corwin‡

ABSTRACT

Self-potential (SP) data from the Cerro Prieto geothermal field in Baja California, Mexico have been inverted using a model consisting of a vertical contact separating regions of different electrical properties. A temperature source is assumed to coincide with the vertical contact between materials with different thermoelectric coupling coefficients. A derivative-free Levenberg-Marquardt algorithm is used to estimate values for the depth, vertical extent, length, and intensity of the source region. The depth to the top of the source is estimated to be about 1.3 ± 0.2 km, which agrees quite well with the depth to the top of the production zone determined from drilling. The vertical extent and length of the source region are estimated to be 11 ± 3 km and 9.9 ± 0.4 km, respectively. There appears to be geologic evidence for the presence of a fault or fault zone within the geothermal field that roughly coincides in location with the self-potential source region. The conductivity on the east side of the production zone is estimated to be 80 percent of the value to the west, which is in general agreement with field resistivity measurements. Thermoelectric coupling coefficients measured in the laboratory on samples of reservoir rock are not large enough to explain the −340 ± 40 mV source intensity predicted by the model, possibly because the laboratory measurements were made at temperatures about 300°C lower than the reservoir value. These results do not rule out the possibility of a streaming potential source mechanism.

INTRODUCTION

The Cerro Prieto geothermal field is located approximately 30 km south of Mexicali, in the state of Baja California, Mexico. The field, which is operated by the Comisión Federal de Electricidad, presently produces 150 MW of electrical power from about 70 geothermal wells. Maximum reservoir temperature is about 300°C to 350°C (Noble et al, 1977). The regional geologic setting of the field in the Imperial-Mexicali valley was described by Noble et al (1977), Vonder Haar and Puente Cruz (1979), Puente Cruz and de la Pena (1979), Vonder Haar (1980), and Lyons and van de Kamp (1980).

In late 1977 and early 1978, a large-scale self-potential (SP) survey was conducted over the Cerro Prieto field (Corwin et al, 1979). Individual readings were reproducible within about 10 mV, which also was the approximate noise level of the point-to-point readings. Survey profile lines and contoured data are shown in Figure 1. The contoured data reveal a well-developed dipolar anomaly of about 160 mV peak-to-trough amplitude and a peak-to-trough distance of about 7 km. There do not appear to be any surface features, such as variations in topography, soil properties, or near-surface geology, which could act as a source for the anomaly. Similar but less well-developed dipolar anomalies have been measured over other major geothermal areas (Corwin and Hoover, 1979).

A preliminary analysis by Corwin et al (1979) indicated that the dipolar form of the anomaly is very similar to one which could be modeled by using multiple point current dipoles distributed along a vertical plane. A more quantitative and physically reasonable method for calculating SP anomalies near vertical contacts was recently described by Fitterman (1979), based on earlier work by Nourbehecht (1963). Here we present results of an analysis of the Cerro Prieto SP data using this method.

SELF-POTENTIAL MODEL

A wide range of possible SP source mechanisms can be described by a cross-coupled flow model developed by Nourbehecht (1963). This formulation can be used to describe streaming potential, thermoelectric effect, and electrochemical source mechanisms. Possible causes of geothermal SP anomalies include streaming potential and thermoelectric effects (Corwin and Hoover, 1979). The former mechanism is suggested by the convection of hot fluid, while the latter mechanism is due to elevated temperature. The flows, forces, and proper units for the three transport mechanisms involved in the thermoelectric effect and streaming potential sources are given in Table 1.

The governing equations for this general class of crosscoupled flow models were derived more fully in Nourbehecht (1963) and Fitterman (1979). A thermoelectric source mechanism will be considered here. The coupled flow equations are

$$\begin{bmatrix} J_{elec} \\ J_{heat} \end{bmatrix} = \begin{bmatrix} \sigma & \sigma C_T \\ T\sigma C_T & K \end{bmatrix} \begin{bmatrix} -\nabla\phi \\ -\nabla T \end{bmatrix}, \qquad (1)$$

where σ is the electrical conductivity, K is the thermal conductivity, C_T is the thermoelectric coupling coefficient, T is

Manuscript received by the Editor March 20, 1980; revised manuscript received January 26, 1981.
*U.S. Geological Survey, MS 964, Box 25046, Denver, CO 80225.
‡Formerly Univ. of California, Berkeley; presently Harding-Lawson Associates, P.O. Box 578, Novato, CA 94947.
0016-8033/82/0601—938. This paper was prepared by an agency of the U.S. government.

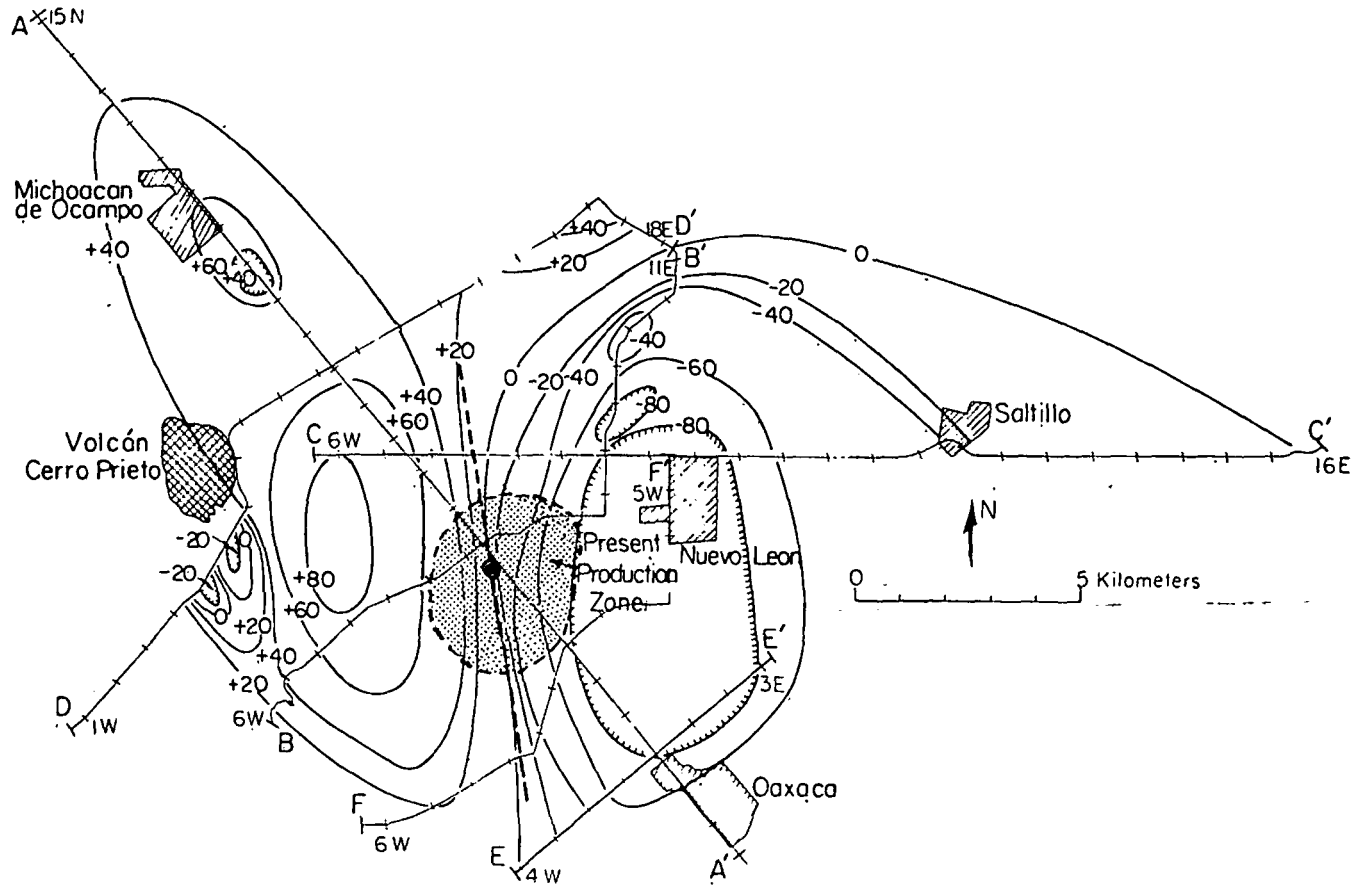

FIG. 1. Self-potential survey lines (A-A', B-B', etc.) and contours from Cerro Prieto area. Contour interval is 20 mV. The dashed line indicates the best estimate of the source plane location.

the temperature, and ϕ is the electric potential. A total electric potential ψ is defined by

$$\psi = \phi + C_T T, \tag{2}$$

such that the current flow is given by

$$\mathbf{J}_{elec} = -\sigma \nabla \psi. \tag{3}$$

The measured quantity is ϕ, but when measurements are made on a surface where T is zero, it has the same value as ψ. The governing equation is

$$\nabla^2 \psi = 0, \tag{4}$$

with boundary conditions of continuity of normal current flow

$$\sigma \hat{\mathbf{n}} \cdot \nabla \psi|_2^1 = 0, \tag{5}$$

and discontinuity of total electric potential at interfaces equal to the difference in thermoelectric coefficient times the temperature,

$$\psi|_2^1 = C_T|_2^1 T = S, \tag{6}$$

where S is a generalized source function. The discontinuity of ψ is the result of ϕ and T continuous while C_T is discontinuous.

The dipolar nature of the Cerro Prieto anomaly is similar to anomalies produced by vertical contact models (Fitterman, 1979), suggesting the use of this type of model for inversion of the data. The model requires a difference in thermoelectric properties across the contact, and the temperature must be nonzero. If the measurements are made on an equipotential of temperature or where $C_T T$ is much less than ψ, it is also necessary for the source term S to be nonconstant so the measured potential ϕ will be nonconstant. For the case of adjoining regions with different but constant values of C_T, this is ensured by having T vary along the contact. Geologically, the juxtaposition of different materials could be caused by a fault. Fractured material within the fault zone would serve as a conduit for hot fluids which would provide the elevated temperatures necessary for a nonconstant SP anomaly.

Using the Green's function developed for this problem, the

Table 1. Transport mechanisms considered to describe geothermal SP anomalies. The combination of fluid flow and electric current gives rise to the electrokinetic effect, while the combination of heat flow and electric current produces the thermoelectric effect. The proper set of units is given in brackets. Note that the heat flow is the total energy transport less any energy transport due to material motion. P is pressure, T is temperature, and ϕ is the electric potential.

Transport mechanism	Flow	Force
Fluid flow	J_{H_2O}[m³/m²/sec]	$-\nabla P$[Pa/m]
Heat flow	J_{heat}[W/m²]	$-\nabla T$[°C/m]
Electric current	J_{elec}[A/m²]	$-\nabla \phi$[V/m]

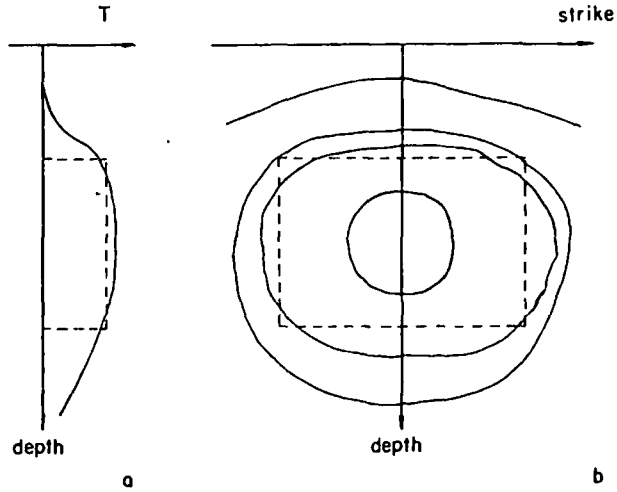

FIG. 2. Expected variation of anomalous temperature along a vertical plane near a geothermal heat source (solid lines). The dashed lines show an approximation of this distribution using the patch model. The left-hand figure shows the distribution along a vertical line through the middle of the source. The right-hand figure shows the variation of the distribution in strike and depth.

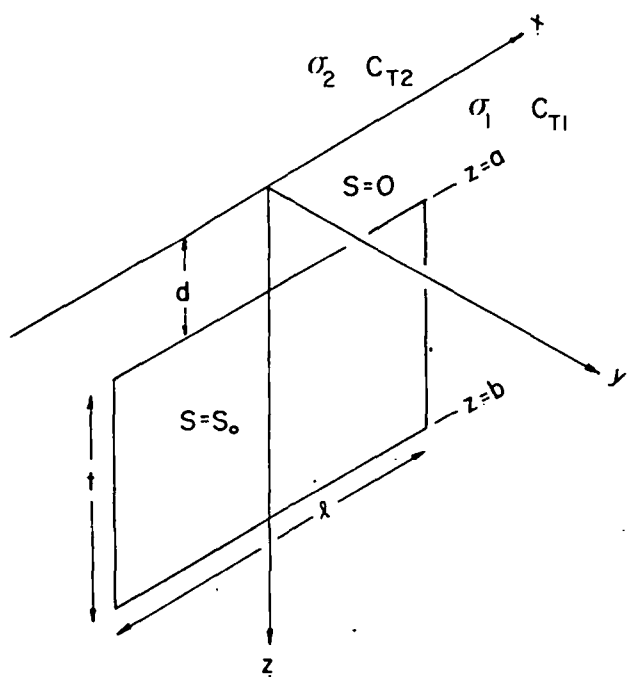

FIG. 3. Geometry of patch model used in inversion. Two regions of different conductivity and thermoelectric coefficient are separated by the plane $y = 0$. The source region has a depth of burial of $d(z = a)$, a depth extent of $t = b - a$, and a length of ℓ. Inside the patch, the source has an intensity of $S_0 = (C_{T1} - C_{T2})T_0$.

anomaly produced by any source distribution S can be determined. From a practical standpoint it is advisable to use a simple model which approximates the true source distribution, but has few parameters and is easy to compute. Figure 2a shows a temperature distribution above the ambient which might be expected to exist in a geothermal system. The profile is characterized by a gradient near the top where heat flow is caused primarily by conduction. Below this region is a zone where convective forces try to produce a region of constant temperature. In the lower portion of the profile, the temperature will return to some ambient value if the geothermal heat source is confined in vertical extent. In the strike direction (Figure 2b), the source intensity decreases from the value in the convective zone if the heat source has a finite strike length. Only the distribution along the vertical contact is shown because this is all the information needed to compute the SP anomaly. Since the temperature has been specified on the contact plane and is assumed to be zero on the surface, the temperature distribution and heat flow in the entire half-space has in principle been described.

Calculation of the SP anomaly due to the contoured distribution in Figure 2 is possible by integration using the appropriate Green's functions. This procedure is quite expensive and not warranted for most geothermal exploration data in view of how little is known of the details of the temperature distribution. A reasonable alternative is to approximate the curved contours shown in Figure 2 by a single rectangular contour similar to the dashed one. Inside this rectangular region, called a patch, the temperature has a constant value, while outside the patch in the contact plane the temperature is zero. Thus the patch model corresponds to a thin, hot rectangular plate from which heat is flowing. The patch model has an easily calculated thermoelectric SP anomaly associated with it. As more is learned about a particular source geometry, better approximations to it can be made by superimposing additional patches of different sizes, intensities, and location.

The surface anomaly produced by the single patch shown in Figure 3 is given by (Fitterman, 1979)

$$\psi_{1,2}(x, y, 0) = \frac{S_0}{\pi(1 + \sigma_1/\sigma_2)_{2\ 1}} [f(x, y; \ell, b) - f(x, y; \ell, a) - f(x, y; -\ell, b) + f(x, y; -\ell, a) \quad (7)$$

where

$$f(x, y; \alpha, \beta) = \tan^{-1} \frac{(x + \alpha/2)\beta}{y[(x + \alpha/2)^2 + y^2 + \beta^2]^{1/2}}. \quad (8)$$

The upper subscript is used for region 1 ($y > 0$), and the lower subscript is used for region 2 ($y < 0$). The function $f(x, y; \alpha, \beta)$ is odd with respect to the y-coordinate. This accounts for the odd

Table 2. Model parameter, standard deviation, and relative error estimates.

Parameter	Value	Standard deviation	Relative error
$a = d$	1.3 km	0.2	0.13
$b = t + d$	13 km	3.	0.26
ℓ	9.9 km	0.4	0.036
σ_1/σ_2	0.80	0.04	0.045
S_0	−340 mV	40.	0.11

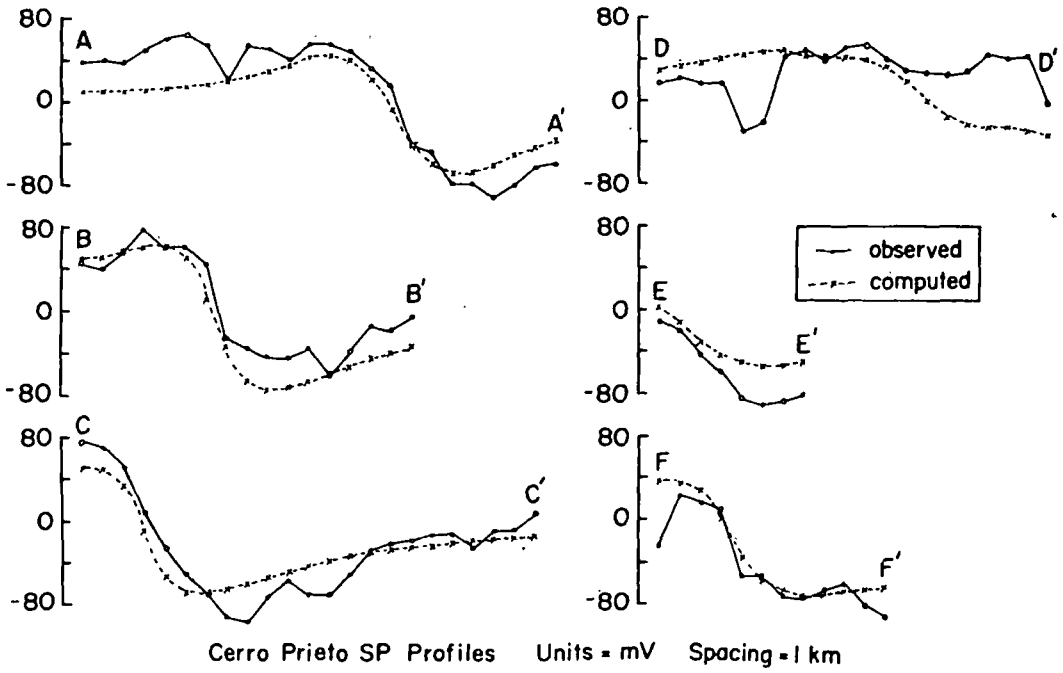

FIG. 4. Comparison of measured (o) and computed (x) potentials along the profiles shown in Figure 1. Model parameters are given in Table 2.

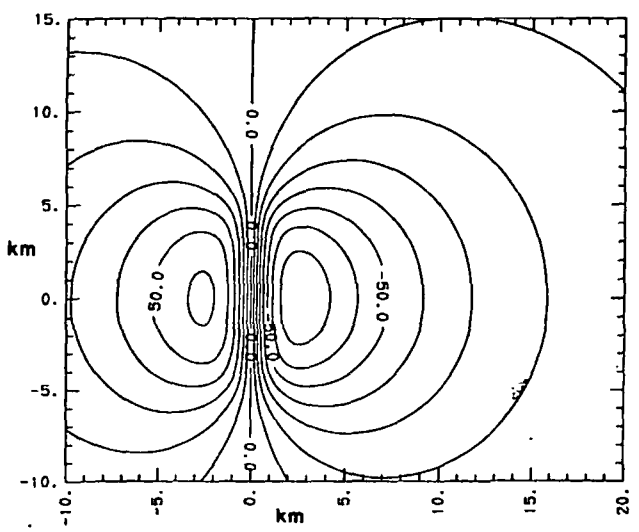

FIG. 5. Contour map of computed potential. Contour interval is 10 mV. Model parameters are given in Table 2.

Table 3. Correlation matrix for unscaled parameters using analytic partial derivatives. Only the lower half of the matrix is shown.

	a	b	ℓ	σ_1/σ_2	S_0
$a = d$	1.000				
$b = t + d$	−0.757	1.000			
ℓ	0.032	0.039	1.000		
σ_1/σ_2	0.0138	−0.008	0.195	1.000	
S_0	−0.937	0.899	−0.036	−0.082	1.000

symmetry of the anomalies when σ_1 and σ_2 are equal. If there is a difference in conductivity, the anomaly is enhanced on the resistive side of the contact and subdued on the conductive side. (See Fitterman, 1979 for examples.)

INVERSION METHODS AND RESULTS

We are now faced with the task of estimating the model parameters. A nonlinear, least-squares technique was used to adjust the model parameters so as to minimize the sum of the squares of the difference between the observed and computed potentials. Numerous discussions of the inverse problem exist in the geophysical literature (Wiggins, 1972; Inman, 1975; Glenn and Ward, 1976). Error minimization for this study was accomplished by means of the Levenberg-Marquardt algorithm *ZXSSQ* from the International Mathematics and Statistics Library (1979). This algorithm uses finite-differences to approximate the partial derivatives needed for the parameter corrections. Details of the method can be found in Levenberg (1944), Marquardt (1963), or Brown and Dennis (1972). Four of the model parameters (a, b, ℓ, and σ_1/σ_2) must always be nonnegative quantities. To ensure this condition, these parameters are logarithmically scaled.

The orientation of the source patch used to model the Cerro Prieto anomaly was placed parallel to the 0 mV contour in the region of steepest gradient (see Figure 1). The model source plane was positioned along the 0 mV contour, midway between the anomaly minimum and maximum. The resulting parameter and error estimates are given in Table 2. The relative error of the parameters ranges from 3 to 26 percent. The conductivity ratio σ_1/σ_2 and source length ℓ have the smallest error bounds (3–5 percent), followed by the depth a to the top of the source and source intensity S_0 (11–12 percent). Examining the correlation matrix (Table 3), one can see that the depth a to the top of the source has a strong inverse correlation with the source intensity

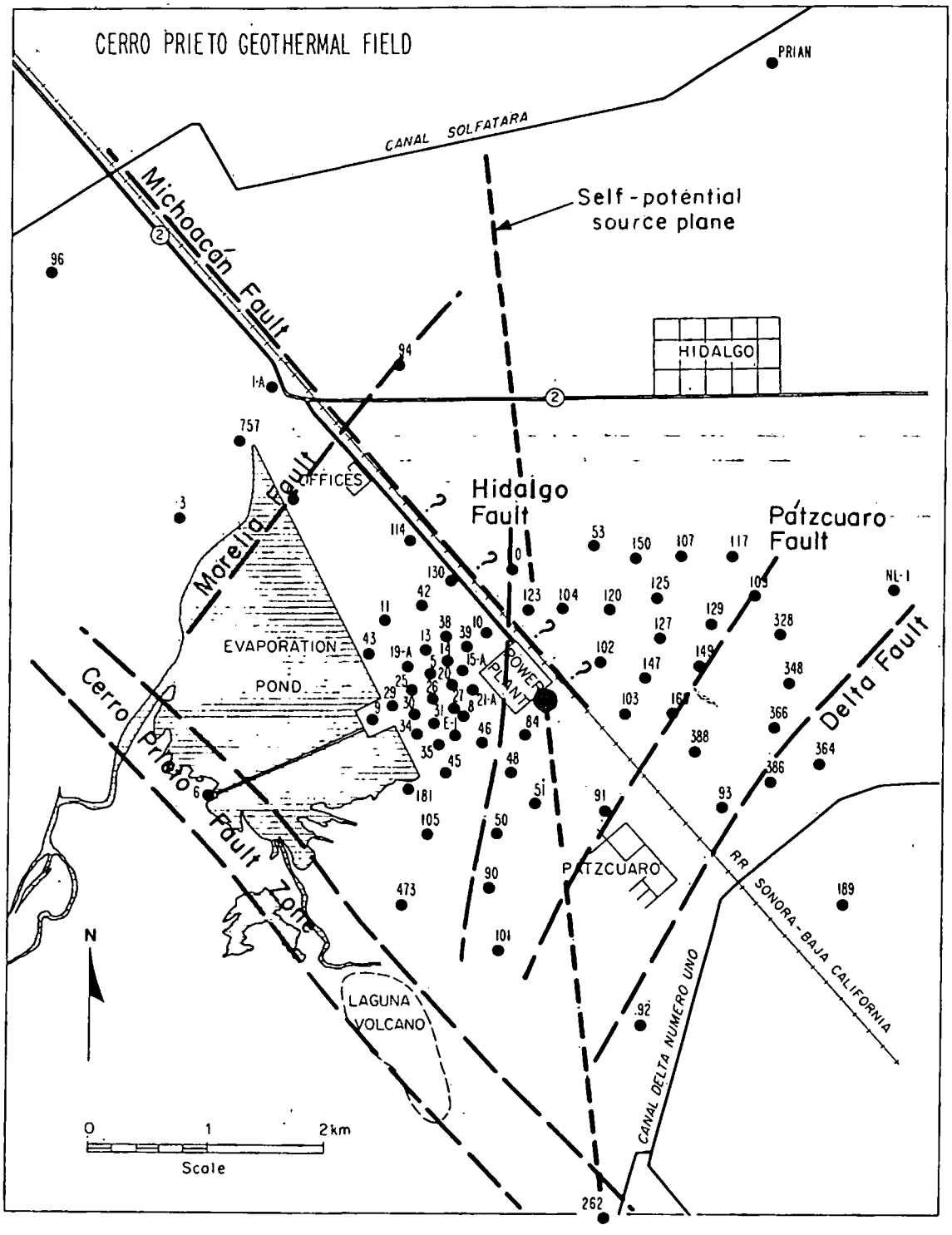

FIG. 6. Map of the Cerro Prieto geothermal field (from Vonder Haar, 1980). The straight line composed of short dashes represents the surface projection of the modeled SP source plane. The other dashed lines represent fault locations. The center of the SP source region is indicated by the large solid circle. The small solid circles are well locations. The symbols above the circles are the well numbers. (The M preceding each well number has been omitted for clarity.)

S_0, and a smaller, but significant, inverse correlation with the depth b to the bottom of the source. The source intensity is also inversely correlated with the depth to the bottom of the source. These strong correlations mean that we can not determine uniquely the model parameters. In view of the fact that we are dealing with potential field data, this is not surprising.

Of much greater concern than the correlation of the model parameters is the possibility that the model geometry is not a good representation of the geology. For example, the interface which is generating the SP anomaly might not be vertical, but rather dipping. The vertical geometry could require an apparent conductivity contrast where one does not exist in order to match the data. Similarly, the actual source intensity might not be constant as specified in the model because of variations in temperature or thermoelectric coefficients in the source region. Automatic inversion techniques cannot be viewed as the geophysicist's panacea, but rather a tool which suggests allowable alternative data interpretations which must be culled using a significant amount of geologic knowledge.

Figure 4 shows the comparison of the data profiles and the computed anomaly. The rms error in the fit is 28 mV. The model shows rather good agreement with the data. Short-wavelength features in the data, which are probably due to near-surface effects, are smoothed over by the model. A contour map of the computed anomaly is shown in Figure 5. Note the general similarity of the computed and measured anomaly (Figure 1). The short-wavelength features of the data, which the model cannot fit, are missing from the computed anomaly.

Self-potential models which use Nourbehecht's (1963) formulation require regions with different crosscoupling coefficients on each side of a boundary. In the patch model the boundary is a vertical plane. We now consider the known geology to see if there is any correspondence between the model parameters and the geology.

CORRELATION OF MODEL AND FIELD GEOLOGY

A wealth of geologic, geophysical, geochemical, and well log data from the Cerro Prieto field is available in the proceedings of two symposia published by the Lawrence Berkeley Laboratory (1979) and the Comisión Federal de Electricidad (1980). Structural models of the field described in these publications and in the numerous reports referenced in them have evolved rapidly in response to the increasing availability of data, resulting in a variety of interpretations. The most recent English language comprehensive studies are those of de la Pena and Puente (1979), Vonder Haar (1980), and Lyons and van de Kamp (1980), each of which considers many, but not all, of the currently available data in formulating their geologic models.

These recent studies conclude that the geothermal reservoir exists within deposits of the ancestral Colorado delta, consisting mainly of complexly interbedded sandstones, siltstones, and shales. The reservoir formation is overlain by about 1 km of unconsolidated silts, clays, and sands. This depth correlates well with the postulated depth of 1.3 ± 0.2 km to the top of the SP source plane. A granodioritic basement at about 1.5 to 3 km depth in the northwest appears to deepen to about 5 km in the southwest. This southeastern basement may consist of mixed volcanics, metasediments, and highly faulted granitic rock. The basement depth is considerably less than the 12 ± 3 km depth to the bottom of the SP source plane, inferring that any geologic structure corresponding to the source plane extends deep into the basement. At this time there is not enough information available even to contour the depth roughly to the top of the basement, not to mention draw any conclusions about possible basement structural features. Lyons and van de Kamp (1980) emphasized the structure of the geothermal field is complex, and it is not accurately visualized as a uniform reservoir overlain by a continuous low-permeability cap and overlying a simply structured basement.

Of central importance to our SP model is the possible existence of a fault or fault zone corresponding in location to our source plane and separating areas of different coupling coefficient and electrical conductivity. A fault map of the Cerro Prieto field given by Vonder Haar (1980) is shown in Figure 6, and one given by Lyons and van de Kamp (1980) is shown in Figure 7. The heavy dashed line in each of these figures represents the trace of our inferred SP source plane.

It is apparent from these two figures that more than one picture of faulting in the Cerro Prieto field may be drawn from similar data. (It also should be noted that these two figures combine faults of varying age, displacement, and vertical extent, as described in the original references.) In view of the compexity of the geology, it is not surprising that there is no single, continuous fault corresponding to the location of our inferred SP source plane. However, the location and strike of the Hidalgo fault shown in Figure 6 are not greatly different from those of the central part of our source plane, and the trace of the source plane also appears to correspond roughly to the general trend of a series of shorter northwest and northeast striking faults shown in Figure 7. Dips for these faults are not explicitly stated, but from stratigraphic

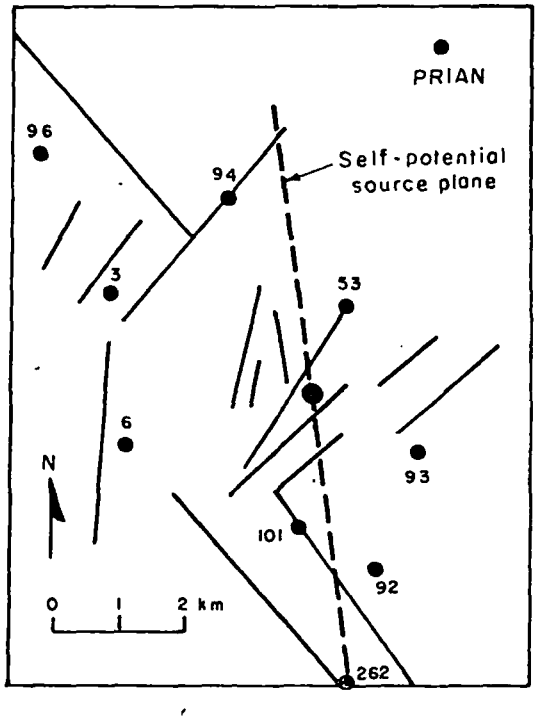

FIG. 7. Location of faults in the Cerro Prieto geothermal field (from Lyons and van de Kamp, 1980). Solid lines represent fault locations, and the dashed line represents the surface projection of the modeled SP source plane. The center of the SP source plane is indicated by the solid circle. Some of the well locations are indicated for correlation with Figure 6.

Table 4. Thermoelectric coupling coefficient from Cerro Prieto geothermal field cores. Undiluted pore fluid is 0.372 M in NaCl and 0.054 M in KCl with a conductivity of 4 mho/m. Measurements were made at a mean temperature of 30°C.

Well	Depth (m)	Rock type	Pore fluid dilution	C_T (mV/°C)
M-53	1708	Sandstone	0	0.037
M-53	1708	Sandstone	100:1	0.144
M-53	1900	Sandstone	0	0.010
M-94	1292	Sandstone	0	0.057
M-94	1292	Shale	0	0.180

cross-sections given by Lyons and van de Kamp (1980), they appear to be close to vertical. Additional evidence for a northerly structural trend in the central part of the field is given by north-trending contours of rock alteration as indicated by shale densification patterns (Lyons and van de Kamp, 1980).

Given the uncertainty of fault locations and possible errors inherent in the location of the SP source plane, it does not seem unreasonable to assume the source plane corresponds to a north-trending fault or zone of faults within the geothermal reservoir, possibly extending into the basement. The strike length of the source plane extends beyond the region where extensive well log data are presently available. However, the plane terminates to the south at its junction with the Cerro Prieto fault (Figure 6), which also forms the southwestern boundary of the present production zone (Vonder Haar, 1980). The plane terminates to the north between Highway 2 and the Canal Solfatara (Figure 6), an area in which a major structural change has been inferred by electrical resistivity data (Wilt et al, 1979).

It may also be significant that the center of the source plane (indicated by the large dot in Figures 6 and 7) is close to the intersection of the northwest-trending Michoacán fault and the north-trending fault or fault zone. According to Vonder Haar (1980), the high productivity of some geothermal wells near this intersection could indicate a zone of relatively high permeability that serves as a conduit for convective circulation of geothermal fluids. This conclusion is supported by a resistivity profile across the field given by Wilt and Goldstein (1980), which shows a zone of relatively high conductivity surfacing in the area of the intersection and dipping under the trace of the SP source plane. Unfortunately, the strike of this conductive zone is not known.

Obviously, the north-trending fault or fault zone does not represent a simple contact separating two different materials having differing thermoelectric coefficients and electrical conductivity. However, different rock types having different thermoelectric coefficients could be brought into contact by vertical offsets along faults. Because most of the individual rock units are less than 50 m thick (Lyons and van de Kamp, 1980), and because vertical fault offsets range up to several hundred meters (Vonder Haar, 1980), it seems likely that different rock types could be in contact across considerable vertical sections of most faults in the field. It is not obvious why one particular fault or fault zone (i.e., the Hidalgo fault of Figure 6) seems to act as an SP source plane even though most of the major faults in the field seem to have considerable vertical offset. If the north-trending faults corresponding to the SP source plane have higher permeability than others in the field, they might serve as the major conduits for hydrothermal circulation, providing increased heat to interact with the thermoelectric coefficient difference. Increased fluid circulation could also lead to extensive hydrothermal alteration along the faults, which could possibly contribute to thermoelectric coefficient variations. Whether the magnitude of possible thermoelectric coefficient differences between actual Cerro Prieto reservoir rocks is quantitatively sufficient to generate the observed SP anomaly is discussed later.

Finally, our SP model requires that the electrical conductivity on the east side of the source plane be 80 percent of that to the west. The conductivity structure of the field is far more complicated than this, but a resistivity profile across the production zone (Wilt and Goldstein, 1980) does show a general decrease in conductivity from west to east.

It should be kept in mind that a streaming potential source mechanism should not be ruled out as a possible cause of the SP anomaly, since one would expect hydrothermal circulation to be associated with the Cerro Prieto geothermal field. However, the modeling technique which we have used requires that there be neither heat nor fluid pressure variation, in the case of a streaming potential source, in the horizontal direction on the surface of the half-space. Since this condition is not realistic for groundwater flow, we have chosen not to attempt a model of a streaming potential source.

In summary, the geology of the Cerro Prieto geothermal field is much more complex than indicated by our simple SP model. However, some evidence does exist for the presence of a north-trending fault or fault zone roughly coincident with our SP source plane. Vertical offsets along these faults, along with hydrothermal alteration caused by possible circulation of geothermal fluids along the faults, could create the thermoelectric coefficient contrast needed for generation of the SP anomaly. The depth to the top of the source plane agrees well with the known depth to the top of the geothermal reservoir, but the bottom of the plane extends deep into the basement. The center of the plane lies close to the intersection of two major fault zones, a region where increased permeability may allow hot fluids to reach the source region. The electrical conductivity of the field decreases from west to east, in agreement with our model.

SOURCE MECHANISM

Values of the thermoelectric coupling coefficient C_T must be known in order to calculate SP anomalies using the analytical method described above. To gain a preliminary idea of the magnitude of these coupling coefficients, a series of laboratory measurements was made on Cerro Prieto reservoir rocks. The apparatus and test procedure used are described in detail in Morrison et al (1978). The tests were made on cylindrical samples measuring 50.8 mm (2 inches) diameter by 31.75 mm (1.25 inch) long taken from geothermal production wells (well locations are shown in Figure 6). The pore fluid used was 0.327 M in NaCl and 0.054 M in KCl, approximately representing the average composition of the fluid from all the producing wells (Mañon et al, 1977). The conductivity of this fluid at room temperature was 4 mho/m. The wells from which the samples were obtained, along with sample depths and rock types, are listed in Table 4.

Results of the thermoelectric coupling coefficient measurements are summarized in Table 4. For the sample from well M-53, 1708 m depth, diluting the pore fluid 100:1 increased C_T from 0.037 to 0.144 mV/°C, indicating that C_T is sensitive to pore fluid conductivity. Because pore fluid conductivity is a function of temperature, it is likely that C_T also varies with temperature. In order to generate the −340 mV source potential in a 300°C reservoir solely by thermoelectric effect, a coupling coefficient con-

trast of about 1 mV/°C would be required. This is about an order of magnitude greater than the measured values. Measurement of C_T under in-situ conditions is necessary to determine realistically the contribution of this mechanism to the measured anomaly.

CONCLUSIONS

The similarity of the measured SP anomaly at Cerro Prieto and those produced by a vertical contact model suggests using this model to determine the source of the Cerro Prieto anomaly. The inversion of SP data is relatively easy to do, but one must be aware of the nonuniqueness problem indicated by correlation of certain model parameters.

The source region of the Cerro Prieto SP anomaly appears to correspond to a north-trending fault or fault zone which crosses the geothermal field. Rock displacement or alteration across this zone could provide the thermoelectric coefficient contrast necessary to interact with the temperature field or to generate the measured SP anomaly. The estimated depth to the top of the source zone is in good agreement with the known depth to the production zone. The estimated increase in resistivity on the east side of the source region agrees with the near-surface resistivity interpretation of Wilt and Goldstein (1980).

The exact source mechanism generating the SP anomaly cannot be determined without more knowledge of the in-situ cross-coupling properties. Laboratory measurements at low temperatures and pressures give values for thermoelectric coupling coefficients which are too low by about an order of magnitude to generate the inferred source voltage from the measured temperature of the reservoir. We have not ruled out the possibility that the observed SP anomaly is generated by a streaming potential mechanism. Modeling using this type of a source mechanism would be helpful in determining the cause of the SP anomaly.

ACKNOWLEDGMENTS

This work was supported in part by the U. S. Geological Survey under contract no. 14-08-0001-16546, and in part by the U. S. Department of Energy under the direction of the Lawrence Berkeley Laboratory, Earth Sciences Division, under contract no. W-7405-ENG-48. We thank S. Vonder Haar and M. J. Wilt of the Lawrence Berkeley Laboratory and the personnel of the Comisión Federal de Electricidad, Coordinadora Ejecutiva de Cerro Prieto, for their cooperation and assistance. Comments by W. R. Sill and T. R. Madden have been helpful in pointing out the limitations of the modeling technique we have used.

REFERENCES

Brown, K. M., and Dennis, J. E., 1972, Derivative free analogues of the Levenberg-Marquardt and Gauss algorithms for nonlinear least-squares approximations: Numer. Math., v. 18, p. 289–297.

Comisión Federal de Electricidad, 1980, Proceedings, Second symposium on the Cerro Prieto geothermal field, October 17–19, 1979, Mexicali, Baja California, Mexico: Comisión Federal de Electricidad de México, in press.

Corwin, R. F., and Hoover, D. B., 1979, The self-potential method in geothermal exploration: Geophysics, v. 44, p. 226–245.

Corwin, R. F., Morrison, H. F., Diaz, S., and Rodriguez, J., 1979, Self-potential studies at the Cerro Prieto geothermal field, September 20–22, 1978, San Diego: Lawrence Berkeley Lab rep. LBL-7098, p. 204–210.

Fitterman, D. V., 1979, Calculations of self-potential anomalies near vertical contacts: Geophysics, v. 44, p. 195–205.

Garcia, S. D., 1975, Estudio Geoeléctrico de la zona geothérmica de Cerro Prieto, Baja California, Mexico: Proc. 2nd U.N. symposium on the development and use of geothermal resources, San Francisco, U.S. Gov. Print. Of., Washington, DC, v. 2, p. 1003–1011.

Glenn, W. E., and Ward, S. H., 1976, Statistical evaluation of electrical sounding methods, part I: Experimental design: Geophysics, v. 41, p. 1207–1221.

Inman, J. R., Jr., 1975, Resistivity inversion with ridge regression: Geophysics, v. 40, p. 798–817.

International Mathematics and Statistics Library, 1979, IMSL Library Edition 6: IMSL, 6th floor, GNB Bldg., 7500 Bellaire Blvd., Houston, TX 77036.

Lawrence Berkeley Laboratory, 1979, Proceedings, First symposium on the Cerro Prieto geothermal field, Baja California, Mexico, Sept. 20–22, 1978, San Diego, California: Lawrence Berkeley Laboratory rep. LBL-7098.

Levenberg, K., 1944, A method for the solution of certain non-linear problems in least squares: Quart. Appl. Math., v. 2, p. 164–168.

Lyons, D. J., and van de Kamp, P. C., 1980, Subsurface geological and geophysical study of the Cerro Prieto geothermal field, Baja California, Mexico: Lawrence Berkeley Lab. rep. LBL-10540.

Mañon, A., Mazor, E., Jiminez, M., Sanchez, A., Fausto, J., and Zenizo, C., 1977, Extensive geochemical studies in the geothermal field of Cerro Prieto, Mexico: Lawrence Berkeley Lab. rep. LBL-7019.

Marquardt, D. W., 1963, An algorithm for least-squares estimation of nonlinear parameters: J. SIAM, v. 11, p. 431–441.

Morrison, H. F., Corwin, R. F., DeMoully, G., and Durand, D., 1978, Interpretation of self-potential data from geothermal areas: Semi-annual technical progress report, U.S.G.S. contract no. 14-08-0001-16546, October 31.

Noble, J. E., Mañon, A., Lippmann, M. J., and Witherspoon, P. A., 1977, A study of the structural control of fluid flow within the Cerro Prieto geothermal field, Baja California, Mexico: Preprint, SPE 52nd an. meet., AIME.

Nourbehecht, B., 1963, Irreversible thermodynamic effects in inhomogeneous media and their applications in certain geoelectric problems: Ph.D. thesis, M.I.T.

de la Pena, A., and Puente, I., 1979, The geothermal field of Cerro Prieto, *in* Geology and Geothermics of the Salton Trough: W. A., Elders, editor, rep. UCR/IGPP-79/23, Inst. of Geophys. and Planetary Phys., Univ. of California, Riverside, p. 20–35.

Puente Cruz, I., and de la Pena, A., 1979, Geology of the Cerro Prieto geothermal field, *in* Proceedings, 1st symposium on the Cerro Prieto Geothermal Field, September 20–22, 1978, San Diego: Lawrence Berkeley Lab rep. LBL-7098, p. 17–40.

Vonder Haar, S., 1980, Geology of the Cerro Prieto geothermal field: Earth Sciences, Lawrence Berkeley Lab, v. 3, p. 1–5.

Vonder Haar, S., and Puente Cruz, I., 1979, Hybrid transform faults and fault intersections in the southern Salton trough geothermal area, Baja California, Mexico, *in* Geology and geothermics of the Salton trough: W. A., Elders, editor, rep. UCR/IGPP-79/23, Inst. of Geophys. and Planetary Phys., Univ. of California, Riverside, p. 95–100.

Wiggins, R. A., 1972, The general linear inverse problem: Implications of surface waves and free oscillations for earth structures: Rev. Geophys. Space Phys., v. 10, p. 251–285.

Wilt, M. J., and Goldstein, N. E., 1980, Resistivity monitoring at Cerro Prieto: Lawrence Berkeley Lab rep. LBL-9549.

Wilt, M. J., Goldstein, N. E., and Razo, A. M., 1979, LBL resistivity studies at Cerro Prieto, *in* Proceedings, 1st symposium on the Cerro Prieto geothermal field, September 20–22, 1978, San Diego: Lawrence Berkeley Lab rep. LBL-7098, p. 179–188.

GEOPHYSICS, VOL. 47, NO. 6 (JUNE 1982); P. 938–945, 7 FIGS., 4 TABLES.

Inversion of self-potential data from the Cerro Prieto geothermal field, Mexico

David V. Fitterman* and Robert F. Corwin‡

ABSTRACT

Self-potential (SP) data from the Cerro Prieto geothermal field in Baja California, Mexico have been inverted using a model consisting of a vertical contact separating regions of different electrical properties. A temperature source is assumed to coincide with the vertical contact between materials with different thermoelectric coupling coefficients. A derivative-free Levenberg-Marquardt algorithm is used to estimate values for the depth, vertical extent, length, and intensity of the source region. The depth to the top of the source is estimated to be about 1.3 ± 0.2 km, which agrees quite well with the depth to the top of the production zone determined from drilling. The vertical extent and length of the source region are estimated to be 11 ± 3 km and 9.9 ± 0.4 km, respectively. There appears to be geologic evidence for the presence of a fault or fault zone within the geothermal field that roughly coincides in location with the self-potential source region. The conductivity on the east side of the production zone is estimated to be 80 percent of the value to the west, which is in general agreement with field resistivity measurements. Thermoelectric coupling coefficients measured in the laboratory on samples of reservoir rock are not large enough to explain the −340 ± 40 mV source intensity predicted by the model, possibly because the laboratory measurements were made at temperatures about 300°C lower than the reservoir value. These results do not rule out the possibility of a streaming potential source mechanism.

INTRODUCTION

The Cerro Prieto geothermal field is located approximately 30 km south of Mexicali, in the state of Baja California, Mexico. The field, which is operated by the Comisión Federal de Electricidad, presently produces 150 MW of electrical power from about 70 geothermal wells. Maximum reservoir temperature is about 300°C to 350°C (Noble et al, 1977). The regional geologic setting of the field in the Imperial-Mexicali valley was described by Noble et al (1977), Vonder Haar and Puente Cruz (1979), Puente Cruz and de la Pena (1979), Vonder Haar (1980), and Lyons and van de Kamp (1980).

In late 1977 and early 1978, a large-scale self-potential (SP) survey was conducted over the Cerro Prieto field (Corwin et al, 1979). Individual readings were reproducible within about 10 mV, which also was the approximate noise level of the point-to-point readings. Survey profile lines and contoured data are shown in Figure 1. The contoured data reveal a well-developed dipolar anomaly of about 160 mV peak-to-trough amplitude and a peak-to-trough distance of about 7 km. There do not appear to be any surface features, such as variations in topography, soil properties, or near-surface geology, which could act as a source for the anomaly. Similar but less well-developed dipolar anomalies have been measured over other major geothermal areas (Corwin and Hoover, 1979).

A preliminary analysis by Corwin et al (1979) indicated that the dipolar form of the anomaly is very similar to one which could be modeled by using multiple point current dipoles distributed along a vertical plane. A more quantitative and physically reasonable method for calculating SP anomalies near vertical contacts was recently described by Fitterman (1979), based on earlier work by Nourbehecht (1963). Here we present results of an analysis of the Cerro Prieto SP data using this method.

SELF-POTENTIAL MODEL

A wide range of possible SP source mechanisms can be described by a cross-coupled flow model developed by Nourbehecht (1963). This formulation can be used to describe streaming potential, thermoelectric effect, and electrochemical source mechanisms. Possible causes of geothermal SP anomalies include streaming potential and thermoelectric effects (Corwin and Hoover, 1979). The former mechanism is suggested by the convection of hot fluid, while the latter mechanism is due to elevated temperature. The flows, forces, and proper units for the three transport mechanisms involved in the thermoelectric effect and streaming potential sources are given in Table 1.

The governing equations for this general class of crosscoupled flow models were derived more fully in Nourbehecht (1963) and Fitterman (1979). A thermoelectric source mechanism will be considered here. The coupled flow equations are

$$\begin{bmatrix} J_{\text{elec}} \\ J_{\text{heat}} \end{bmatrix} = \begin{bmatrix} \sigma & \sigma C_T \\ T\sigma C_T & K \end{bmatrix} \begin{bmatrix} -\nabla\phi \\ -\nabla T \end{bmatrix}, \qquad (1)$$

where σ is the electrical conductivity, K is the thermal conductivity, C_T is the thermoelectric coupling coefficient, T is

Manuscript received by the Editor March 20, 1980; revised manuscript received January 26, 1981.
*U.S. Geological Survey, MS 964, Box 25046, Denver, CO 80225.
‡Formerly Univ. of California, Berkeley; presently Harding-Lawson Associates, P.O. Box 578, Novato, CA 94947.
0016-8033/82/0601—938. This paper was prepared by an agency of the U.S. government.

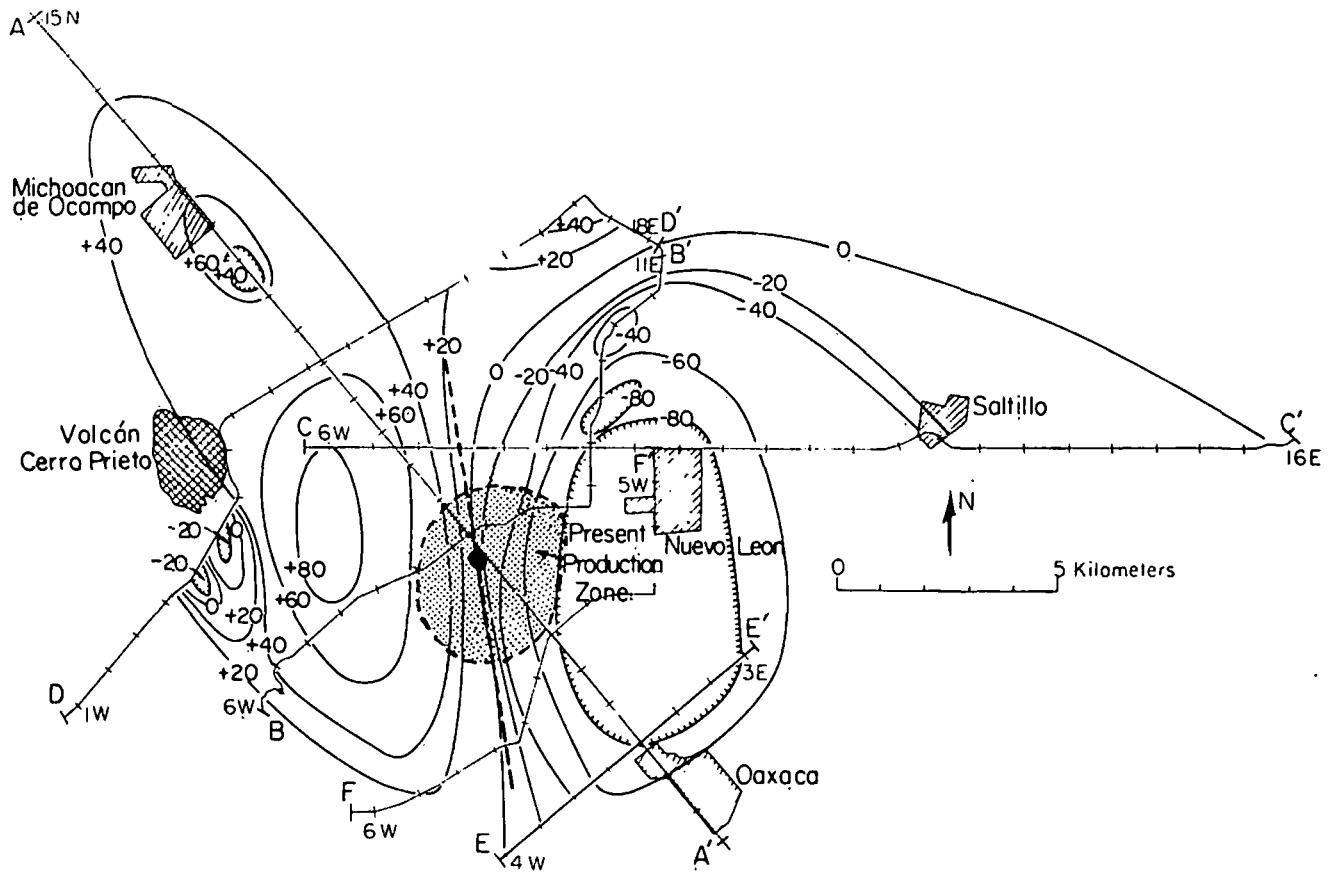

FIG. 1. Self-potential survey lines (A-A', B-B', etc.) and contours from Cerro Prieto area. Contour interval is 20 mV. The dashed line indicates the best estimate of the source plane location.

the temperature, and ϕ is the electric potential. A total electric potential ψ is defined by

$$\psi = \phi + C_T T, \tag{2}$$

such that the current flow is given by

$$\mathbf{J}_{elec} = -\sigma \nabla \psi. \tag{3}$$

The measured quantity is ϕ, but when measurements are made on a surface where T is zero, it has the same value as ψ. The governing equation is

$$\nabla^2 \psi = 0, \tag{4}$$

with boundary conditions of continuity of normal current flow

$$\sigma \hat{\mathbf{n}} \cdot \nabla \psi|_2^1 = 0, \tag{5}$$

and discontinuity of total electric potential at interfaces equal to the difference in thermoelectric coefficient times the temperature,

$$\psi|_2^1 = C_T|_2^1 T = S, \tag{6}$$

where S is a generalized source function. The discontinuity of ψ is the result of ϕ and T continuous while C_T is discontinuous.

The dipolar nature of the Cerro Prieto anomaly is similar to anomalies produced by vertical contact models (Fitterman, 1979), suggesting the use of this type of model for inversion of the data. The model requires a difference in thermoelectric properties across the contact, and the temperature must be nonzero. If the measurements are made on an equipotential of temperature or where $C_T T$ is much less than ψ, it is also necessary for the source term S to be nonconstant so the measured potential ϕ will be nonconstant. For the case of adjoining regions with different but constant values of C_T, this is ensured by having T vary along the contact. Geologically, the juxtaposition of different materials could be caused by a fault. Fractured material within the fault zone would serve as a conduit for hot fluids which would provide the elevated temperatures necessary for a nonconstant SP anomaly.

Using the Green's function developed for this problem, the

Table 1. Transport mechanisms considered to describe geothermal SP anomalies. The combination of fluid flow and electric current gives rise to the electrokinetic effect, while the combination of heat flow and electric current produces the thermoelectric effect. The proper set of units is given in brackets. Note that the heat flow is the total energy transport less any energy transport due to material motion. P is pressure, T is temperature, and ϕ is the electric potential.

Transport mechanism	Flow	Force
Fluid flow	J_{H_2O} [m³/m²/sec]	$-\nabla P$ [Pa/m]
Heat flow	J_{heat} [W/m²]	$-\nabla T$ [°C/m]
Electric current	J_{elec} [A/m²]	$-\nabla \phi$ [V/m]

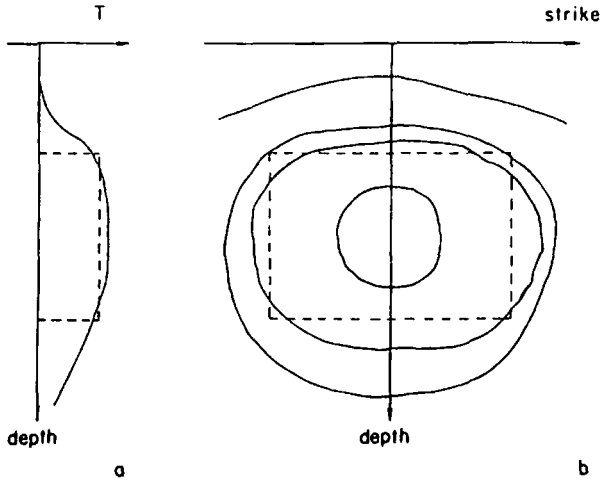

FIG. 2. Expected variation of anomalous temperature along a vertical plane near a geothermal heat source (solid lines). The dashed lines show an approximation of this distribution using the patch model. The left-hand figure shows the distribution along a vertical line through the middle of the source. The right-hand figure shows the variation of the distribution in strike and depth.

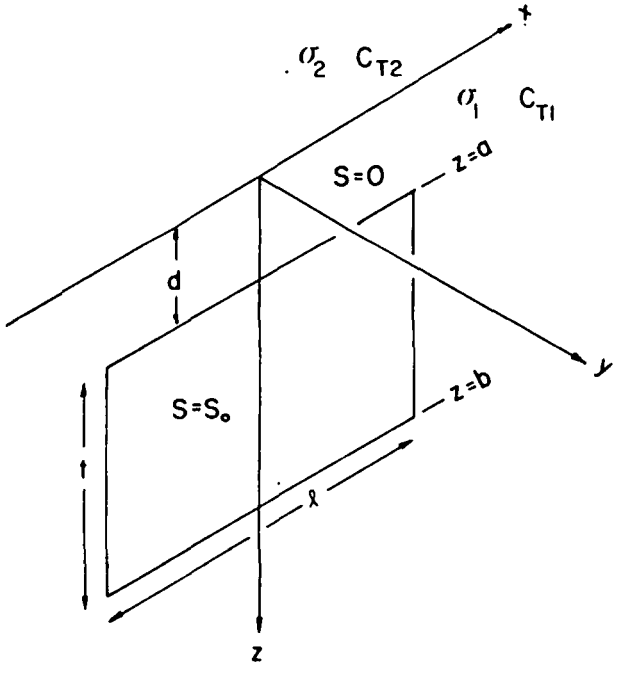

FIG. 3. Geometry of patch model used in inversion. Two regions of different conductivity and thermoelectric coefficient are separated by the plane $y = 0$. The source region has a depth of burial of $d(z = a)$, a depth extent of $t = b - a$, and a length of ℓ. Inside the patch, the source has an intensity of $S_0 = (C_{T1} - C_{T2})T_0$.

anomaly produced by any source distribution S can be determined. From a practical standpoint it is advisable to use a simple model which approximates the true source distribution, but has few parameters and is easy to compute. Figure 2a shows a temperature distribution above the ambient which might be expected to exist in a geothermal system. The profile is characterized by a gradient near the top where heat flow is caused primarily by conduction. Below this region is a zone where convective forces try to produce a region of constant temperature. In the lower portion of the profile, the temperature will return to some ambient value if the geothermal heat source is confined in vertical extent. In the strike direction (Figure 2b), the source intensity decreases from the value in the convective zone if the heat source has a finite strike length. Only the distribution along the vertical contact is shown because this is all the information needed to compute the SP anomaly. Since the temperature has been specified on the contact plane and is assumed to be zero on the surface, the temperature distribution and heat flow in the entire half-space has in principle been described.

Calculation of the SP anomaly due to the contoured distribution in Figure 2 is possible by integration using the appropriate Green's functions. This procedure is quite expensive and not warranted for most geothermal exploration data in view of how little is known of the details of the temperature distribution. A reasonable alternative is to approximate the curved contours shown in Figure 2 by a single rectangular contour similar to the dashed one. Inside this rectangular region, called a patch, the temperature has a constant value, while outside the patch in the contact plane the temperature is zero. Thus the patch model corresponds to a thin, hot rectangular plate from which heat is flowing. The patch model has an easily calculated thermoelectric SP anomaly associated with it. As more is learned about a particular source geometry, better approximations to it can be made by superimposing additional patches of different sizes, intensities, and location.

The surface anomaly produced by the single patch shown in Figure 3 is given by (Fitterman, 1979)

$$\psi_{1,2}(x, y, 0) = \frac{S_0}{\pi(1 + \sigma_1/\sigma_2)}[f(x, y; \ell, b) - f(x, y; \ell, a) - f(x, y; -\ell, b) + f(x, y; -\ell, a) \quad (7)$$

where

$$f(x, y; \alpha, \beta) = \tan^{-1}\frac{(x + \alpha/2)\beta}{y[(x + \alpha/2)^2 + y^2 + \beta^2]^{1/2}}. \quad (8)$$

The upper subscript is used for region 1 ($y > 0$), and the lower subscript is used for region 2 ($y < 0$). The function $f(x, y; \alpha, \beta)$ is odd with respect to the y-coordinate. This accounts for the odd

Table 2. Model parameter, standard deviation, and relative error estimates.

Parameter	Value	Standard deviation	Relative error
$a = d$	1.3 km	0.2	0.13
$b = t + d$	13 km	3.	0.26
ℓ	9.9 km	0.4	0.036
σ_1/σ_2	0.80	0.04	0.045
S_0	−340 mV	40.	0.11

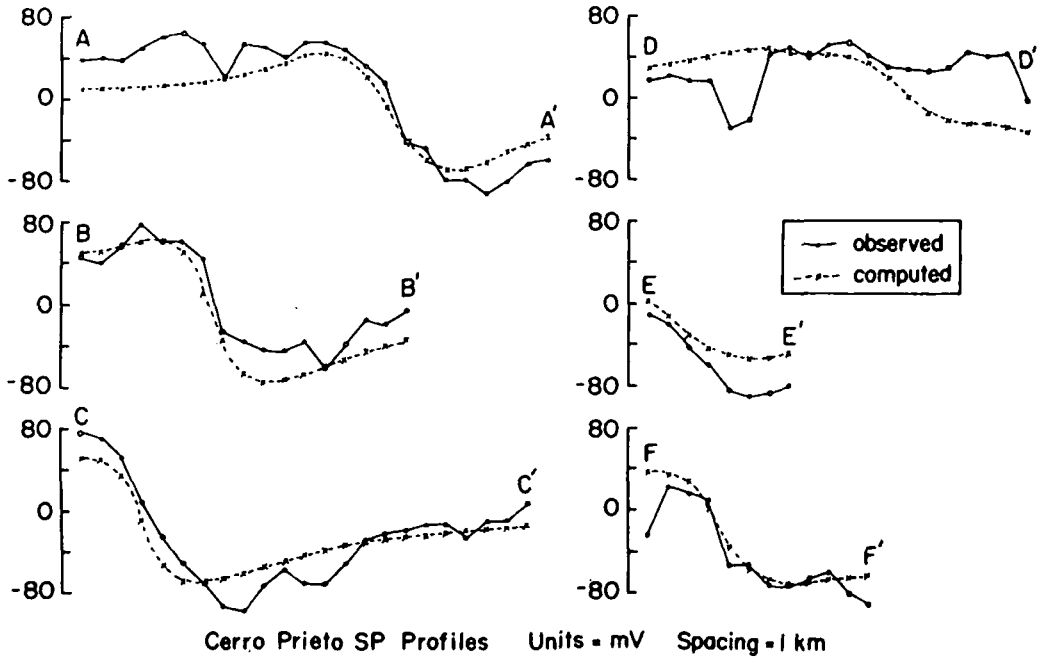

FIG. 4. Comparison of measured (o) and computed (x) potentials along the profiles shown in Figure 1. Model parameters are given in Table 2.

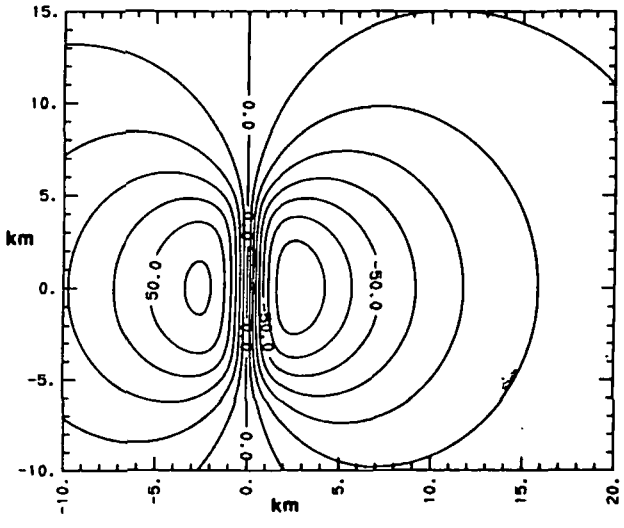

FIG. 5. Contour map of computed potential. Contour interval is 10 mV. Model parameters are given in Table 2.

Table 3. Correlation matrix for unscaled parameters using analytic partial derivatives. Only the lower half of the matrix is shown.

	a	b	ℓ	σ_1/σ_2	S_0
$a = d$	1.000				
$b = t + d$	−0.757	1.000			
ℓ	0.032	0.039	1.000		
σ_1/σ_2	0.0138	−0.008	0.195	1.000	
S_0	−0.937	0.899	−0.036	−0.082	1.000

symmetry of the anomalies when σ_1 and σ_2 are equal. If there is a difference in conductivity, the anomaly is enhanced on the resistive side of the contact and subdued on the conductive side. (See Fitterman, 1979 for examples.)

INVERSION METHODS AND RESULTS

We are now faced with the task of estimating the model parameters. A nonlinear, least-squares technique was used to adjust the model parameters so as to minimize the sum of the squares of the difference between the observed and computed potentials. Numerous discussions of the inverse problem exist in the geophysical literature (Wiggins, 1972; Inman, 1975; Glenn and Ward, 1976). Error minimization for this study was accomplished by means of the Levenberg-Marquardt algorithm *ZXSSQ* from the International Mathematics and Statistics Library (1979). This algorithm uses finite-differences to approximate the partial derivatives needed for the parameter corrections. Details of the method can be found in Levenberg (1944), Marquardt (1963), or Brown and Dennis (1972). Four of the model parameters (a, b, ℓ, and σ_1/σ_2) must always be nonnegative quantities. To ensure this condition, these parameters are logarithmically scaled.

The orientation of the source patch used to model the Cerro Prieto anomaly was placed parallel to the 0 mV contour in the region of steepest gradient (see Figure 1). The model source plane was positioned along the 0 mV contour, midway between the anomaly minimum and maximum. The resulting parameter and error estimates are given in Table 2. The relative error of the parameters ranges from 3 to 26 percent. The conductivity ratio σ_1/σ_2 and source length ℓ have the smallest error bounds (3–5 percent), followed by the depth a to the top of the source and source intensity S_0 (11–12 percent). Examining the correlation matrix (Table 3), one can see that the depth a to the top of the source has a strong inverse correlation with the source intensity

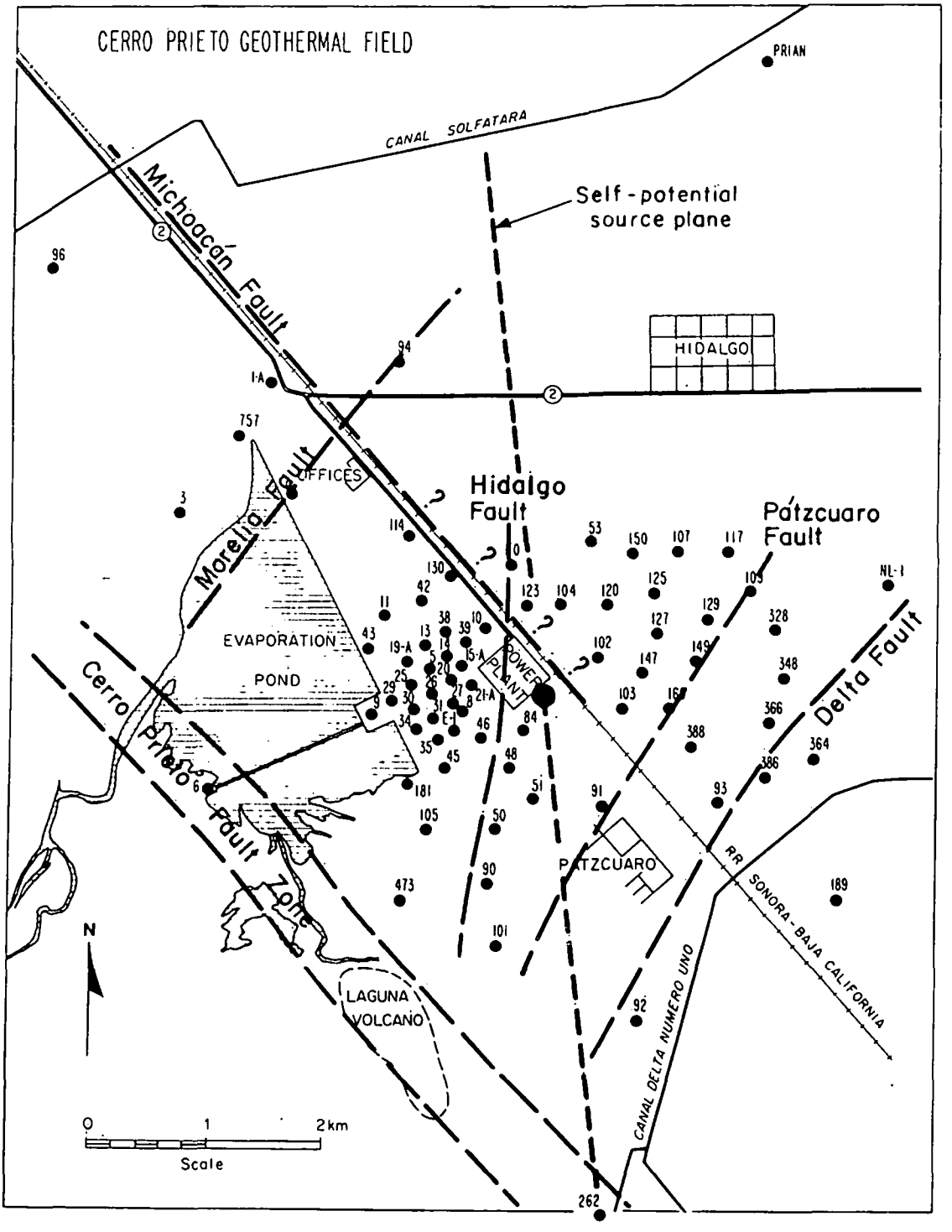

FIG. 6. Map of the Cerro Prieto geothermal field (from Vonder Haar, 1980). The straight line composed of short dashes represents the surface projection of the modeled SP source plane. The other dashed lines represent fault locations. The center of the SP source region is indicated by the large solid circle. The small solid circles are well locations. The symbols above the circles are the well numbers. (The M preceding each well number has been omitted for clarity.)

S_0, and a smaller, but significant, inverse correlation with the depth b to the bottom of the source. The source intensity is also inversely correlated with the depth to the bottom of the source. These strong correlations mean that we can not determine uniquely the model parameters. In view of the fact that we are dealing with potential field data, this is not surprising.

Of much greater concern than the correlation of the model parameters is the possibility that the model geometry is not a good representation of the geology. For example, the interface which is generating the SP anomaly might not be vertical, but rather dipping. The vertical geometry could require an apparent conductivity contrast where one does not exist in order to match the data. Similarly, the actual source intensity might not be constant as specified in the model because of variations in temperature or thermoelectric coefficients in the source region. Automatic inversion techniques cannot be viewed as the geophysicist's panacea, but rather a tool which suggests allowable alternative data interpretations which must be culled using a significant amount of geologic knowledge.

Figure 4 shows the comparison of the data profiles and the computed anomaly. The rms error in the fit is 28 mV. The model shows rather good agreement with the data. Short-wavelength features in the data, which are probably due to near-surface effects, are smoothed over by the model. A contour map of the computed anomaly is shown in Figure 5. Note the general similarity of the computed and measured anomaly (Figure 1). The short-wavelength features of the data, which the model cannot fit, are missing from the computed anomaly.

Self-potential models which use Nourbehecht's (1963) formulation require regions with different crosscoupling coefficients on each side of a boundary. In the patch model the boundary is a vertical plane. We now consider the known geology to see if there is any correspondence between the model parameters and the geology.

CORRELATION OF MODEL AND FIELD GEOLOGY

A wealth of geologic, geophysical, geochemical, and well log data from the Cerro Prieto field is available in the proceedings of two symposia published by the Lawrence Berkeley Laboratory (1979) and the Comisión Federal de Electricidad (1980). Structural models of the field described in these publications and in the numerous reports referenced in them have evolved rapidly in response to the increasing availability of data, resulting in a variety of interpretations. The most recent English language comprehensive studies are those of de la Pena and Puente (1979), Vonder Haar (1980), and Lyons and van de Kamp (1980), each of which considers many, but not all, of the currently available data in formulating their geologic models.

These recent studies conclude that the geothermal reservoir exists within deposits of the ancestral Colorado delta, consisting mainly of complexly interbedded sandstones, siltstones, and shales. The reservoir formation is overlain by about 1 km of unconsolidated silts, clays, and sands. This depth correlates well with the postulated depth of 1.3 ± 0.2 km to the top of the SP source plane. A granodioritic basement at about 1.5 to 3 km depth in the northwest appears to deepen to about 5 km in the southwest. This southeastern basement may consist of mixed volcanics, metasediments, and highly faulted granitic rock. The basement depth is considerably less than the 12 ± 3 km depth to the bottom of the SP source plane, inferring that any geologic structure corresponding to the source plane extends deep into the basement. At this time there is not enough information available even to contour the depth roughly to the top of the basement, not to mention draw any conclusions about possible basement structural features. Lyons and van de Kamp (1980) emphasized the structure of the geothermal field is complex, and it is not accurately visualized as a uniform reservoir overlain by a continuous low-permeability cap and overlying a simply structured basement.

Of central importance to our SP model is the possible existence of a fault or fault zone corresponding in location to our source plane and separating areas of different coupling coefficient and electrical conductivity. A fault map of the Cerro Prieto field given by Vonder Haar (1980) is shown in Figure 6, and one given by Lyons and van de Kamp (1980) is shown in Figure 7. The heavy dashed line in each of these figures represents the trace of our inferred SP source plane.

It is apparent from these two figures that more than one picture of faulting in the Cerro Prieto field may be drawn from similar data. (It also should be noted that these two figures combine faults of varying age, displacement, and vertical extent, as described in the original references.) In view of the compexity of the geology, it is not surprising that there is no single, continuous fault corresponding to the location of our inferred SP source plane. However, the location and strike of the Hidalgo fault shown in Figure 6 are not greatly different from those of the central part of our source plane, and the trace of the source plane also appears to correspond roughly to the general trend of a series of shorter northwest and northeast striking faults shown in Figure 7. Dips for these faults are not explicitly stated, but from stratigraphic

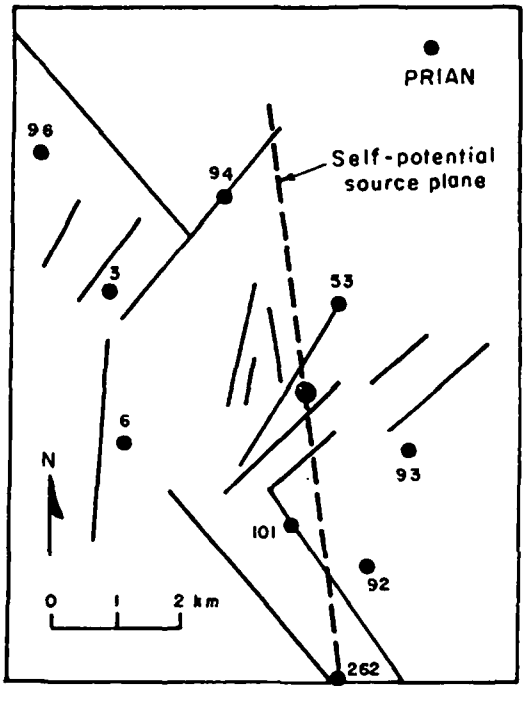

FIG. 7. Location of faults in the Cerro Prieto geothermal field (from Lyons and van de Kamp, 1980). Solid lines represent fault locations, and the dashed line represents the surface projection of the modeled SP source plane. The center of the SP source plane is indicated by the solid circle. Some of the well locations are indicated for correlation with Figure 6.

Table 4. Thermoelectric coupling coefficient from Cerro Prieto geothermal field cores. Undiluted pore fluid is 0.372 M in NaCl and 0.054 M in KCl with a conductivity of 4 mho/m. Measurements were made at a mean temperature of 30°C.

Well	Depth (m)	Rock type	Pore fluid dilution	C_T (mV/°C)
M-53	1708	Sandstone	0	0.037
M-53	1708	Sandstone	100:1	0.144
M-53	1900	Sandstone	0	0.010
M-94	1292	Sandstone	0	0.057
M-94	1292	Shale	0	0.180

cross-sections given by Lyons and van de Kamp (1980), they appear to be close to vertical. Additional evidence for a northerly structural trend in the central part of the field is given by north-trending contours of rock alteration as indicated by shale densification patterns (Lyons and van de Kamp, 1980).

Given the uncertainty of fault locations and possible errors inherent in the location of the SP source plane, it does not seem unreasonable to assume the source plane corresponds to a north-trending fault or zone of faults within the geothermal reservoir, possibly extending into the basement. The strike length of the source plane extends beyond the region where extensive well log data are presently available. However, the plane terminates to the south at its junction with the Cerro Prieto fault (Figure 6), which also forms the southwestern boundary of the present production zone (Vonder Haar, 1980). The plane terminates to the north between Highway 2 and the Canal Solfatara (Figure 6), an area in which a major structural change has been inferred by electrical resistivity data (Wilt et al, 1979).

It may also be significant that the center of the source plane (indicated by the large dot in Figures 6 and 7) is close to the intersection of the northwest-trending Michoacán fault and the north-trending fault or fault zone. According to Vonder Haar (1980), the high productivity of some geothermal wells near this intersection could indicate a zone of relatively high permeability that serves as a conduit for convective circulation of geothermal fluids. This conclusion is supported by a resistivity profile across the field given by Wilt and Goldstein (1980), which shows a zone of relatively high conductivity surfacing in the area of the intersection and dipping under the trace of the SP source plane. Unfortunately, the strike of this conductive zone is not known.

Obviously, the north-trending fault or fault zone does not represent a simple contact separating two different materials having differing thermoelectric coefficients and electrical conductivity. However, different rock types having different thermoelectric coefficients could be brought into contact by vertical offsets along faults. Because most of the individual rock units are less than 50 m thick (Lyons and van de Kamp, 1980), and because vertical fault offsets range up to several hundred meters (Vonder Haar, 1980), it seems likely that different rock types could be in contact across considerable vertical sections of most faults in the field. It is not obvious why one particular fault or fault zone (i.e., the Hidalgo fault of Figure 6) seems to act as an SP source plane even though most of the major faults in the field seem to have considerable vertical offset. If the north-trending faults corresponding to the SP source plane have higher permeability than others in the field, they might serve as the major conduits for hydrothermal circulation, providing increased heat to interact with the thermoelectric coefficient difference. Increased fluid circulation could also lead to extensive hydrothermal alteration along the faults, which could possibly contribute to thermoelectric coefficient variations. Whether the magnitude of possible thermoelectric coefficient differences between actual Cerro Prieto reservoir rocks is quantitatively sufficient to generate the observed SP anomaly is discussed later.

Finally, our SP model requires that the electrical conductivity on the east side of the source plane be 80 percent of that to the west. The conductivity structure of the field is far more complicated than this, but a resistivity profile across the production zone (Wilt and Goldstein, 1980) does show a general decrease in conductivity from west to east.

It should be kept in mind that a streaming potential source mechanism should not be ruled out as a possible cause of the SP anomaly, since one would expect hydrothermal circulation to be associated with the Cerro Prieto geothermal field. However, the modeling technique which we have used requires that there be neither heat nor fluid pressure variation, in the case of a streaming potential source, in the horizontal direction on the surface of the half-space. Since this condition is not realistic for groundwater flow, we have chosen not to attempt a model of a streaming potential source.

In summary, the geology of the Cerro Prieto geothermal field is much more complex than indicated by our simple SP model. However, some evidence does exist for the presence of a north-trending fault or fault zone roughly coincident with our SP source plane. Vertical offsets along these faults, along with hydrothermal alteration caused by possible circulation of geothermal fluids along the faults, could create the thermoelectric coefficient contrast needed for generation of the SP anomaly. The depth to the top of the source plane agrees well with the known depth to the top of the geothermal reservoir, but the bottom of the plane extends deep into the basement. The center of the plane lies close to the intersection of two major fault zones, a region where increased permeability may allow hot fluids to reach the source region. The electrical conductivity of the field decreases from west to east, in agreement with our model.

SOURCE MECHANISM

Values of the thermoelectric coupling coefficient C_T must be known in order to calculate SP anomalies using the analytical method described above. To gain a preliminary idea of the magnitude of these coupling coefficients, a series of laboratory measurements was made on Cerro Prieto reservoir rocks. The apparatus and test procedure used are described in detail in Morrison et al (1978). The tests were made on cylindrical samples measuring 50.8 mm (2 inches) diameter by 31.75 mm (1.25 inch) long taken from geothermal production wells (well locations are shown in Figure 6). The pore fluid used was 0.327 M in NaCl and 0.054 M in KCl, approximately representing the average composition of the fluid from all the producing wells (Mañon et al, 1977). The conductivity of this fluid at room temperature was 4 mho/m. The wells from which the samples were obtained, along with sample depths and rock types, are listed in Table 4.

Results of the thermoelectric coupling coefficient measurements are summarized in Table 4. For the sample from well M-53, 1708 m depth, diluting the pore fluid 100:1 increased C_T from 0.037 to 0.144 mV/°C, indicating that C_T is sensitive to pore fluid conductivity. Because pore fluid conductivity is a function of temperature, it is likely that C_T also varies with temperature. In order to generate the −340 mV source potential in a 300°C reservoir solely by thermoelectric effect, a coupling coefficient con-

trast of about 1 mV/°C would be required. This is about an order of magnitude greater than the measured values. Measurement of C_γ under in-situ conditions is necessary to determine realistically the contribution of this mechanism to the measured anomaly.

CONCLUSIONS

The similarity of the measured SP anomaly at Cerro Prieto and those produced by a vertical contact model suggests using this model to determine the source of the Cerro Prieto anomaly. The inversion of SP data is relatively easy to do, but one must be aware of the nonuniqueness problem indicated by correlation of certain model parameters.

The source region of the Cerro Prieto SP anomaly appears to correspond to a north-trending fault or fault zone which crosses the geothermal field. Rock displacement or alteration across this zone could provide the thermoelectric coefficient contrast necessary to interact with the temperature field or to generate the measured SP anomaly. The estimated depth to the top of the source zone is in good agreement with the known depth to the production zone. The estimated increase in resistivity on the east side of the source region agrees with the near-surface resistivity interpretation of Wilt and Goldstein (1980).

The exact source mechanism generating the SP anomaly cannot be determined without more knowledge of the in-situ cross-coupling properties. Laboratory measurements at low temperatures and pressures give values for thermoelectric coupling coefficients which are too low by about an order of magnitude to generate the inferred source voltage from the measured temperature of the reservoir. We have not ruled out the possibility that the observed SP anomaly is generated by a streaming potential mechanism. Modeling using this type of a source mechanism would be helpful in determining the cause of the SP anomaly.

ACKNOWLEDGMENTS

This work was supported in part by the U. S. Geological Survey under contract no. 14-08-0001-16546, and in part by the U. S. Department of Energy under the direction of the Lawrence Berkeley Laboratory, Earth Sciences Division, under contract no. W-7405-ENG-48. We thank S. Vonder Haar and M. J. Wilt of the Lawrence Berkeley Laboratory and the personnel of the Comisión Federal de Electricidad, Coordinadora Ejecutiva de Cerro Prieto, for their cooperation and assistance. Comments by W. R. Sill and T. R. Madden have been helpful in pointing out the limitations of the modeling technique we have used.

REFERENCES

Brown, K. M., and Dennis, J. E., 1972, Derivative free analogues of the Levenberg-Marquardt and Gauss algorithms for nonlinear least-squares approximations: Numer. Math., v. 18, p. 289–297.

Comisión Federal de Electricidad, 1980, Proceedings, Second symposium on the Cerro Prieto geothermal field, October 17–19, 1979, Mexicali, Baja California, Mexico: Comisión Federal de Electricidad de México, in press.

Corwin, R. F., and Hoover, D. B., 1979, The self-potential method in geothermal exploration: Geophysics, v. 44, p. 226–245.

Corwin, R. F., Morrison, H. F., Diaz, S., and Rodriguez, J., 1979, Self-potential studies at the Cerro Prieto geothermal field, September 20–22, 1978, San Diego: Lawrence Berkeley Lab rep. LBL-7098, p. 204–210.

Fitterman, D. V., 1979, Calculations of self-potential anomalies near vertical contacts: Geophysics, v. 44, p. 195–205.

Garcia, S. D., 1975, Estudio Geoeléctrico de la zona geothérmica de Cerro Prieto, Baja California, Mexico: Proc. 2nd U.N. symposium on the development and use of geothermal resources, San Francisco, U. S. Gov. Print. Of., Washington, DC, v. 2, p. 1003–1011.

Glenn, W. E., and Ward, S. H., 1976, Statistical evaluation of electrical sounding methods, part I: Experimental design: Geophysics, v. 41, p. 1207–1221.

Inman, J. R., Jr., 1975, Resistivity inversion with ridge regression: Geophysics, v. 40, p. 798–817.

International Mathematics and Statistics Library, 1979, IMSL Library Edition 6: IMSL, 6th floor, GNB Bldg., 7500 Bellaire Blvd., Houston, TX 77036.

Lawrence Berkeley Laboratory, 1979, Proceedings, First symposium on the Cerro Prieto geothermal field, Baja California, Mexico, Sept. 20–22, 1978, San Diego, California: Lawrence Berkeley Laboratory rep. LBL-7098.

Levenberg, K., 1944, A method for the solution of certain non-linear problems in least squares: Quart. Appl. Math., v. 2, p. 164–168.

Lyons, D. J., and van de Kamp, P. C., 1980, Subsurface geological and geophysical study of the Cerro Prieto geothermal field, Baja California, Mexico: Lawrence Berkeley Lab. rep. LBL-10540.

Mañon, A., Mazor, E., Jiminez, M., Sanchez, A., Fausto, J., and Zenizo, C., 1977, Extensive geochemical studies in the geothermal field of Cerro Prieto, Mexico: Lawrence Berkeley Lab. rep. LBL-7019.

Marquardt, D. W., 1963, An algorithm for least-squares estimation of nonlinear parameters: J. SIAM, v. 11, p. 431–441.

Morrison, H. F., Corwin, R. F., DeMoully, G., and Durand, D., 1978, Interpretation of self-potential data from geothermal areas: Semi-annual technical progress report, U.S.G.S. contract no. 14-08-0001-16546, October 31.

Noble, J. E., Mañon, A., Lippmann, M. J., and Witherspoon, P. A., 1977, A study of the structural control of fluid flow within the Cerro Prieto geothermal field, Baja California, Mexico: Preprint, SPE 52nd an. meet., AIME.

Nourbehecht, B., 1963, Irreversible thermodynamic effects in inhomogeneous media and their applications in certain geoelectric problems: Ph.D. thesis. M.I.T.

de la Pena, A., and Puente, I., 1979, The geothermal field of Cerro Prieto, *in* Geology and Geothermics of the Salton Trough: W. A., Elders, editor, rep. UCR/IGPP-79/23, Inst. of Geophys. and Planetary Phys., Univ. of California, Riverside, p. 20–35.

Puente Cruz, I., and de la Pena, A., 1979, Geology of the Cerro Prieto geothermal field, *in* Proceedings, 1st symposium on the Cerro Prieto Geothermal Field, September 20–22, 1978, San Diego: Lawrence Berkeley Lab rep. LBL-7098, p. 17–40.

Vonder Haar, S., 1980, Geology of the Cerro Prieto geothermal field: Earth Sciences, Lawrence Berkeley Lab, v. 3, p. 1–5.

Vonder Haar, S., and Puente Cruz, I., 1979, Hybrid transform faults and fault intersections in the southern Salton trough geothermal area, Baja California, Mexico, *in* Geology and geothermics of the Salton trough: W. A., Elders, editor, rep. UCR/IGPP-79/23, Inst. of Geophys. and Planetary Phys., Univ. of California, Riverside, p. 95–100.

Wiggins, R. A., 1972, The general linear inverse problem: Implications of surface waves and free oscillations for earth structures: Rev. Geophys. Space Phys., v. 10, p. 251–285.

Wilt, M. J., and Goldstein, N. E., 1980, Resistivity monitoring at Cerro Prieto: Lawrence Berkeley Lab rep. LBL-9549.

Wilt, M. J., Goldstein, N. E., and Razo, A. M., 1979, LBL resistivity studies at Cerro Prieto, *in* Proceedings, 1st symposium on the Cerro Prieto geothermal field, September 20–22, 1978, San Diego: Lawrence Berkeley Lab rep. LBL-7098, p. 179–188.

A Comparative Study of Hot-Water Chemistry and Bedrock Resistivity in the Southern Lowlands of Iceland

VALGARDUR STEFÁNSSON
STEFÁN ARNÓRSSON
National Energy Authority, Laugavegur 116, Reykjavík, Iceland

ABSTRACT

The low-temperature area on the east side of the volcanic zone in southwestern Iceland is investigated by means of the chemical properties of the hot water and the electrical resistivity of the bedrock. The combined geochemical and resistivity results, along with analysis of the geological structure, give a much more reliable picture of this area than the individual methods do separately. Three distinct hydrothermal systems inferred from the Cl:B ratio of the thermal water are separated by high-resistivity boundaries which are known to contain a high proportion of massive basaltic dykes and intrusions in a few localities. There is a good regional agreement between high temperatures of last equilibrium with chalcedony/quartz of the thermal water and low rock resistivity. The regional geological structure is complemented by an overall northeast-southwest resistivity structure, and dipping formations containing thermal water are traced down to 500 to 1000 m depth by resistivity soundings. Superimposed on the northeast-southwest structure is an east-west resistivity structure which coincides with a local anomaly in the chemical composition of the thermal water. This is suggested to be connected with a seismically active east-west transform fault.

INTRODUCTION

A regional investigation of the low-temperature area on the east side of the volcanic zone in southwestern Iceland has been in progress for several years. The first overall picture of the area was achieved by geochemical methods (Arnórsson, 1970). On the basis of the Cl:B ratios in the thermal water, three hydrothermal systems could be distinguished.

Since 1970 a rather extensive resistivity survey has been performed in the area, parallel with a detailed geological mapping. The geological, geochemical, and geophysical results together form a rather comprehensive picture of the geohydrology of the area, and the conformity of three independent exploration methods improves the reliability of the model achieved. Further, this combination of survey methods demonstrates how the characteristics of a geothermal reservoir can be revealed by inexpensive surface exploration.

This paper presents the results obtained so far from the geochemical and resistivity methods. The results of the geological investigation have been applied in the interpretation. No attempt is made, however, to review the geological studies.

The geochemical results presented here are based on new data from the area as well as more comprehensive interpretation of the previous data (Arnórsson, 1970). Underground temperatures are estimated in three different ways, and a discussion on the hydrogen sulfide and carbonate content of the geothermal waters is given.

The specific resistivity of the area is obtained from numerous dc resistivity soundings. This survey is still in progress. It is, however, believed that the results obtained so far give a reliable general picture of the regional distribution of the resistivity.

GEOLOGICAL FEATURES

The southern lowlands low-temperature area is located in Quaternary rocks just east of the western active volcanic zone (Fig. 1). The bedrock consists mostly of basalt lavas and hyaloclastite formations (pillow lavas, pillow breccias, and hyaloclastites). Acid volcanics occur in the vicinity of Geysir and Flúdir in the northeastern and eastern parts of the area. The lavas were formed during interglacials of the Quaternary epoch, whereas the hyaloclastite formations formed during the glacial periods in meltwater chambers within the ice sheet.

The basalt lavas dip a few degrees toward the northwest under the active volcanic belt. Toward the east where the rocks are oldest, the hyaloclastite formations are reworked, at least partly, and tend to form sheets of variable thickness between the lavas. In the west, on the other hand, the hyaloclastite formations form mountains protruding above the plains. These mountains still reflect to some extent the shape of the meltwater chambers as a result of limited erosion.

Differentiated and intrusive rocks which characterize central complexes occur at Geysir and near Flúdir. A complex of dense basalt intrusions also occurs just north of Vördufell at the boundary of the three main hydrothermal systems.

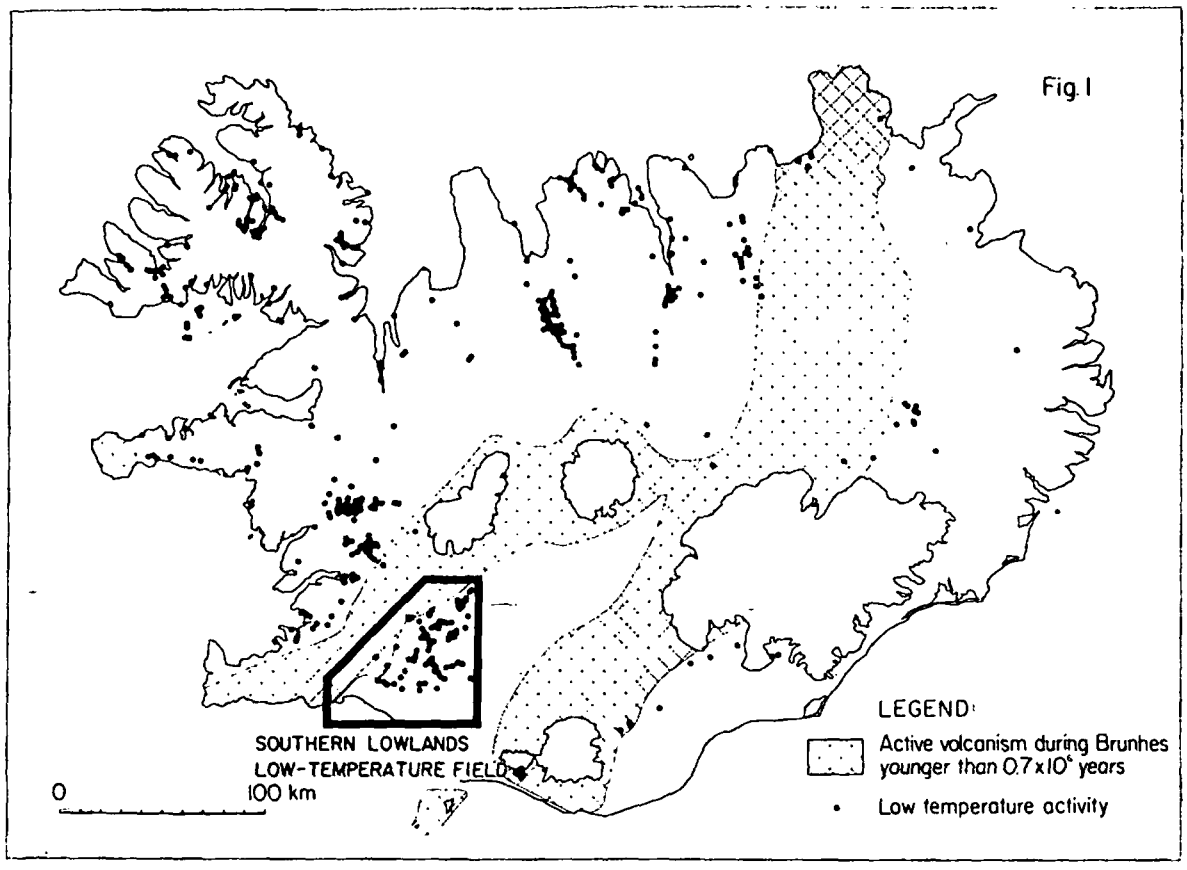

Figure 1. The location of the southern lowlands low-temperature field in relation to the active volcanic zone.

Northeast-southwest faults, approximately parallel to the axis of the active volcanic zone, are pronounced in the area.

The regional thermal gradient is high in the area, ranging from about 140°C/km at the edge of the volcanic zone to about 60°C/km 50 km to the east (Pálmason, 1973). The flow of thermal water from natural springs in the whole area amounts to about 300 liters/sec.

GEOCHEMICAL STUDIES

Silica temperatures, that is, temperatures which correspond with equilibrium between chalcedony or quartz and un-ionized silica in the thermal water, have been estimated for the majority of thermal springs and drill holes (Fig. 2). The principles and assumptions involved in estimation of silica temperatures were outlined by Arnórsson (1975).

The silica temperatures tend to be 0 to 40°C higher than the measured temperatures in the springs and drill holes (Fig. 3). A few samples show, however, greater supersaturation by as much as 100°C. Several samples are undersaturated by a few degrees but this undersaturation is not regarded as significant. For the majority of the thermal springs and shallow drill holes, the chalcedony and quartz supersaturation are considered to have resulted from cooling of the water in the upflow zones, either by conduction or flashing; so silica temperatures give an idea of underground temperature conditions below the zone of conductive cooling and flashing. Some warm spring waters around major upflow zones are considered to have formed by mixing of cold ground water with thermal water. In this case the silica temperature values bear a more complicated relation to the underground temperatures since the mixing will lead to pH lowering and chalcedony and quartz supersaturation for the temperature of the mixture. In other words these factors bring about changes in the un-ionized silica content of the water, which is not so in the case of conductive cooling.

Underground temperature estimates from the Na-K-Ca geothermometer as defined by Fournier and Truesdell (1973) yield values which give the same overall picture for underground temperatures as the silica geothermometer does. This is partly reflected in Figure 4. There is a considerable scatter of points in this figure, particularly at low temperatures, which reflects discrepancy between the two geothermometers. At silica temperatures above 100°C the Na-K-Ca geothermometer tends to give a little higher values than chalcedony equilibrium temperatures.

In general, the Na-K-Ca geothermometer shows greater deviation above measured temperatures in springs than does the silica geothermometer (Fig. 4). It is believed that the Na-K-Ca geothermometer may yield unreliable values toward high temperatures for many of the warm springs which appear in peat soil. Equilibrium may not be reached at the low temperatures of these springs, and the water is likely to be high in potassium due to the relatively high mobility of this element in the soil. Discrepancy between the two geothermometers is to be expected for thermal waters which have been diluted with cold ground waters.

The thermal activity in the southern lowlands has been divided into three major hydrothermal systems on the basis of the chlorine and boron contents of the thermal waters (Arnórsson, 1970). A fourth hydrothermal system occurs

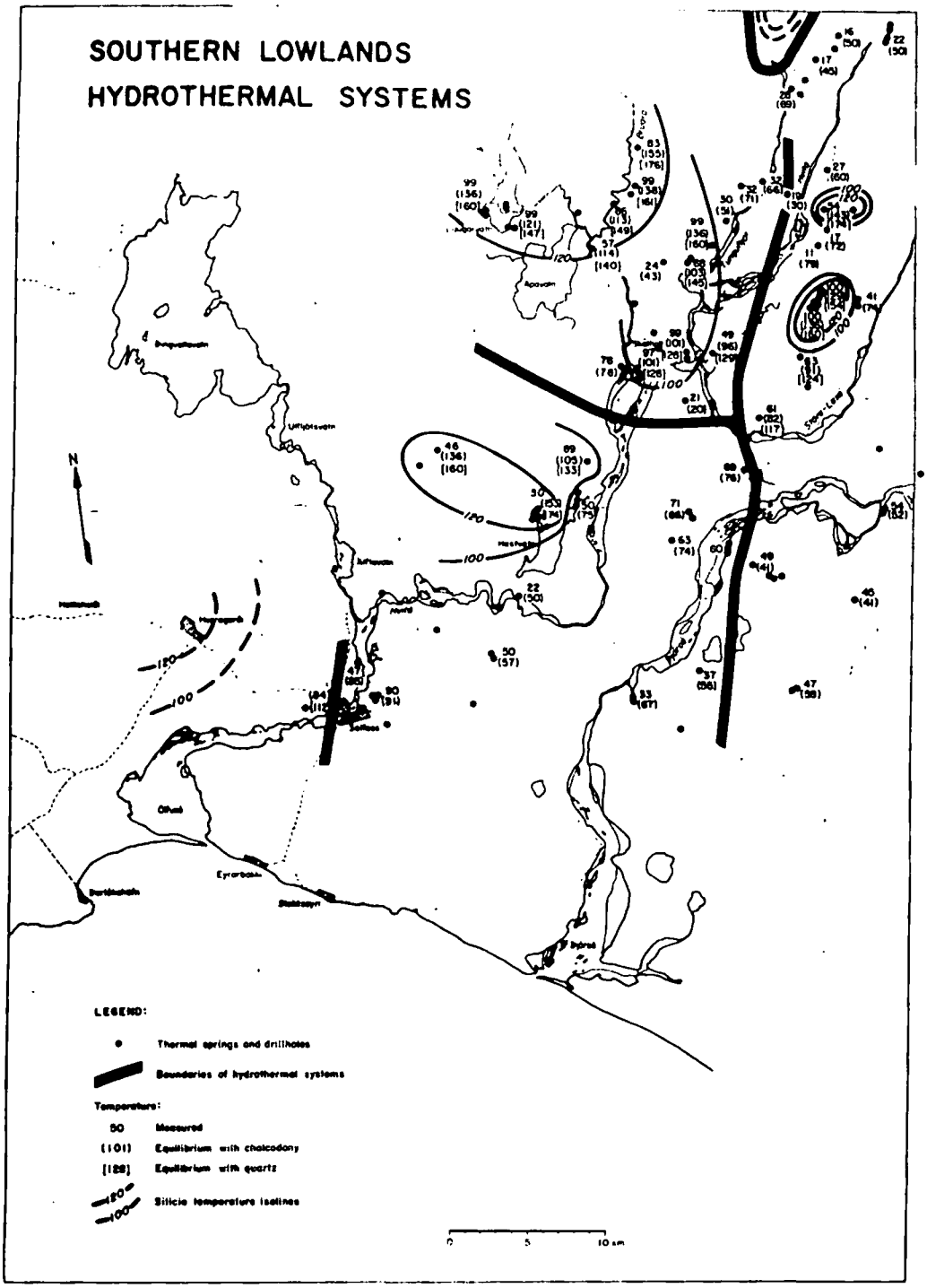

Figure 2. Hydrothermal systems in the southern lowlands as deduced from the Cl-B content of the thermal water. Silica temperature estimates are given for the majority of thermal springs and drill holes.

to the west of hydrothermal system II (see Fig. 2), and a fifth system, which is of the high-temperature type, occurs north of hydrothermal systems I and III. New data on chlorine and boron not included in the previous study fall into the picture of the three main hydrothermal systems (Fig. 5). Much of the additional data include warm springs, some of which are located around major upflow zones of hot water, and they are believed to have originated by mixing of this hot water with cold ground water.

For hydrothermal systems II and III the chlorine and boron concentrations fall approximately on a line between about 5 to 10 ppm chlorine and 0 ppm boron and the densest cluster of points corresponding to the hot waters of each system. This is what would be expected if the warm waters had really formed by mixing of hot water and cold ground waters. The cold ground waters contain 5 to 10 ppm of chlorine and about 0 ppm of boron.

Warm springs are rather widespread in the northwestern corner of the southern lowlands but no hot springs exist in that area. Due to the similar concentrations of boron and chlorine in these waters and cold ground waters, it cannot be established with any certainty to which hydrother-

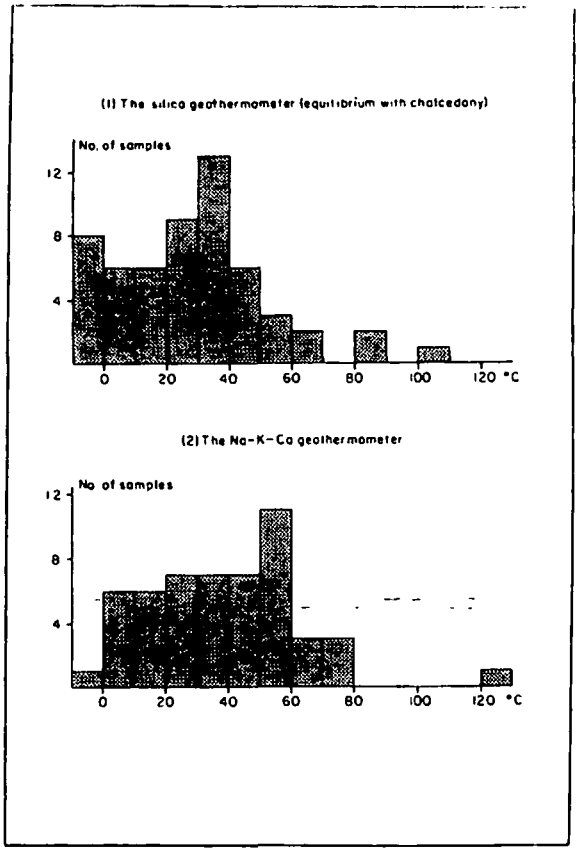

Figure 3. Supersaturation corresponding to differences between measured temperatures in springs and drill holes.

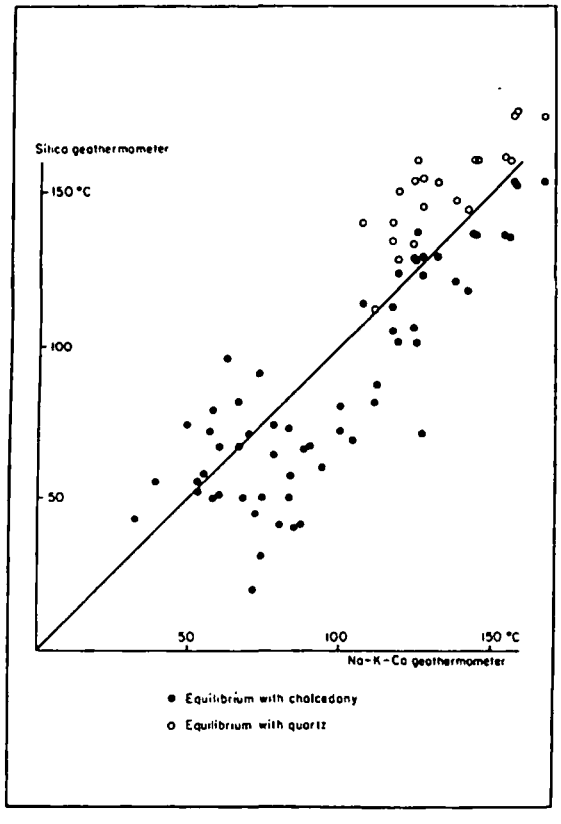

Figure 4. Comparison between underground temperatures as estimated by (1) the silica geothermometer; (2) the Na-K-Ca geothermometer.

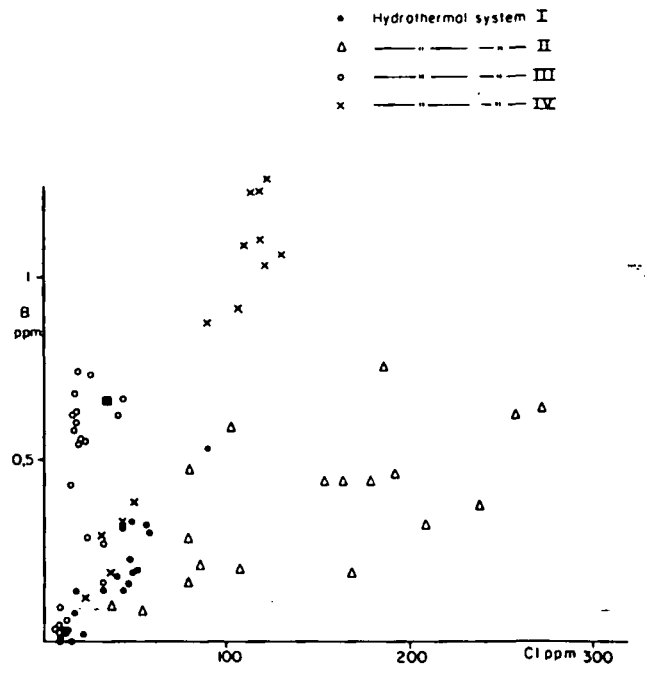

Figure 5. Cl-B relationships in thermal waters in the southern lowlands.

mal system these warm springs belong or whether they really form a separate system.

Within each of the three major hydrothermal systems as defined by the chlorine and boron contents of the thermal waters, there is a rather regular distribution in the values of the silica temperatures (Fig. 2). Thus, the highest silica temperatures occur in the northernmost part of hydrothermal system I and in the western part of hydrothermal system II, in both cases nearest to the active volcanic belt. If the warm springs discussed in the previous paragraph are excluded, the highest silica temperatures occur in the northernmost part of hydrothermal system III. Within each area the highest silica temperatures, corresponding to equilibrium with quartz, are in the range of 170 to 180°C. If, on the other hand, equilibrium with chalcedony is assumed, highest silica temperatures of 150 to 160°C are obtained for each hydrothermal system. On the outskirts of each system silica temperatures have dropped to some 40 to 80°C.

An attempt has been made to draw isolines for silica temperatures of 120°C (equilibrium with chalcedony) inside each hydrothermal system (Fig. 2). Due to lack of hot springs and drill holes in parts of the southern lowlands, these isolines should be regarded as only tentative. This refers particularly to hydrothermal system III and the isolines on the western boundary of systems I and II. Apparently, hydrothermal system I has the greatest areal extent.

With a few exceptions, the waters from springs and drill holes in the southern lowlands possess chemical characteristics typical for the low-temperature areas in Iceland. The exceptions include two major hot-spring centers around Laugarvatn in the northwestern corner of hydrothermal system I and the two spring localities in hydrothermal system II having the highest silica temperatures for that area. The former is characterized by an unusually high content of hydrogen sulfide (20 to 25 ppm) but the latter is characterized by carbonate water, and the carbonate may be of juvenile origin.

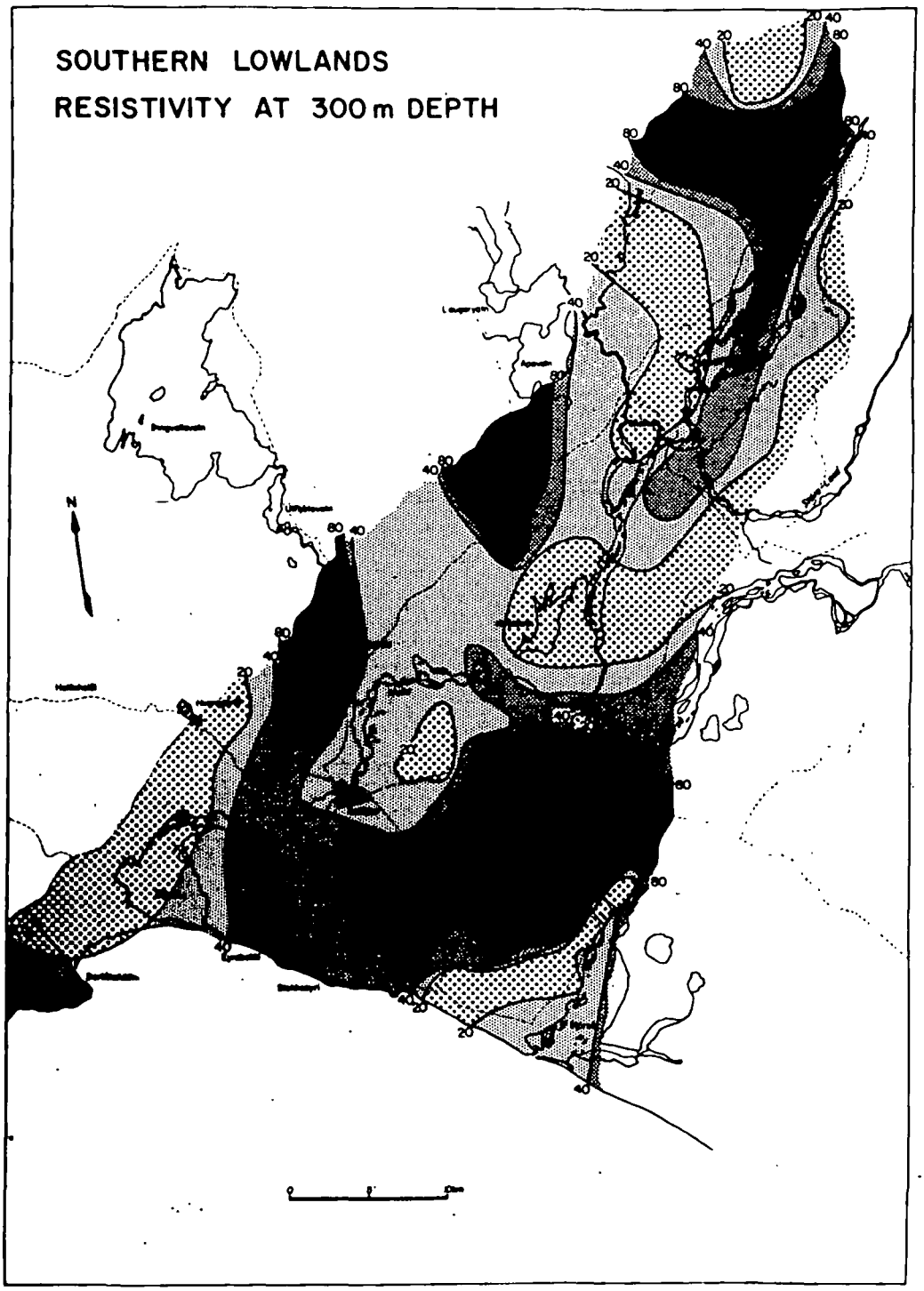

Figure 6. True resistivity at 300 m depth.

The hydrogen sulfide content of boiling springs in the low-temperature areas tends to be in the range of 1 to 2 ppm and lower in cooler springs. Thermal waters with temperatures of less than about 50°C contain generally no detectable hydrogen sulfide, or less than 0.1 ppm. By contrast, some hot springs and, invariably, drill holes from the high-temperature areas contain substantial concentrations of hydrogen sulfide, 30 to 250 ppm. For example, thermal water at 200°C feeding drill holes in Hveragerdi in the Hengill high-temperature area contains about 30 ppm of hydrogen sulfide. Hydrogen sulfide of 20 to 25 ppm in the hot springs by Laugarvatn are therefore indicative of high-temperature activity rather than low-temperature activity. Laugarvatn is adjacent to the active volcanic zone; and the high hydrogen sulfide content in the hot springs there could well reflect the existence of a hidden high-temperature area, whether it would be located directly under Laugarvatn or within the active volcanic zone to the north or to the west.

As with many other warm carbonate waters in Iceland, the silica content of the carbonate waters in hydrothermal system II is not far from opal saturation at the temperature

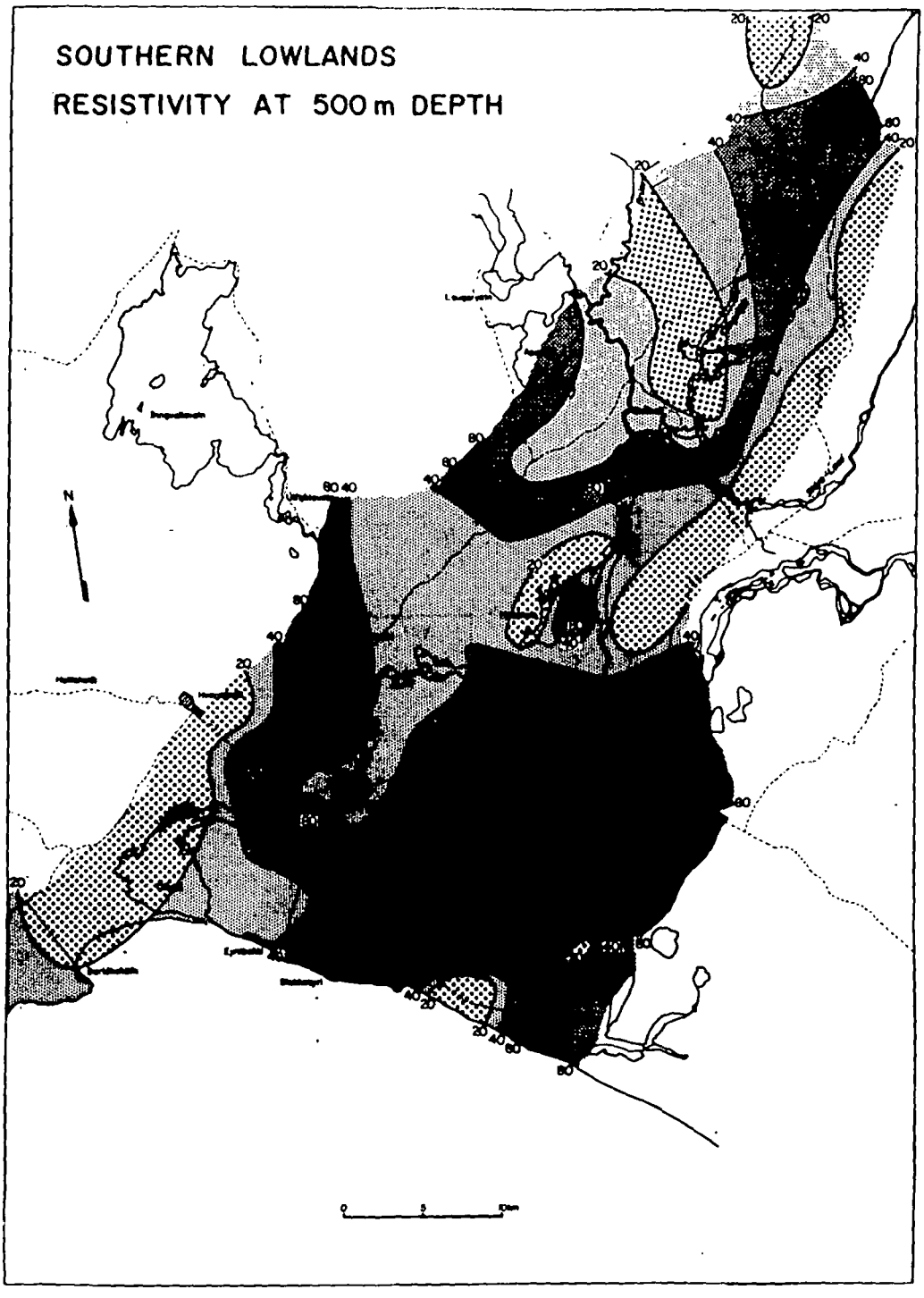

Figure 7. True resistivity at 500 m depth.

in the springs. Due to the high silica supersaturation, whether it refers to equilibrium with quartz or chalcedony, a doubt has been thrown on the reliability of underground temperature estimates by the silica geothermometer for such waters. Yet, the Na-K-Ca geothermometer yields temperature values which are intermediate for chalcedony and quartz equilibrium temperatures. This good comparison rather supports the interpretation that high underground temperatures really exist where the carbonate springs occur in hydrothermal system II.

RESISTIVITY STUDIES

The specific electrical resistivity of the bedrock has been obtained from direct current resistivity soundings. A symmetrical Schlumberger electrode configuration has been used and the maximum current arm AB/2 is 900 to 1500 m, depending on local circumstances.

In the interpretation, horizontal resistivity layers have been assumed on a local basis, that is, within the range of each sounding. Comparison with theoretical master curves (Orellana and Mooney, 1966; van Dam and Meulenkamp, 1969) has given the resistivity layers.

To date, there have been about 180 resistivity soundings in the area. On the basis of these measurements, resistivity maps at 300, 500, and 900 m depth have been made (Figs. 6, 7, and 8). This kind of representation gives an areal view of the true resistivity in the bedrock. It can easily be seen that the area is divided into several low resistivity

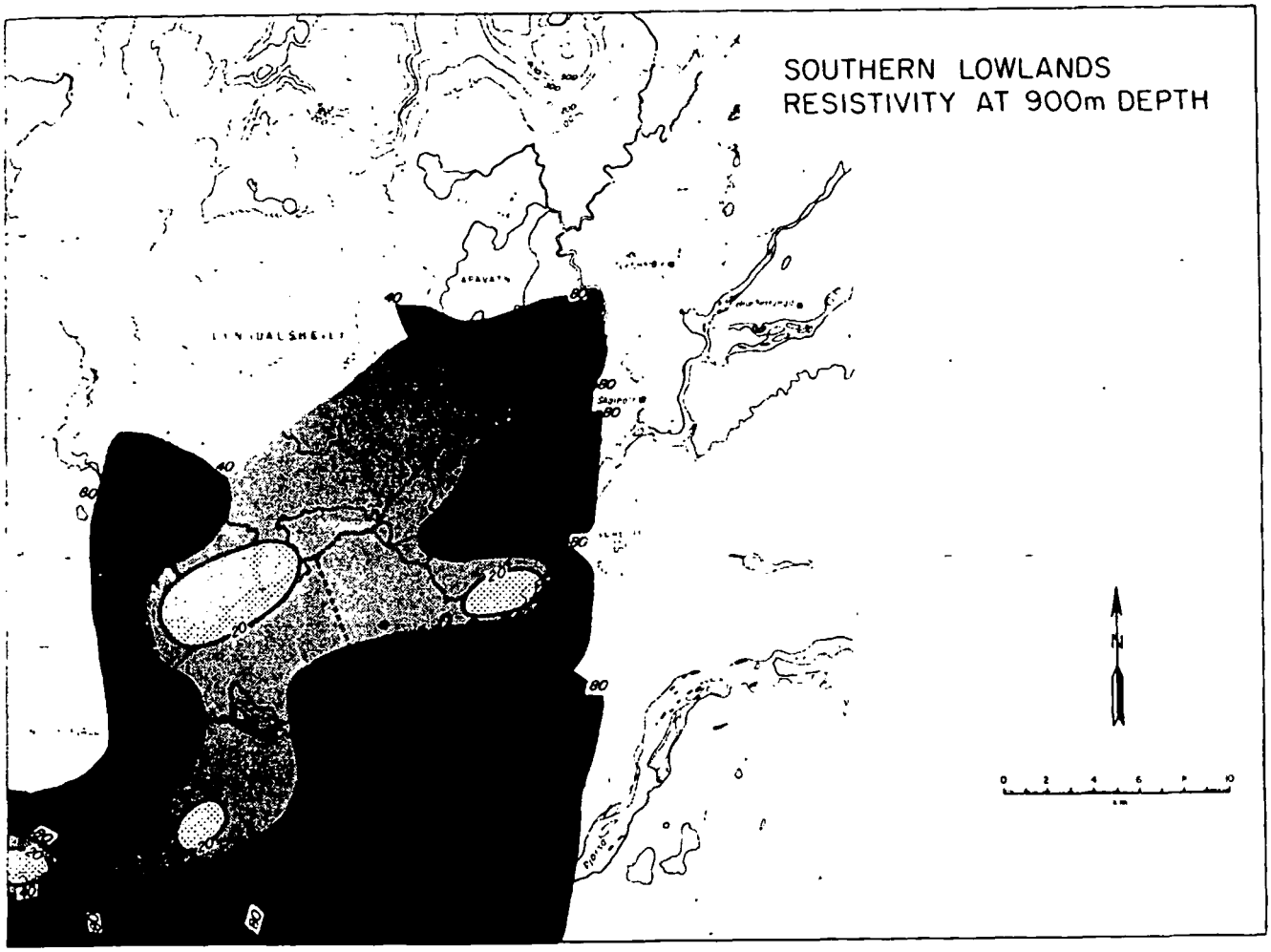

Figure 8. True resistivity at 900 m depth.

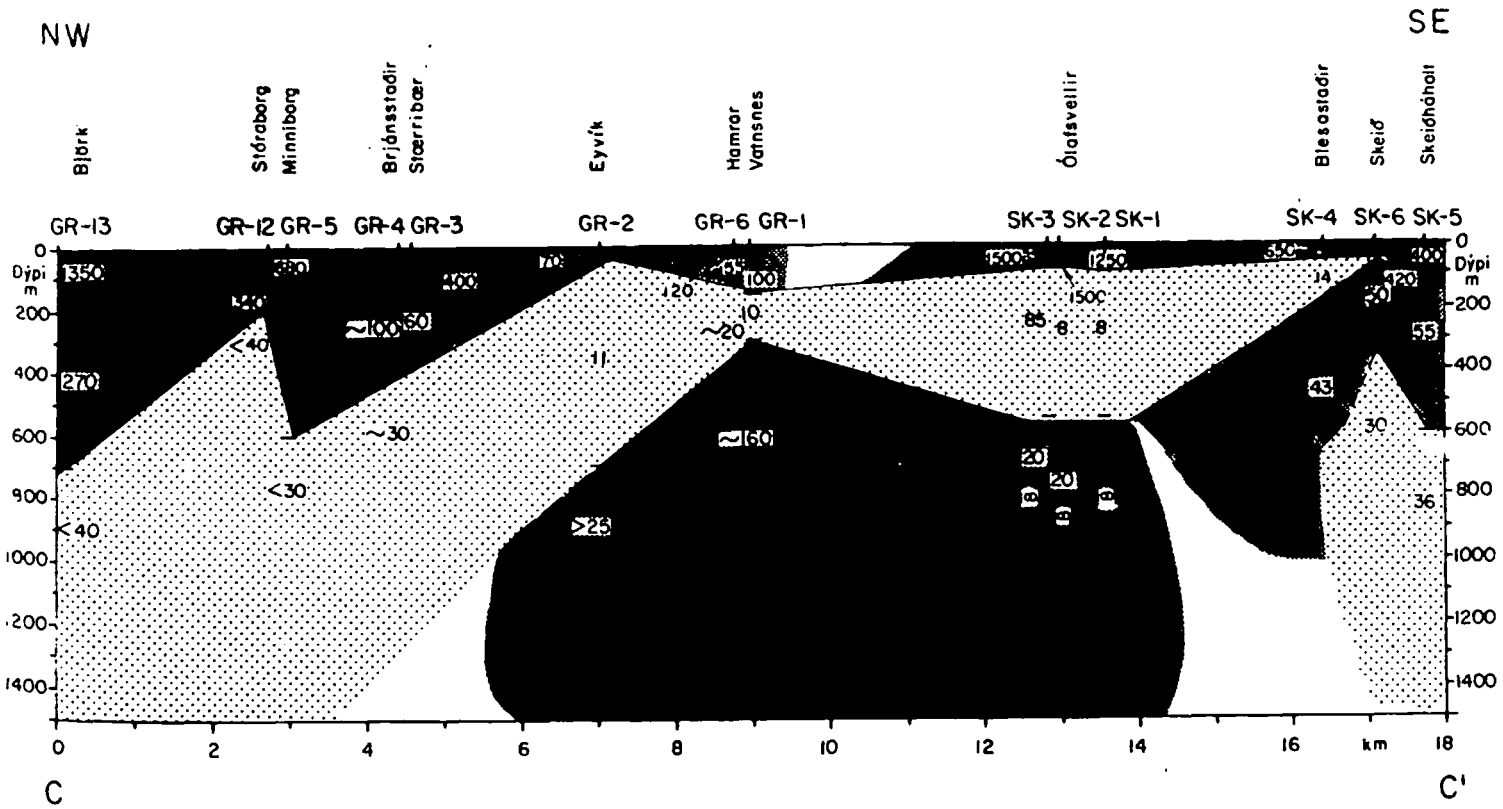

Figure 9. Resistivity section across the area in northwest-southeast direction perpendicular to the strike.

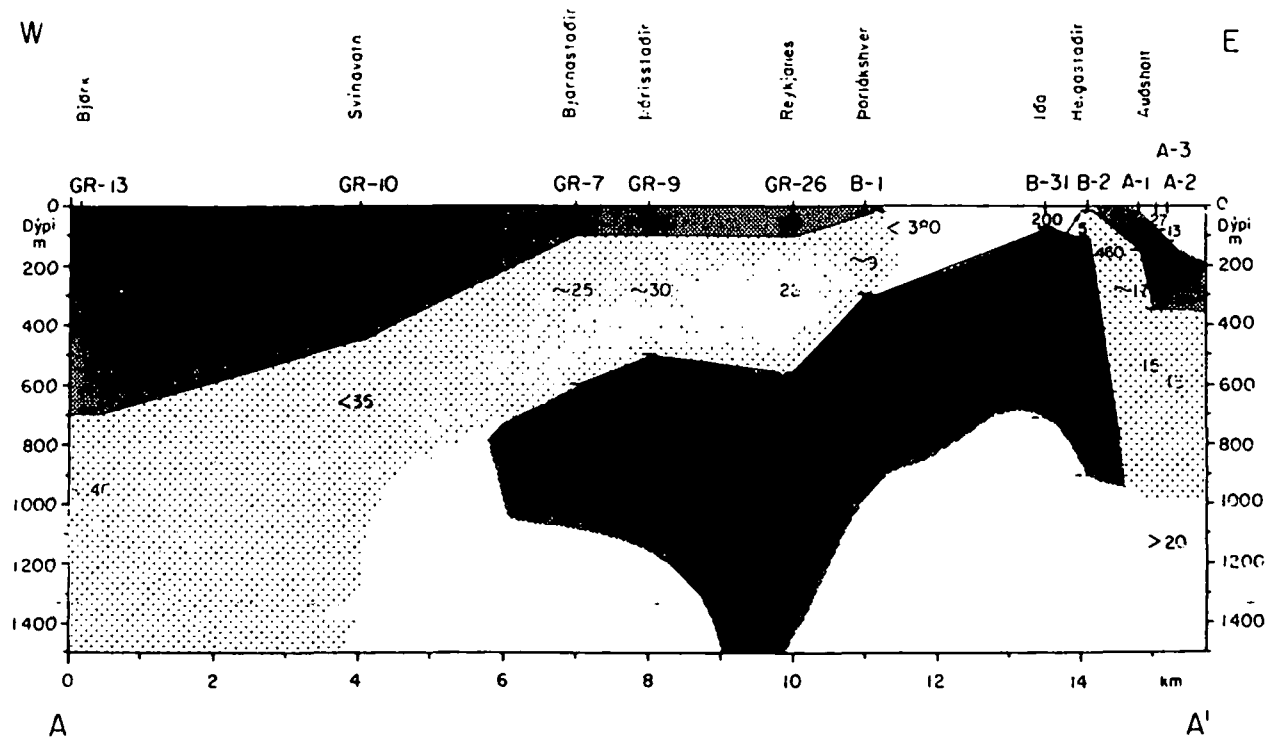

Figure 10. Resistivity section across the intersection of two hydrothermal systems.

(≤20 ohm·m) areas which are more or less separated by high-resistivity boundaries. However, the distribution of resistivity in the bedrock is a three-dimensional problem, and the vertical variations are not easily represented on an areal map. In Figure 9 a cross section of the resistivity across the area is shown. The dip of resistivity layers is about 5 degrees toward the northwest, which is the same as the dip of geological formations in the area.

In the vicinity of Vördufell, where the intersection between hydrothermal systems I, II, and III is located, a rather high resistivity is found with sharp boundaries to the east and west. In the cross section shown in Figure 10, an example of this high-resistivity wall is shown. This high-resistivity wall is found to have a southwest-northeast direction and can be seen in Figure 9 in the middle of the section. At this place the wall does not reach the surface.

GEOHYDROLOGICAL MODEL

The combination of the chemical and resistivity data makes it possible to obtain a model for the geothermal systems in the southern lowlands. In Figure 11 the main results of the chemical investigation are drawn together with the true resistivity at 500 m depth. In this way the results of the two exploration methods can be compared easily. As can be seen the Cl-B boundaries generally coincide with high resistivity in the bedrock. This correlation indicates that on the boundaries there are impermeable walls of some kind. The best location of such walls is on the boundary between hydrothermal systems I and III. Several massive basalt intrusions occur here (Fransson, personal commun., 1974) and they could be the cause of the high resistivity.

It can be observed, further, that several of the greatest natural springs belonging to hydrothermal system I are located near the boundaries (Thorlákshver, Laugarás, Reykholt). A possible explanation for this is that the impermeable walls bring the thermal water to the surface as is schematically shown in Figure 12. This hypothesis should be compared to the resistivity section shown in Figure 10.

Further investigation of Figure 11 shows that the centers of the hydrothermal systems, where the highest silica temperature is measured, generally coincide with low resistivity (≤20 ohm·m) in the bedrock. In some places this correlation is remarkably good, as for example in the Biskupstungur area (hydrothermal system I).

In general it seems clear that geothermal properties can be mapped by resistivity soundings, and the picture achieved is the same as obtained by chemical methods. The main result of the comparative study is, therefore, that the reliability of the model is greatly strengthened by the use of the two independent methods instead of one.

The overall pattern of the resistivity data in the area investigated indicates a southwest-northeast trend which is in agreement with the structural trend dominating the geology. A similar structure of resistivity data has been found in the low-temperature areas on the western side of the volcanic zone. The influence of geological structure on hydrothermal systems is discussed by Tómasson, Fridleifsson, and Stefánsson (1975). However, in the middle of the area investigated (Grímsnes) a clear east-west structure in the resistivity data is found. This east-west resistivity structure is located on a line following the 64-degree latitude line. From seismic activity an east-west transform fault has been proposed in this area (Björnsson and Einarsson, 1974; Fig. 13). Further, the warm water occurring in this east-west region is very high in carbonate, and postglacial volcanic eruptions have occurred in the vicinity of the warm carbonate springs in hydrothermal system II. It seems conceivable that the warm springs in this area are mostly derived from

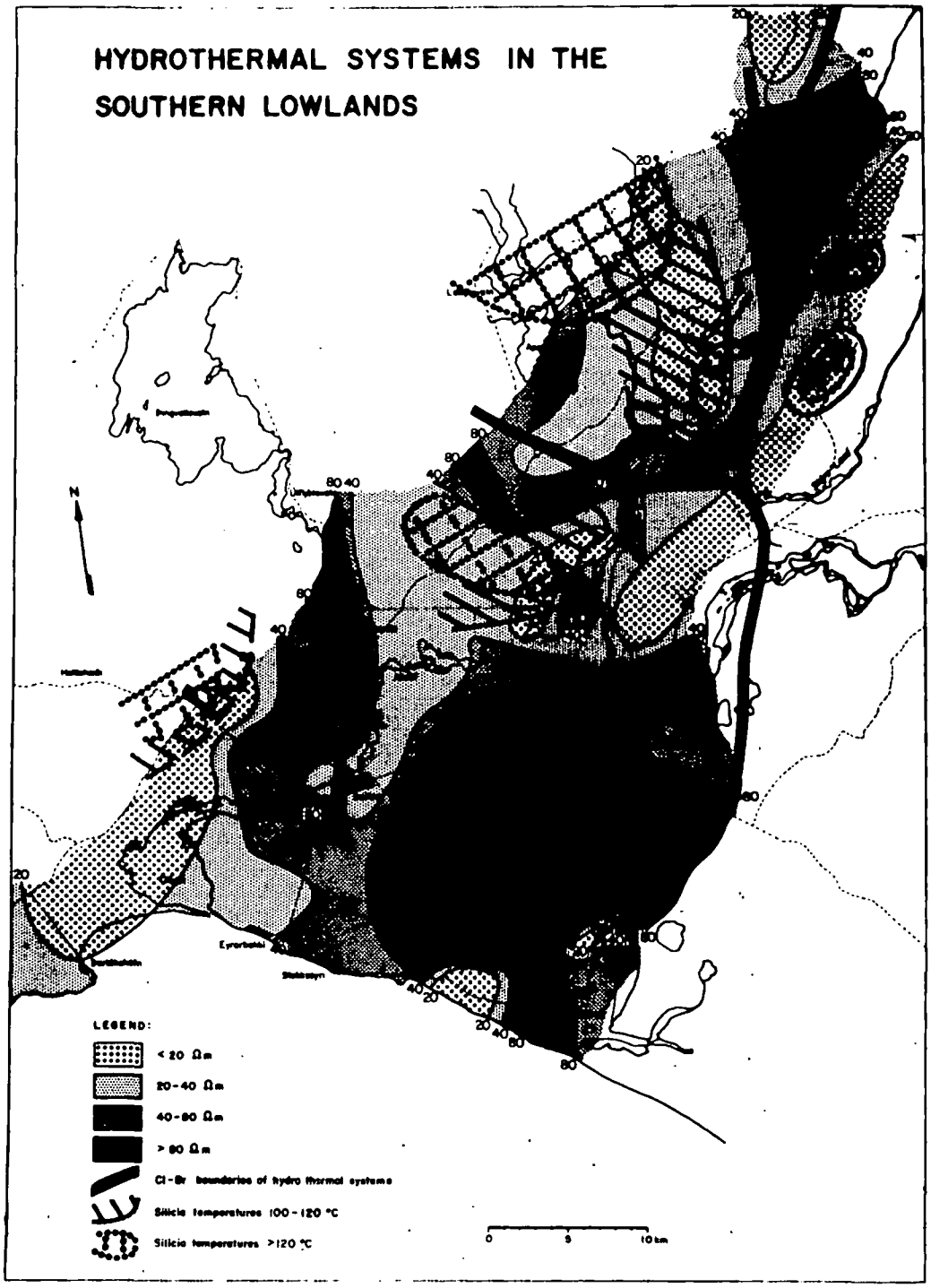

Figure 11. The true resistivity at 500 m depth and the hydrothermal systems as deduced from geochemical methods.

shallow-level instrusions and that the mentioned transform fault structure may aid transport of this juvenile carbonate towards the surface.

The results from the chemical and resistivity investigations are in agreement with the proposed east-west transform fault.

REFERENCES CITED

Arnórsson, S., 1970, Geochemical studies of thermal waters in the southern lowlands of Iceland: UN Symposium on the Development and Utilization of Geothermal Resources, Pisa, Proceedings (Geothermics, Spec. Iss. 2), v. 2, pt. 1, p. 547.

——, 1975, Application of the silica geothermometer in low-temperature hydrothermal areas in Iceland: Am. Jour. Sci.

Björnsson, S., and Einarsson, P., 1974, Seismicity of Iceland, *in* Kristjánsson, L., ed., Geodynamics of Iceland and the North Atlantic area: Dordrecht, Holland, D. Reidel, p. 225-239.

Fournier, R. O., and Truesdell, A. H., 1973, An empirical Na-K-Ca geothermometer for natural waters: Geochim. et Cosmochim. Acta, v. 37, p. 1255.

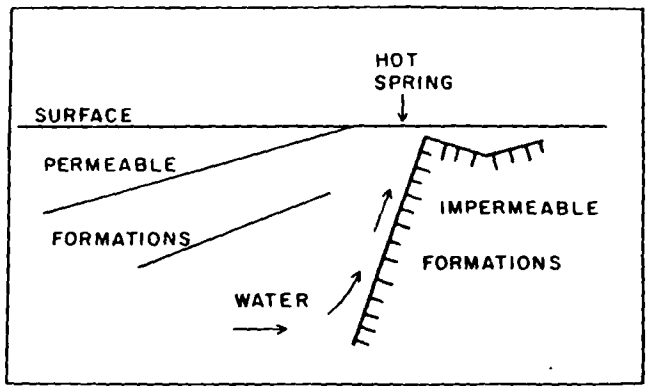

Figure 12. A schematic model for hot springs occurring at boundaries between massive and permeable formations.

Orellana, E., and Mooney, H. M., 1966, Master tables and curves for vertical electrical sounding over layered structures: Madrid, Interciencia, 150 p., 66 tables.

Pálmason, G., 1973, Kinematics and heat flow in a volcanic rift zone, with application to Iceland: Royal Astron. Soc. Geophys. Jour., v. 33, p. 451.

Tómasson, J., Fridleifsson, I. B., and Stefánsson, V., 1975, A hydrological model for the flow of thermal water in SW-Iceland, with a special reference to the Reykir and Reykjavík thermal areas: Second UN Symposium for the Development and Use of Geothermal Resources, San Francisco, Proceedings, Lawrence Berkeley Lab., Univ. of California.

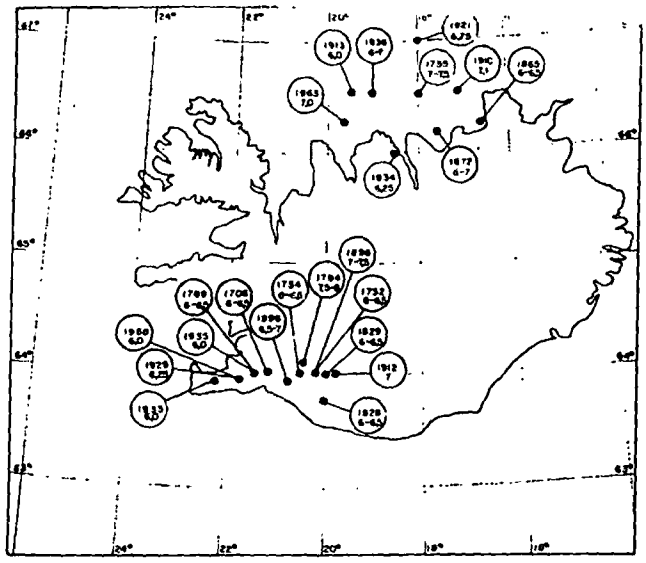

Figure 13. Estimated magnitudes and locations of major destructive earthquakes in Iceland since 1700. Epicenters are shown as black dots. Encircled numbers indicate the year of occurrence and estimated surface magnitude of the earthquake. From Björnsson and Einarsson (1974).

Van Dam, J. C., and Meulenkamp, J. J., 1969, Standard graphs for resistivity prospecting: The Hague, European Assoc. Expl. Geophys., 167 p.

Geothermal Resources Council, TRANSACTIONS Vol. 7, October 1983

COMPARISON OF INTERPRETED RESULTS OF RESISTIVITY SOUNDING CURVES WITH WELL DATA IN EL TATIO GEOTHERMAL FIELD, CHILE

Seibe ONODERA

Department of Mining, Faculty of Engineering
Kyushu University

ABSTRACT

Comparison of the interpreted result of a resistivity sounding curve with the data of a well drilled in the neighborhood of the resistivity station is treated as an important problem of geothermal exploration's aftercare. As a result, it becomes clear that temperature log in the well is correlated with the resistivity step distribution, which is plotted by using the solution of the iterative least-squares interpretation for the resistivity sounding curve.

Some of geoelectrical indications are discussed for the location of permeable levels, which correspond to geothermal reservoir, the variation point of temperature log, the correlation of formations with resistivity layers, and their interface depths from the surface.

INTRODUCTION

In development of geothermal resources a discovery well proves commercially an existence of geothermal fluids. Moreover, it gives important information on geologic sequences, its petrological properties and geothermal reservoirs. At present, geothermal well data include geologic section, alteration index, drillability log, caliper log, temperature log, pressure log, escaped portion and percolated rate of circulating mud water, water table, etc.

On the other hand, universal validity of direct and indirect geophysical indications obtained by the application of geophysical methods to geothermal exploration leads to a useful geothermal exploration method.

Based on the standpoint above, the author carried out the present investigation. The object of this paper is to find the correlation of geoelectrical indications with geothermal well data.

LOCATION OF GEOTHERMAL WELLS AND RESISTIVITY STATIONS

Figure 1 shows the map illustrating the location of geothermal wells and resistivity sounding stations in El Tatio geothermal field. Hot springs are situated in the hatched area. The result of temperature measurements at a depth of 2 m is given by the iso-temperature contour map.

For convenience of comparison, the data of #1, #9, #10, and #7 Wells and the results of interpretation of resistivity sounding curves observed near the site of each well were taken into consideration.

In this geothermal field, as a rule, resistivity sounding curves for the Schlumberger array were observed in the direction of NS and EW spreads of increasing electrode separations. This is a new and good idea in the field work of resistivity soundings to determine strikes and inclinations of formations.

REINTERPRETATION OF RESISTIVITY SOUNDING CURVES

Based on the assumption of multiple-layered model, the iterative least-squares interpretation of resistivity sounding curves were performed by using a current graphic display apparatus connected to the Geothermal Resistivity Interpretation System.

The results obtained are listed in Table 1. The first numeral for the notation of resistivity sounding curves, 1-EW, 9-NS, 10NS, 10EW, and 7-EW, denotes the resistivity sounding station and the next Roman letters show the direction of spreading the electrode system.

In general, this interpretation produces many solutions with preconditions of convergence. These solutions can be grouped by accuracy ranges denoted by κ and depend upon intial values. A best automatic fitting condition can be obtained when convergence factor is sufficient small for the accuracy requried. In the case of interpreting field curves it may be said that the iterate gives a good result, if κ is less than 10 per pent, although it depends upon smoothness of an observed curve.

As listed in the Table, we see that the assumption of a four layer model for the interpretation of the 9-NS curve gives more precise result than that of a five

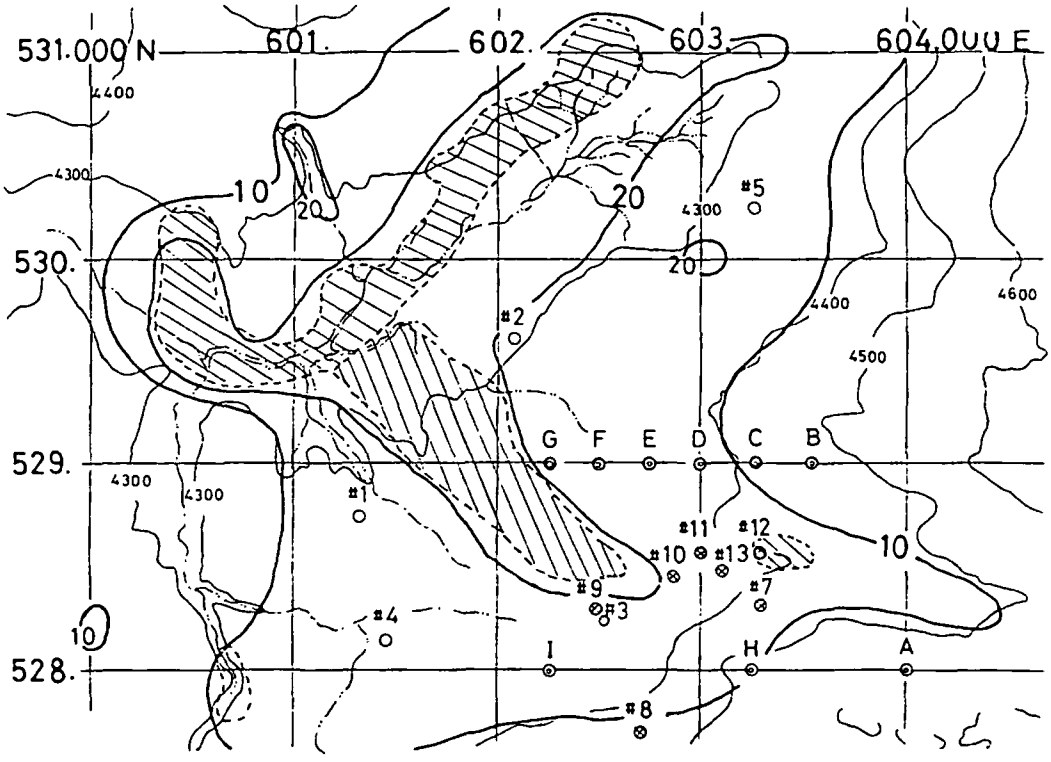

Fig. 1. Map showing the location of wells and resistivity sounding stations in El Tatio geothermal field

Table 1. Numerical values of the solutions obtained by the iterative least-squares interpretation of resistivity sounding curves observed at stations, 1-EW, 7-EW, 9-NS, 10NS, and 10EW

RS curves	ρ_1	ρ_2	ρ_3	ρ_4	ρ_5	h_1	h_2	h_3	h_4	κ	Curve types
1-EW	340.206	1309.455	108.411	.....	.....	6.406	220.707	.....	.....	0.09126	2(12)
1-EW	346.580	1379.465	76.064	.....	.....	6.323	243.151	.....	.....	0.06781	
7-EW	522.622	67.592	1.670	4.655	207.346	3.176	13.157	84.824	478.269	0.09685	13(2211)
7-EW	567.315	78917	1.773	5.097	824.181	2.886	12.176	185.410	541.282	0.13251	
9-NS	6.878	1.702	2.710	3.787	.....	10.473	29.163	443.800	.....	0.06170	5(211)
9-NS	6.893	1.740	2.721	3.823	.....	10.362	30.620	459.597	.....	0.06086	
9-NS	7.222	22.422	0.325	3.078	3.804	3.816	6.833	12.079	506.619	0.21298	5(1211)
10NS	55.060	12.309	0.908	4.876	.....	7.989	23.255	88.134	.....	0.07994	7(221)
10NS	55.381	13.522	0.863	4.814	.....	7.740	22.681	85.435	.....	0.08227	
10EW	122.755	28.416	0.942	4.345	.....	5.206	20.014	66.009	.....	0.06482	7(221)
10EW	137.586	36.205	1.105	4.382	.....	4.407	18.176	85.421	.....	0.05475	

κ denotes the root mean square of the relative errors of approximations in apparent resistivities (calculated) corresponding to the exact apparent resistivity values (given) for electrode separation available.

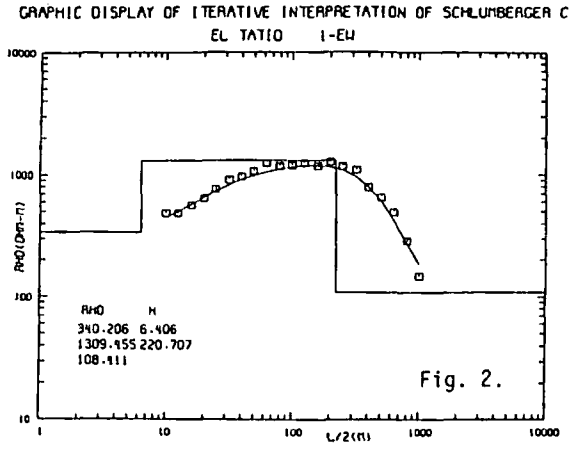

Fig. 2.

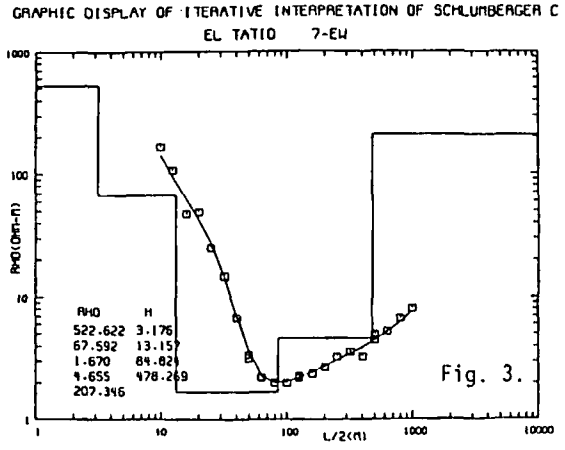

Fig. 3.

layer one.

Some examples of graphic display are shown in Figures 2, 3, and 4. In these

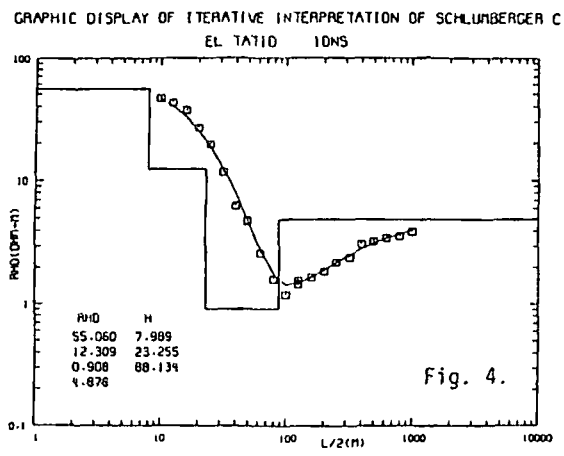

Fig. 4.

Figures, the values of apparent resistivities are plotted as ordinates, and the lengths of half electrode separations of the Schlumberger array as abscissas. Regular square marks represent observed apparent resistivities corresponding to the selected electrode spacings, and the solid curve in each Figure shows the theoretical resistivity sounding curve gained by the automatic curve fitting.

The solution of the iterative least-squares interpretation of resistivity sounding curves is given by the resistivity step distribution, of which numerical values of apparent resistivities in ohm-m for the successive layers and of depths in m of interfaces for the assumed multiple-layered earth are plotted below Labels,RHO and H, respectively, on the left hand lower corner of each Figure.

The resistivity sounding curve of 1-EW observed near #1 Well shows essentially the type 2(12) of a 3-layer case, the 7-EW curve represent the type 13(2211) of a 5-layer case, the 9-NS curve expresses the type 5(211) of a 4-layer case,and the 10NS and 10EW illustrate the type 7(221) of a 4-layer case.

If except for the curve type of 7-EW resistivity sounding curve, the residual curve types of three fall under the category in the classification of the Schlumberger resistivity sounding curves in geothermal fields (Onodera, 1982).

The Well #7, which was drilled into the geoelectrical structure determined by resistivity exploration, produced a useful mixture of steam and hot water. Consequently, the curve type of 13(2211) of the 7-EW resistivity sounding curve should also be included in the statistical table showing the number of production wells per curve type (Onodera, 1982).

EXISTING DATA FOR WELLS

According to A.LAHSEN and P.TRUJILLO (1975), Some of Wells proved the presence of three permeable levels, namely, the first level, formed by volcanic sands and gravels so that its permeabilty is high,is located in the Tucle dacites formation at a depth ranging from 150 m to 245 m; the second one, on the whole low permeability, in the Puripical ignimbrite from 480 m to 600 m; and the third zone in the base of the Rio Salado volcanic group from 745 m to 1580 m. These are listed in Table 2.

Table 2. Permeable levels proved by Wells

Wells	Permeable levels	Depth ranges	Degree of permeabi.	Temperature	Formations
7	1st	170-245m	high	160°C	Tucle
	2nd	480-530	----	228	Puripicar
	3rd	745-890	high	260	Penaliri
9	1st	141-180	high	160	Tucle
	2nd	550-600	low	224	Puripicar
	3rd	1150-1580	low	200	Penaliri
10	1st	150-190	high	160	Tucle
	2nd	550-600	low	230	Puripicar
	3rd	700-800	----	235	Penaliri

Further, geologic sections are prepared for #7, #9, and #10 Wells, and their temperature logs are also measured. These will be used for the matter of comparison described later.

COMPARISON OF INTERPRETED RESULTS OF RESISTIVITY SOUNDING CURVES WITH WELL DATA

It needs to research this interesting problem, in order to extract geoelectrical indications of reservoir from resistivity data and to find the real worth of resistivity exploration for geothermal fields.

Comparison of Solution for 7-EW Resistivity Sounding Curve with Data of #7 Well

Plotting the comprehensive figure by use of observed apparent resistivities for the selected half electrode spacings, its solution represented by the resistivity step distribution, of which numerical values are listed in the second major line of Table 1 and is shown in Figure 2, the temperature log for #7 Well, and the geologic section for the well, together with information of permeable levels for the well listed in Table 2, then we have Figure 5.

As seen from the Figure, the comparison between the resistivity step distribution and the geologic section is relatively difficult.

After careful examination, it is demonstrated that the resistivity step distribution is correlated significantly with the temperature log. That is to say, the fourth resistivity layer with 4.655 (or 5.097) ohm-m in resistivity corresponds to the part showing 160 °C of the temperature log and the depth of the fourth interface of 478.269 (or 541.282) m indicates both

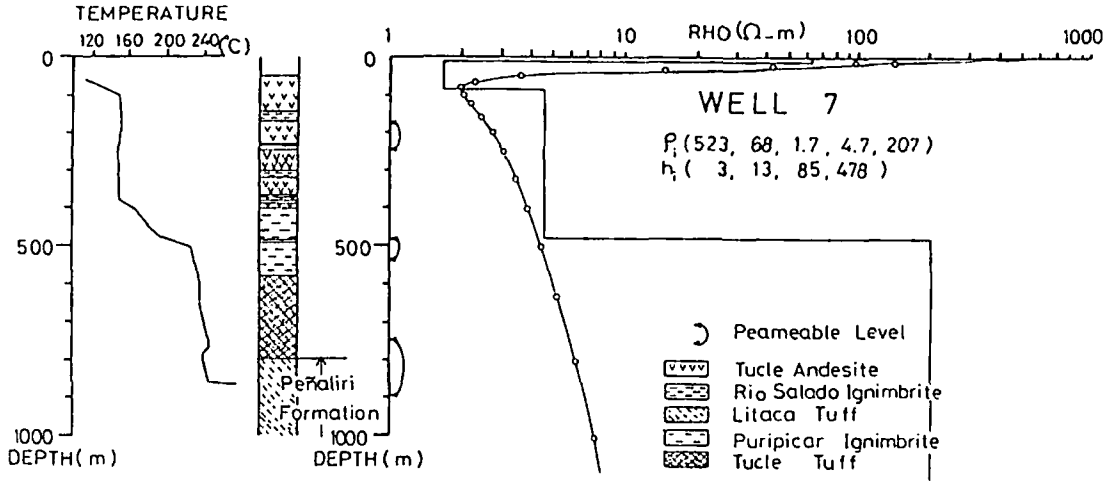

Fig. 5. Comparison of the interpreted result of the 7-EW resistivity sounding curve with the data of Well #7

a variation point from 160 °C to 240 °C of the temperature log and the upper depth of the second level in the Puripicar ignimbrite. In addition, the depth of the third interface of 84.824 m is roughly equal to the first variation point of the temperature log.

Unfortunately, the result of interpretation of the resistivity sounding curve does not reveal the presence of the first and third permeable levels. According to such resolving power of resistivity sounding curve, it is known naturally that either the scale of the second permeable level is larger than that of the first and third ones or it has no resistivity contrast between upper and lower formations.

Correlation of Interpreted Result of 9-NS Resistivity Sounding Curve with Data of #9 Well

Similar to the example above, we can see from Figure 6 that the result of interpretation of the 9-NS resistivity sounding curve is correlated with the temperature log for Well #9. That is, the third interface between the third and fourth resistivity layers indicates the maximum variation point of the temperature log. Especially, it should be remarked that the depth of the third interface of 443.800 m (or 400.000 m) coincides with the upper depth of Puripicar ignimbrite formation.

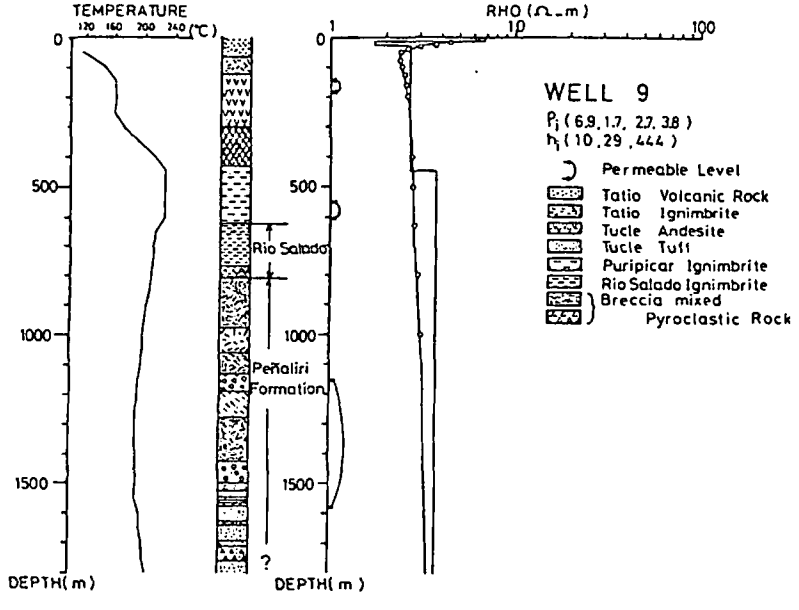

Fig. 6. Correlation of the interpreted result of the 9-NS resistivity sounding curve with the data of Well #9

Correlation of Result Obtained by Interpretation of Resistivity Sounding Curve with Data of #10 Well

Figure 7 shows the example of the resistivity step distribution correlated with the geologic section and the temperature log.

In this case, the depth of the third interface of 88.134 m corresponds to the depth of Tucle andesite, and also indicates the variation point of the temperature log.

A significant reason is that there is no effective resistivity contrast in the successive geological formation below the Tucle andesite, since the observed resistivity sounding curve is very smooth. Note that resistivity exploration can not be applied to an area giving such a

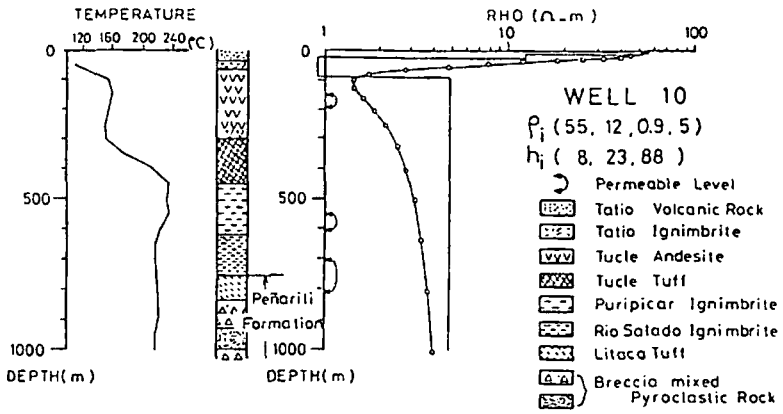

Fig. 7. Correlation of the result obtained by the interpretation of the resistivity sounding curve with the data of Well #10

geoelectrical condition.

COMPARISON OF RESISTIVITY SECTION WITH GEOLOGIC SECTION AND TEMPERATURE PROFILE

Comprising the section of resistivity layers, determined by adequate solutions for the interpretation of resistivity sounding curves, 1-EW, 9-NS, and 7-EW, in the geologic section along Wells, #1, #9, and #7, then we have Figure 8.

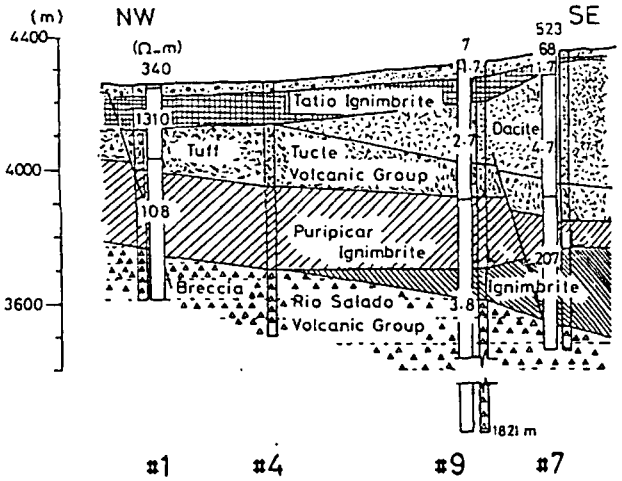

Fig. 8. Correlation of resistivity layers with geologic section and the distribution of permeable levels

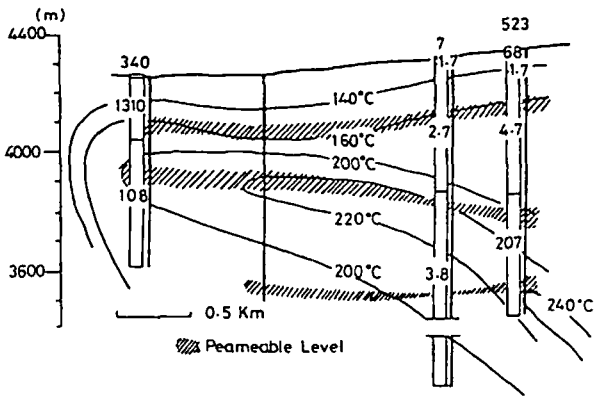

Fig. 9. Correlation of resistivity layers with temperature profiles and the distribution of permeable levels

As a result of comparative studies, it is concluded that the combination of Tatio ignimbrite and tuff formation is indicated by the second resistivity layer of 1309.455 ohm-m; the successive formation (Puripicar ignimbrite and breccia) is given by the third resistivity layer of 108.411 ohm-m; and the depth (260 m from the surface) of the boundary between tuff and breccia formations is roughly equal to the depth of the third interface of 220.70 7 m.

In the last case resistivity measurements in depth determination estimates an error of -15 per cent, approximately. And the resistivity sounding curve has no resolving power of indicating the boundary depth of Tatio ignimbrite and Tucle tuff formation and also that of Puripicar ignimbrite and breccia formation.

In the correlation between geologic section near #9 Well and the interpreted result of resistivity sounding curve at station, 9-NS, only the boundary depth of Tucle volcanic group and Puripicar ignimbrite is given by the third depth of interface of 443.800 m with close accuracy.

Figure 9 shows the correlation of resistivity layers with temperature profile and the distribution of three permeable levels. Appart from the second resistivity layer of 1309.455 ohm-m in the solution of the 1-EW resistivity sounding curve and the fourth resistivity layer of 3.787 ohm-m in that of the 9-NS one, we can find that the deepest interface of resistivity layers for each solution indicates roughly the upper depth of the second permeable level, simultaneously coincides roughly with the upper contour of 200 ^{o}C of the temperature profile along the traverse of wells, #1, #9, and #7.

It follows from the fact illustrated above that the basic data to be correlated with the result of interpreting resistivity sounding curves lies significantly in the temperature distribution of the well, which is related to the temperature distribution of underground.

In other words, it is not too much to say that the function of resistivity exploration is dependent upon resistivity contrast controlled by temperature.

CONCLUDING REMARKS

For the sake of comparison between the interpreted result and the well data available, firstly, the author presented appropriate solutions to the observed resistivity sounding curves by making use of the iterative least-squares interpretation. Here, one of principal materials in the present investigation was obatined for the practical grounds of correlation.

Summarizing the results of the research, it was concluded that the solutions of the iterative interpretation for given resistivity sounding curves were correlated with the temperature log in each well drilled in the neighborhood of the resistivity sounding stations, although there is not enough of the necessary basic data.

Resistivity measurements gave the resistivity values of the formations such that 1 ohm-m order for the Tatio ignimbrite, 5 ohm-m order for the Tucle andesite and 100-200 ohm-m order for the Puripicar ignimbrite.

Unfortunately, it was impossible to determine resistivity values of the Penaliri formation, in which the third permeable level exists.

Geoelectrical indications for detecting the first level located in the Tucle formation was given by the segment, gradually increasing state of apparent resistivity curve, past a position of showing the minimum indication of the Schlumberger resistivity sounding curves as shown in Figures 5, 6, and 7.

The schlumberger resistivity sounding curves, which indicated the existence of the second permeable level in the Puripicar formation, were measured at stations, 7-EW and 9-NS.

With the results of interpretation of these curves, similar correlation with the temperature logs for #7 and #9 Wells was observed. In fact, both resistivity and depth of the formations were fairly determined, and the deepest depth of the solutions indicated the variation point of temperature logs.

These practical examples of comparison will be useful as a basis of resistivity soundings in geothermal fields. These are the merit of resistivity soundings, but the method has its demerit that no information for detecting geothermal resources is obtained, as far as resolving power is concerned.

ACKNOWLEDGEMENTS

To carry out this study, the author received many useful data from participants of 10, Renato Tomas FERNANDEZ(1970), Raul Israel JERALDO (1971), Patricio TRUJILLO (1974), Raul Alfonso BRAVO (1975), Ljubomir Milivoj TOMASEVIC MUNOZ (1976), Gerd REINKE (1977), Hernan Nobuyuki FUJII (1977), Claudo CADIZ CHAVARRIA (1978), M. Ruperto BERRIOS (1979), and Ricardo SANDOVAL SALAS (1980), who came from Chile to attend the International Group Training Course in Geothermal Energy.

While, to carry out resistivity data processing, the current graphic display apparatus connected to the Automatic Resistivity Interpretation System was installed by the GRANT-IN-AID for Scientific Research in 1980.

Here, I would like to extend my sincere thanks to the participants and to the Organization for their academic friendship and for the financial support, respectively.

REFERENCES

ELC-Electroconsult (1975), APROVECHAMIENTO DEL CAMPO GEOTERMICO DE EL TATIO EN EL NORTE DE CHILE

LAHSEN,A. and P.TRUJILLO (1975), The Geothermal Field of El Tatio, Chile, PROCEEDINGS, Second United Nations Symposium on the Develpment and Use of Geothermal Resources, vol. 1, 170-177.

ONODERA,S.(1982), Classification of Schlumberger Resistivity Sounding Curves in Geothermal Field,Geothermal Resources Council, Transactions, vol.6, 145-148.

PATRICIO TRUJILLO R.,RAUL BRAVO E., HERNAN CUSICANQUI R., RAUL JERALDO V. Y CARLOS MUNOZ J. (1974), CAMPO GEOTERMICO EL TATIO, CORFO, COMITE PARA EL APROVECHAMIENTO DE LA ENERGIA GEOTERMICA, AREA TECNICA

Raul GERALDO, Raul BRAVO Y Carlos MUNOZ (1974), INFORME POZOS Nº 7, 10 y 11, COMITE PARA EL APROVECHAMIENTO DE LA ENERGIA GEOTERMICA-CORFO.

Geothermal Resources Council, TRANSACTIONS Vol. 7, October 1983

Electrical

SELF-POTENTIAL SURVEY RESULTS MAKUSHIN VOLCANO GEOTHERMAL AREA, UNALASKA ISLAND, ALASKA

Robert F. Corwin
Harding Lawson Associates
P. O. Box 578
Novato, California 94948

and

David V. Fitterman
U.S. Geological Survey
M.S. 964, Box 25046, Federal Center
Denver, Colorado 80225

ABSTRACT

A self-potential survey covering about 78 line-km was conducted in the Makushin Volcano area of Unalaska Island, in the Aleutian island chain. Two major anomalies were seen; one of -600 mV maximum negative amplitude covering about 15 km^2, and the second of -500 mV maximum negative amplitude covering about 7 km^2. The anomalies do not appear to be caused by artificial sources, variations in soil properties, conductive mineral deposits, or topographic effects.

A preliminary analysis of geothermal source mechanisms indicated that the depth to the source lies between about 0.30 and 0.50 km for both anomalies, which corresponds to the depth to high temperature gradient measured beneath one of the anomalies. These self-potential source regions may correspond to areas where anomalously high flows of heat and/or fluid intersect geological boundaries.

INTRODUCTION

This paper describes the results of a self-potential survey conducted in the area of Makushin Volcano, on the Aleutian island of Unalaska, Alaska. The purpose of the survey, which was performed in April and May of 1982, was to locate and delineate possible geothermal resources. The paper presents a description of the survey area, the field conditions, and the equipment and field procedure used for the self-potential survey; followed by a description of the survey results and an interpretation of these results in terms of both nongeothermal and geothermal sources.

SURVEY DESCRIPTION AND FIELD PROCEDURE

Figure 1 shows the locations of the self-potential survey lines superimposed on a topographic map of the survey area. The survey covered approximately 78 line-kilometers. The terrain in the survey area is extremely rugged, and no roads exist in the area. Much of the survey area was covered by deep snow and/or frozen soil.

Self-potential readings were made using the "fixed-base" survey procedure (Corwin and Hoover, 1975). Contact with the soil was made using nonpolarizing copper-copper sulfate electrodes (Tinker & Rasor Model 6B), and voltages and contact resistances were read on a Fluke Model 8020A digital multimeter with an input impedance of 10 megohms. Comparison with readings from a very high-impedance meter (Geonics Model SP-19; 500 megohms) indicated that source contact resistances of up to 2 or 3 megohms did not significantly affect the accuracy of the readings on the Fluke meter. Nominal station spacing was 200 meters, with closer spacing in some areas where detail was desired, and wider spacing in areas where no soil was present or where hazardous terrain or snow conditions precluded stopping for a measurement. Point A (Figure 1), at the mouth of Makushin Valley, was assumed to be at zero potential, and all values are referenced and tied to this point.

Because potentials caused by time-varying telluric currents can affect self-potential readings, telluric voltages were continuously monitored on a strip chart recorder connected across a stationary electrode dipole pair located about 1 km south of point D (Figure 1). Maximum telluric variations on this monitor for a day of high telluric activity were about ±12 mV/km, with a period of about 30 seconds. When this type of telluric activity was present during a self-potential measurement, it was compensated by reading for several minutes and averaging several successive peak values. No significant longer-period telluric variations were seen.

SURVEY RESULTS

The self-potential survey results are summarized in the form of a contour map on Figure 1. Figure 2 shows a field data profile along a line through the major anomalous area. Along with the measured self-potential values, Figure 2 also shows self-potential values smoothed by use of a 5-point unweighted running mean and a topographic profile. Linear distances along the survey line are given in kilometers, and elevations in feet because these are the units used on the base map (Figure 1). The topography on Figure 2 is plotted upside down in order to make

it easier to notice possible correlations between self-potential and elevation, as discussed later. The self-potential contours shown on Figure 1 are taken from the smoothed curves, in order to reduce unnecessary contour detail and the effects of near-surface sources.

Well-established background levels similar to those just to the west of point I and just to the east of point C (see Figures 1 and 2) are seen over most of the survey area. Such areas are characterized by flat or very slowly rising or falling trend lines, by point-to-point variations that rarely exceed about ±50 mV, and by absolute self-potential levels between ±100 mV (one contour interval on Figure 1). Two anomalous areas stand out clearly from this background: the Sugarloaf negative anomaly of about -600 mV amplitude, centered about 1 kilometer northeast of Sugarloaf Cone; and the Fox Canyon negative anomaly of about -500 mV amplitude, centered about 3 kilometers southwest of Sugarloaf Cone.

Both of these anomalies are traversed by a sufficient number of survey lines so that their true shapes and amplitudes are reasonably well defined. Cumulative tie-in errors around all closed loops were well under 100 mV, so the measured self-potential value at any given field data point should be reproducible within one contour interval. Although the smoothing process produces slight distortions in the shapes of the anomalies, these distortions should not significantly affect the geologic interpretations of the anomalies discussed below.

INTERPRETATION

Non-geothermal Sources

There are many possible sources of self-potential variations that are not related to geothermal activity. These include artificial sources, soil property variations, conductive mineral deposits, streaming potentials generated by the flow of nongeothermal ground water, and

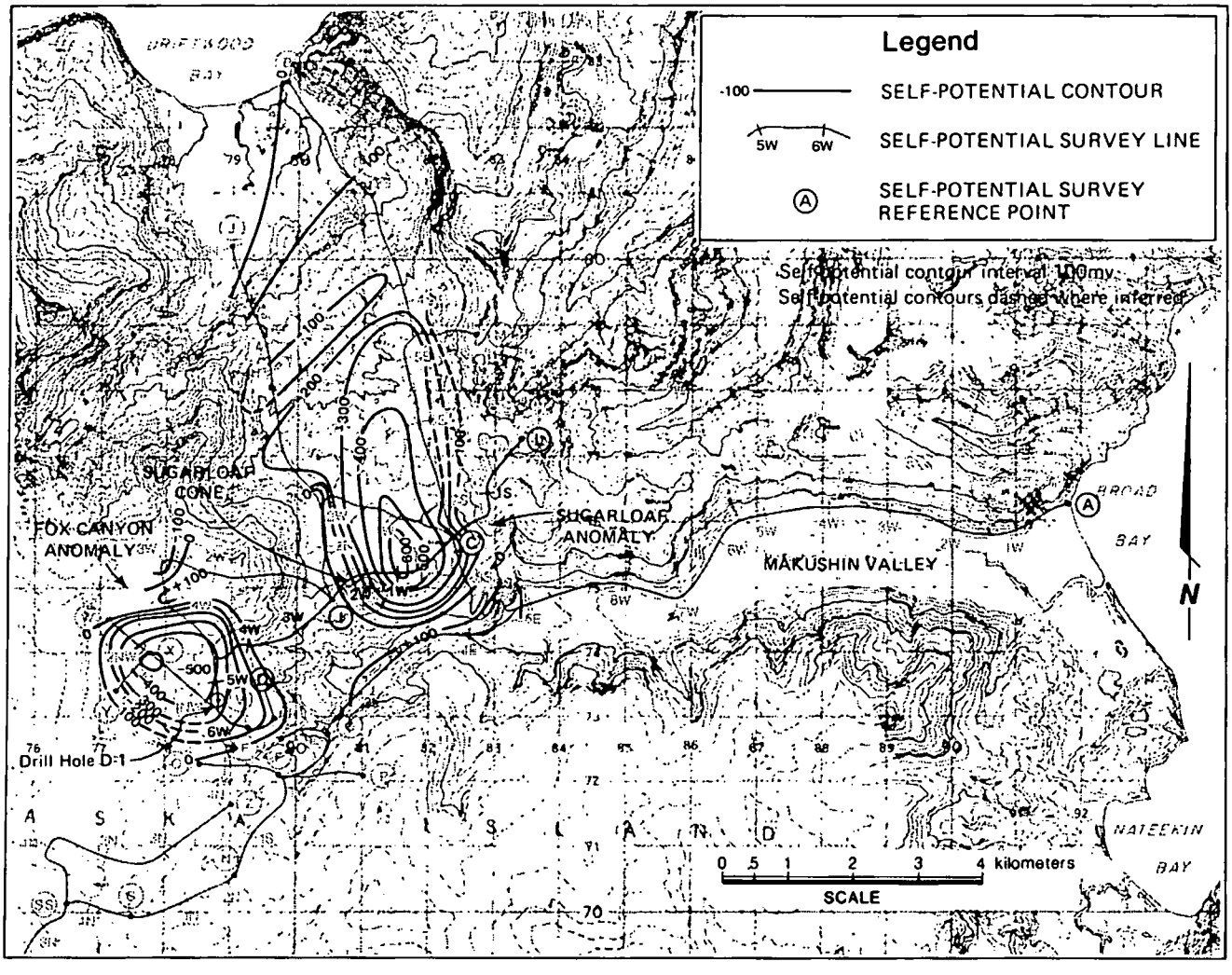

Figure 1. Self-Potential Survey Lines and Contours

topographic effects. Before assigning a geothermal origin to the Sugarloaf and Fox Canyon anomalies, the possibility that one or more of these other sources may be responsible for, or contribute to, the observed anomalies is evaluated below.

Artificial sources such as buried pipelines, well casings, cathodic protection systems, electrical machinery grounds, etc. can develop large electric potential fields in the earth. As this survey area is totally undeveloped, and as virtually no evidence of human activity was seen in the area of the anomalies, it is safe to conclude that artificial sources did not contribute to the observed anomalies.

Variations in soil properties such as moisture content, pore fluid chemistry, and soil type are known to affect self-potential readings. Soil properties in the survey area ranged from unfrozen, fully water-saturated tundra muskeg bog in the lower valleys to deep snow or frozen and/or extremely rocky soil at higher elevations. Snow cover was present over much of the survey area, but in most cases it proved possible to dig through the snow to soil beneath. Previous experience, and several measurements made in this survey area, indicate that readings made in snow cover are not significantly different than those made in the soil beneath the snow, providing that the voltmeter used has sufficiently high input impedance.

Laboratory experiments have shown that the maximum effect of soil property variations on a given self-potential reading is limited to a few tens of mV; far less than the amplitudes of the observed anomalies in this area. Additionally, field experiments have shown that self-potential readings do not change significantly between thawed and frozen soil conditions. Therefore, the lack of correlation between self-potential and soil property variations typical for the entire survey area makes it unlikely that soil property variations contribute significantly to the observed large anomalies, although they probably are responsible for much of the point-to-point "geologic noise" seen in the data profiles.

Both massive and disseminated deposits of electronically conductive minerals, including pyrite, chalcopyrite, graphite, and a number of others, are known to generate self-potential anomalies. These anomalies are almost always negative in polarity, centered over the deposit, and range in amplitude from a few tens of mV to more than 1 volt. The wavelength and shape of the anomaly depend on the size, geometry, and depth of burial of the deposit (Sato and Mooney, 1960).

The amplitude, shape, polarity, and wavelength of the Sugarloaf and Fox Canyon anomalies are similar to those seen over large disseminated deposits of graphite or sulfides. As such deposits often are related to volcanic activity

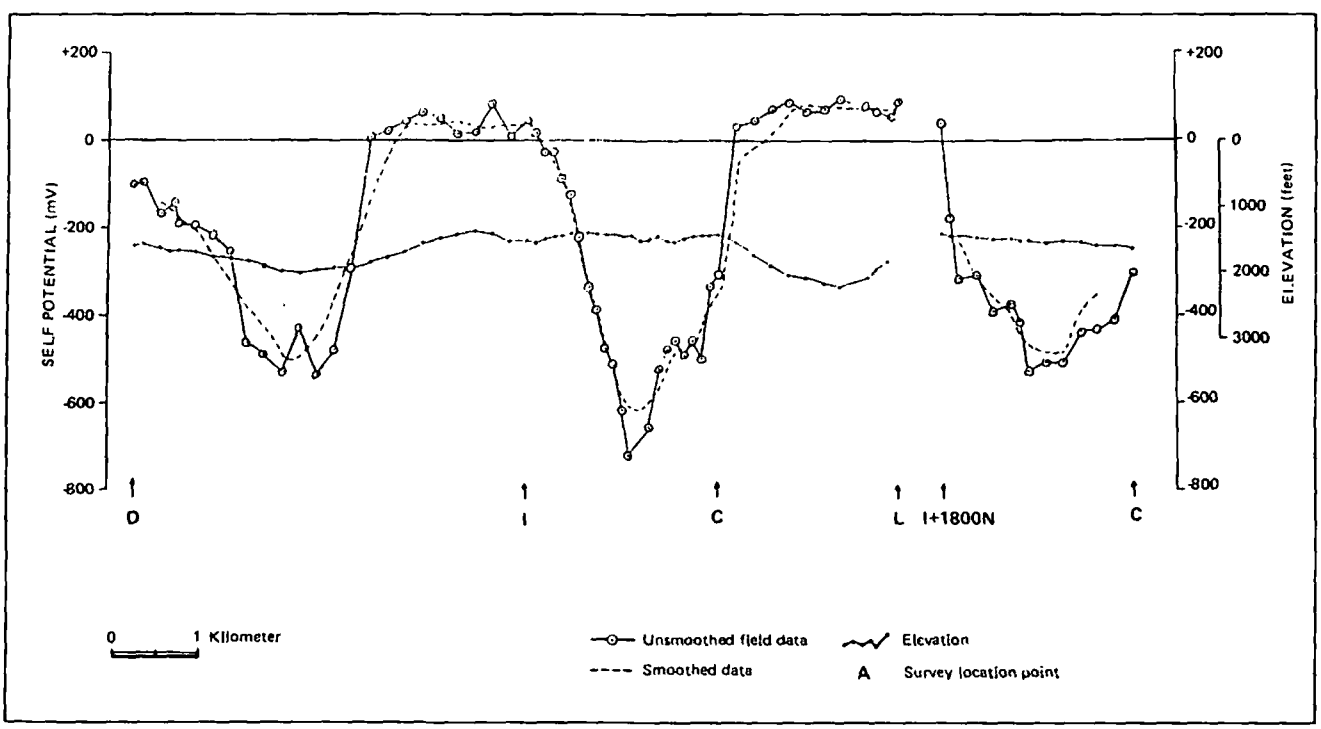

Figure 2. Self-Potential Data and Elevation: Line D-I-C-L

of the type seen in the Makushin area, and as mineral deposits have been discovered elsewhere on the island, consideration must be given to the possibility that all or part of the negative anomalies may be related to conductive sulfide mineral deposits (graphite deposits probably would not be found in this geologic setting).

Drill Hole D-1 (Figure 1), located close to the -400 mV contour of the Fox Canyon anomaly, was completed to a depth of 1440 feet in July 1982. A very minor amount of pyrite (probably less than 1 percent) was seen between 785 and 805 feet beneath the surface, and about 5 percent pyrite was seen from about 1220 feet down to the bottom of the hole at 1440 feet. As it is very doubtful that this amount and distribution of pyrite could generate an anomaly as large and extensive as that seen in Fox Canyon (Sato and Mooney, 1960), a conductive mineral source for either of the anomalies seems unlikely.

Topographic effects are known to occasionally produce very large self-potential anomalies, especially in volcanic areas (examples include the East Rift zone of the island of Hawaii and Adagdak volcano on the Aleutian island of Adak [Corwin and Hoover, 1975]). These anomalies presumably are generated by streaming potentials (discussed later) caused by the downhill flow of near-surface water, and usually become more negative with increasing elevation (the so-called "negative summit" phenomenon).

Examination of the profiles on Figure 2 indicates that the two major negative anomalies do not appear to show any significant topographic correlation. Conversely, some of the lines with the greatest topographic relief show little or no self-potential activity. However, the Sugarloaf negative anomaly is roughly confined to what appears to be a valley-filling lava flow surrounding Sugarloaf Cone. The eastern and western margins of this anomaly closely parallel the steep upslopes that bound the valley, while the southern margin of the anomaly roughly parallels a steep downward slope where the Sugarloaf Cone plateau drops off into Makushin Valley. Similarly, the northwestern and southeastern margins of the Fox Canyon anomaly are roughly parallel to steep upward slopes. Therefore, there may be some indirect contribution of topography to the two major anomalies.

Geothermal Sources

The remaining possible cause of the observed self-potential anomalies is geothermal activity. The preliminary temperature readings in Drill Hole D-1 (Figure 1) show a very high temperature gradient beginning at 1000 feet depth, indicating that a significant geothermal source may exist beneath the Fox Canyon anomaly.

In this discussion we will make qualitative use of a quantitative self-potential modeling approach described by Sill (1983) and Fitterman (1979, 1983). Very briefly summarizing this approach, geothermal systems are characterized by temperature, fluid flow, and geochemical conditions that contrast with those of the surrounding environment. These contrasts can generate subsurface electric current flows which in turn can generate surface self-potential anomalies. The mechanisms by which temperature, pressure, or geochemical gradients generate electric current flows are respectively called thermoelectric, electrokinetic, and electrochemical coupling. Voltages generated by pressure gradients driving a fluid flow through a porous medium also are commonly called streaming potentials. The physical bases for these coupling phenomena are given in advanced texts on physical chemistry and electrochemistry such as MacInnes (1961). Because surface anomalies generated by electrochemical coupling are thought to be small (a few tens of mV at most), the following discussion will be limited to thermoelectric and electrokinetic coupling.

The source geometry of a self-potential anomaly may be approximated by a continuous subsurface charge distribution, by a distribution of point current sources and sinks, or by some combination of these. Quantitatively relating the polarity and amplitude of these charges or current sources to the magnitude and direction of the heat or fluid flows causing them is difficult, because coupling coefficients for in-situ geothermal conditions are not available. Finally, the surface anomaly patterns may be distorted by changes in topography, permeability, or resistivity that are not related to the geothermal source.

Considering these complexities and uncertainties, and the lack of detailed geological and geophysical data in the area, the most realistic interpretation of the Unalaska self-potential data would consist of the simplest source model geometry that could produce the observed anomalies and not be inconsistent with the known geology. In the analysis below, we discuss three such models for the observed anomalies.

Conductive Dike Model. Before beginning a separate analysis of each of the anomalies, we must determine whether the Fox Canyon and Sugarloaf anomalies may be interrelated; i.e., are parts of a single large anomaly. An anomaly pattern similar to the observed pattern could be generated by a source geometry like that shown in Figure 3, consisting of a pair of vertical or nearly vertical planes of dipolar charge (Fitterman, 1983). The "conductive dike" region between the planes is more conductive (less resistive) than the areas outside the planes (i.e., ρ_2 is less than ρ_1 or ρ_3). The plane running just to the east of Fumarole #8

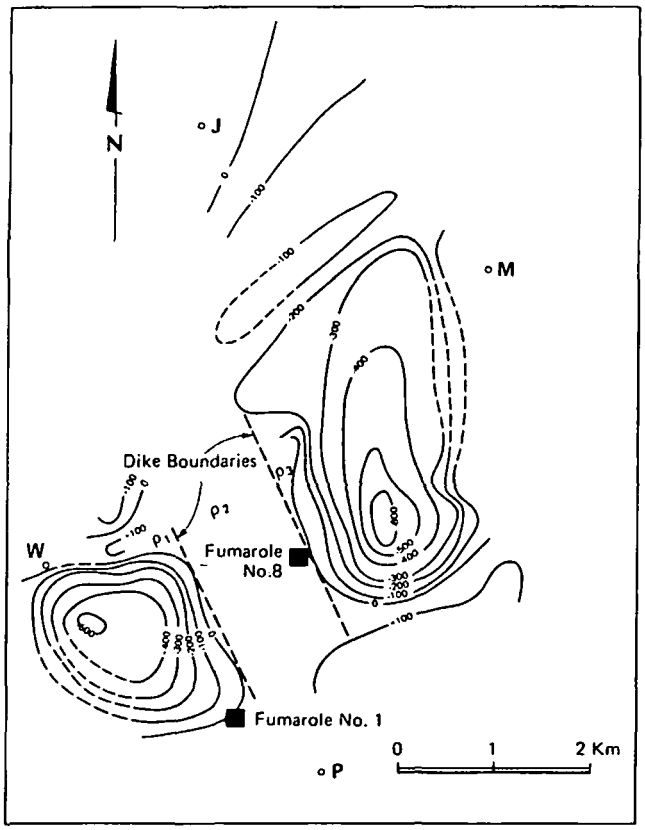

Figure 3. Observed Self-Potential Anomalies and Location of Conductive Dike Model

would be polarized with the positive side facing southwest, while the plane just to the east of Fumarole #1 would have its positive side facing northeast. Geologically, this geometry would correspond to a pair of faults or fractures coincident with the polarized planes. (For simplicity, we will refer to faults and/or fractures simply as faults.) The dipolar charge distribution would be produced by heat and/or fluid flow along the faults, which could be acting as conduits for geothermal fluid flow. Geothermal fluid inundating the central area between the faults could account for the low resistivity of this area.

An analysis of this situation indicated that it is possible to obtain a reasonable match between the measured field data and the calculated anomaly for several different conductive dike models, but all the final models required the resistivity contrasts between the central and outlying areas to be 1000:1 and the potentials along the source planes to be greater than 6000 mV. As both of these are unreasonably large, it seems unlikely that this type of model represents the actual geology.

Point and Line Source Models. In this and the following section, we will consider the Fox Canyon and Sugarloaf anomalies as having separate sources, and will define some simple source geometries that could generate self-potential patterns similar to the observed anomalies.

The simplest source geometry for a roughly circular anomaly pattern in a homogeneous earth is a single infinitesimally small (point) source of electric current. The anomaly pattern generated by such a current source is circular in form, and the deeper the source of a given anomaly is located, the broader the wavelength of the anomaly must be. A related principle is that a source region of finite size may be buried at a shallower depth than a point source producing an anomaly of given wavelength, but cannot be deeper. Thus this principle can be used to establish a rough maximum depth to the source region of a given self-potential anomaly.

From Figure 1, it is evident that the Fox Canyon anomaly is very roughly circular in form, so a point source analysis of the type described above could be used to estimate an approximate maximum depth to the source of this anomaly. For the central portion of the anomaly, a point source centered just to the east of the -500 mV contour and located at a depth of about 0.4 km (1300 ft) gives a fair approximation to the field data. This implies that the depth to the source of the Fox Canyon anomaly is no greater than about 1300 feet.

Results from Drill Hole D-1 (Figure 1) indicate that the temperature gradient increases abruptly from zero to a relatively constant value of about 35°F/100 ft at a depth of about 1000 ft (0.31 km), and that this gradient continues at least to the bottom of the drill hole at about 1425 ft (0.43 km). Thus the self-potential source region may be located close to or somewhat below the 1000-foot depth, where a large vertical heat flow component intersects a geologic boundary; or where vertical fractures may be introducing heat and/or fluid into a host formation.

The simplest source geometry for an elongated anomaly such as the one seen at Sugarloaf is an infinitesimally thin line source of current (essentially, a linear extension of the point source described above). As for the point source, a line source giving a reasonable fit to the observed data can be used to obtain an estimate of the maximum depth to the actual source.

The location of a line source giving a reasonable fit to the Sugarloaf anomaly is shown on Figure 4. The line plunges 10° to the north, with the northernmost end at a depth of 0.49 km (1600 ft) and the southernmost end at 0.21 km (690 ft), giving a fair estimate of the maximum

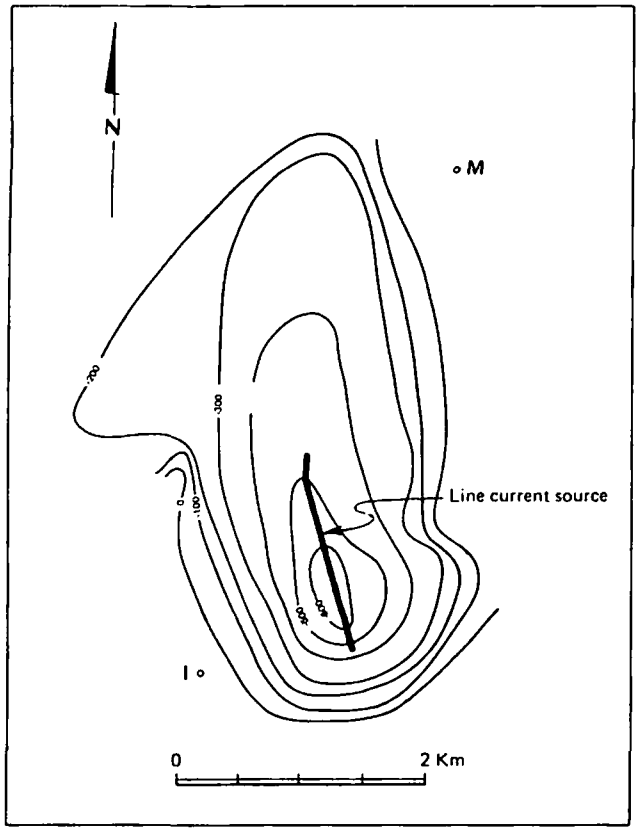

Figure 4. Observed Sugarloaf Self-Potential Anomaly and Location of Line Current Source

depth to the source region. The average depth of about 0.35 km (1150 ft) to the line source is comparable to that for the Fox Canyon anomaly, and suggests that the geology and temperature profile in the Sugarloaf area may be comparable to those in the Fox Canyon area. Geologically, the line source would represent the top of a fault serving as a conduit for geothermal fluids.

Dipolar Plane Models. A more quantitative estimate of source geometry and depth may be made by approximating the self-potential source region by a two-dimensional dipolar plane instead of a point or line source (Fitterman, 1979). A preliminary analysis of the Fox Canyon and Sugarloaf anomalies indicates that the depth to the center of a source plane for the Fox Canyon anomaly is about 0.47 km (1500 ft). The plane, which is polarized with the negative side up, measures about 1.6 km (5250 ft) in the east-west direction and about 2.0 km (6560 ft) north-south, and dips about 11° to the west. A source plane for the Sugarloaf anomaly is buried at a depth of about 0.29 km (940 ft) and is flat-lying. It measures about 1.25 km (4100 ft) east-west and 2.0 km (6560 ft) north-south. This plane also is polarized with the negative side up. It should be noted that the depths given for these planes are estimates of the actual values, rather than the maximum values obtained from the point and line source analyses.

While this preliminary dipolar plane model does not necessarily give the best possible fit to the observed data, it does provide a useful first estimate of source region depths and configurations. The dipolar potential on the two source planes could be generated by a component of heat and/or fluid flow crossing or parallel to a geological boundary; or by some combination of parallel and transverse flow.

Comparing these results with those obtained from the point and line source analyses, the average dipolar plane source depth of 0.47 km for the Fox Canyon anomaly is somewhat greater than the 0.40 km maximum depth estimated for the point source, while the 0.29 km depth to the Sugarloaf dipolar plane source is somewhat less than the 0.35 km average maximum depth for the line source. Considering the approximations and uncertainties inherent in all these models, the differences between the source depths obtained using these two types of models are reasonable.

CONCLUSIONS

The most probable source of the two large self-potential anomalies seen in the survey area appears to be geothermal activity. The maximum depth to the top of the geothermal source region is about 0.40 to 0.47 km (1300 to 1500 ft) for the Fox Canyon anomaly and about 0.29 to 0.35 km (950 to 1150 ft) for the Sugarloaf anomaly. The anomalies appear to be generated by the flow of heat and/or fluid in the vicinity of geologic boundaries in the source regions.

REFERENCES

Corwin, R. F., and Hoover, D. B., 1979, The self-potential method in geothermal exploration: Geophysics, Vol. 44, No. 2, p. 226-245.

Fitterman, D. V., 1979, Calculation of self-potential anomalies near vertical contacts: Geophysics, Vol. 44, No. 2, p. 195-205.

Fitterman, D. V., 1983, Modeling of self-potential anomalies near vertical dikes: Geophysics, Vol. 48, No. 2, p. 171-180.

MacInnes, D. A., 1961, The principles of electrochemistry: Dover, New York, 478 p.

Sato, M., and Mooney, H. M., 1960, The electrochemical mechanism of sulfide self-potentials: Geophysics, Vol. 25, No. 1, p. 226-249.

Sill, W. R., 1983, Self-potential modeling from primary flows: Geophysics, Vol. 48, No. 1, p. 76-86.

GEOPHYSICS, VOL. 47, NO. 1 (JANUARY 1982); P. 100–116, 21 FIGS.

Controlled-source audiomagnetotellurics in geothermal exploration

Stewart K. Sandberg* and Gerald W. Hohmann‡

ABSTRACT

Theoretical and field tests indicate that the controlled-source audiomagnetotelluric (CSAMT) method provides an efficient means of delineating the shallow resistivity pattern above a hydrothermal system. Utilizing a transmitter overcomes the main limitation of conventional audiomagnetotellurics—variable and unreliable natural source fields. Reliable CSAMT measurements can be made with a simple scalar receiver. Our calculations for a half-space show that the plane-wave assumption is valid when the transmitter is more than 3 skin depths away in the broadside configuration and more than 5 skin depths away in the collinear configuration. Three-dimensional (3-D) numerical modeling results for a bipole source 5 skin depths away compare well with those for a plane-wave source, showing that the method is valid.

A CSAMT survey at the Roosevelt Hot Springs geothermal area in Utah produced apparent resistivity contour maps at four frequencies: 32, 98, 977, and 5208 Hz. These maps show the same features as those of a dipole-dipole resistivity map. We also collected detailed CSAMT data at 10 frequencies on two profiles. Two-dimensional (2-D) plane-wave modeling (transverse magnetic mode) of the resulting pseudo-sections yields models similar to those derived by modeling the dipole-dipole resistivity data. However, CSAMT resolved details not shown by the resistivity modeling. Thus, high resolution along with an efficient field procedure make CSAMT an attractive tool for geothermal exploration.

INTRODUCTION

Dipole-dipole resistivity and scalar audiomagnetotelluric (AMT) surveys frequently are conducted to delineate the shallow resistivity pattern above a hydrothermal system. The former method is slow and expensive, while the latter is not dependable. Natural fields in the AMT band ($10–10^4$ Hz) are due to thunderstorm energy propagating in the earth-ionosphere cavity; therefore, the source fields at certain times of the day or in certain seasons may be so weak that it is impossible to obtain reliable data. Furthermore, tensor measurements are required, because the source field direction varies with time. These limitations can be overcome by utilizing a controlled source, i.e., a grounded wire driven at one or several frequencies and located far enough away that the incident field at the receiver approximates a plane wave.

Strangway et al (1973) discussed the application of natural-field AMT in mineral exploration. Hoover et al (1976), Hoover and Long (1976), Hoover et al (1978), and Long and Kaufman (1980) described reconnaissance natural-field AMT investigations with station spacings of several kilometers in geothermal areas. However, in geothermal exploration AMT may be most useful for detailed mapping of near-surface low-resistivity zones due to rock alteration and saline pore fluids.

Goldstein and Strangway (1975) introduced the use of a controlled source for AMT surveys and discussed applications in mineral exploration. If the source is located several skin depths from the observation point, the electromagnetic (EM) field behaves as a plane wave, and the conventional magnetotelluric (MT) formula for apparent resistivity can be used to reduce the data.

We investigate the validity of the plane-wave approximation for half-space and three-dimensional (3-D) models. Then we describe the results and interpretation of a controlled-source audiomagnetotelluric (CSAMT) survey at the Roosevelt Hot Springs KGRA (known geothermal resource area) in Utah.

PLANE-WAVE APPROXIMATION

Expressions for the magnetic and electric fields due to an infinitesimal grounded electric dipole on a half-space were presented by Goldstein and Strangway (1975). We integrated the infinitesimal dipole solution numerically over a finite length source to simulate a field situation. Solutions were calculated over a 3¼ × 3¼ mile (5.23 × 5.23 km) grid for a 2000 ft (609.6 m) transmitter, a half-space resistivity of 100 Ω-m, and a frequency of 32.02 Hz.

AMT scalar apparent resistivities are calculated according to the relation

$$\rho_a = \frac{1}{\mu\omega}\frac{|E|^2}{|H|^2},$$

where E and H are perpendicular horizontal electric and magnetic field components, respectively. For our half-space model, the transmitter bipole is oriented along the x-axis.

Figure 1 shows apparent resistivities calculated using the component of the electric field parallel to the transmitter. For

Presented at the 50th Annual International SEG Meeting, November 18, 1980 in Houston. Manuscript received by the Editor September 2, 1980; revised manuscript received April 30, 1981.
*Amoco Minerals Co., 333 West Hampden, Englewood, CO 80110.
‡Dept. of Geology and Geophysics, University of Utah, Salt Lake City, UT 84112.

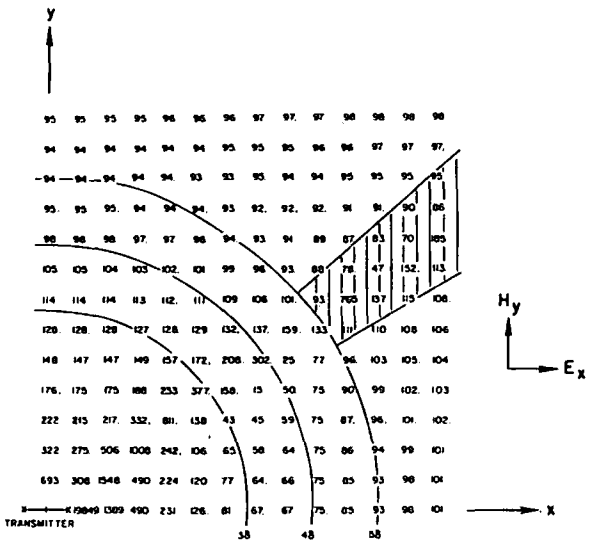

FIG. 1. Apparent resistivities calculated using E_x and H_y with the transmitter bipole parallel to the x-axis. Station spacing 1/4 mi (402.34 m), transmitter bipole 2000 ft (609.6 m) long, half-space resistivity = 100 Ω-m, frequency = 32.02 Hz, skin depth (δ) = 884 m (.55 mi). Three, four, and five skin depth distances from the center of the transmitter are shown. The shaded area is the region of minimum coupling.

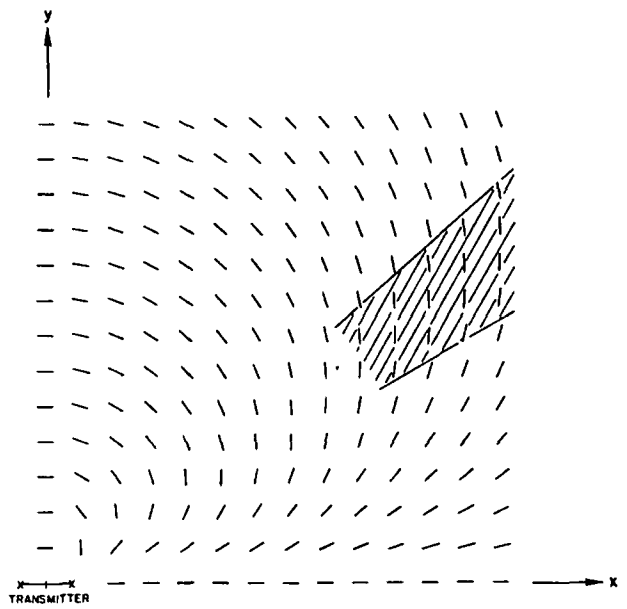

FIG. 2. Orientations of the major axes of the electric field polarization ellipses. The shaded area is the same as that in Figure 1.

reference, distances of 3, 4, and 5 skin depths ($\delta = \sqrt{2/\mu\omega\sigma}$) are shown. Apparent resistivities are within ten percent of the true half-space resistivity (100 Ω-m) when measured more than three skin depths broadside to the transmitter, and more than five skin depths collinear with the transmitter. The broadside configuration refers to measuring the electric field parallel to the transmitter bipole and on its center line. Collinear refers to measuring the electric field parallel to the transmitter bipole and on its axis. However, resistivities in the shaded region of Figure 1, although far enough away, are not within ten percent of 100 Ω-m because the electric and magnetic fields are almost perpendicular to the measuring directions.

Orientations of the major axes of the electric and magnetic field polarization ellipses are plotted in plan view in Figures 2 and 3, respectively. The shaded areas in these figures correspond to the minimum coupling area in Figure 1. Note that in the shaded areas E_x and H_y (the field components used in the apparent resistivity calculations of Figure 1) are small. Apparent resistivities calculated using these small inaccurate components are erratic; the same would be true of field data. Goldstein and Strangway (1975) showed similar regions of minimum coupling on apparent resistivity grids from an infinitesimal electric dipole source.

Figure 4 shows apparent resistivities calculated using the component of the electric field perpendicular to the transmitter bipole. At distances from the transmitter greater than three skin depths, calculated apparent resistivities are everywhere within ten percent of the true half-space resistivity. Minimum coupling in this orientation occurs along the x- and y-axes; no apparent resistivity values are shown on the axes because the E_y and H_x fields are zero.

Profiling parallel to the transmitter bipole (broadside configuration) requires measuring electric and magnetic fields in directions which are not maximum coupling orientations. A profile along a radial path perpendicular to or collinear with the bipole will preserve maximum coupling along the entire profile, and it is therefore recommended.

Kan and Clay (1979) showed half-space solutions for the fields within the earth using a dipole transmitter and stated that the plane-wave source approximation is valid beyond about six skin depths. Their results are based on phases of the fields in the earth.

Three-dimensional (3-D) modeling was employed to simulate the CSAMT technique in the general case and to check the plane-wave approximation for an inhomogeneity in a half-space. The program modeled a bipole source on a 3-D earth using an integral equation solution (Hohmann, 1975). A similar program (Ting and Hohmann, 1981) simulated a plane-wave source over the same 3-D earth for comparison. The 3-D earth consisted of a homogeneous half-space in which a conductive rectangular prism 300 × 600 × 50 m thick was buried 50 m deep. The frequency was 100 Hz, the half-space resistivity was 100 Ω-m, and the prism resistivity was 10 Ω-m.

The first source was located approximately five skin depths from the body, representing a transmitter-receiver separation adequate for the broadside configuration and just large enough for the collinear configuration. Figure 5a shows a plan map of apparent resistivities calculated on profiles across the buried prism using E_y and H_x with transmitter electrodes located 2600 and 3200 m from the origin on the y-axis. The nearest source electrode is 4.9 skin depths from the nearest edge of the body, and the geometry corresponds to the collinear configuration.

In Figure 5b, apparent resistivities are calculated in the same manner, except the source is a plane wave with the electric field polarization in the y-direction. A comparison of Figures 5a and 5b shows the validity of the plane-wave approximation for an inhomogeneous earth. Discrepancies are larger on the source side of the body because it is closer to the transmitter bipole.

Figure 6a shows apparent resistivities calculated from E_x and

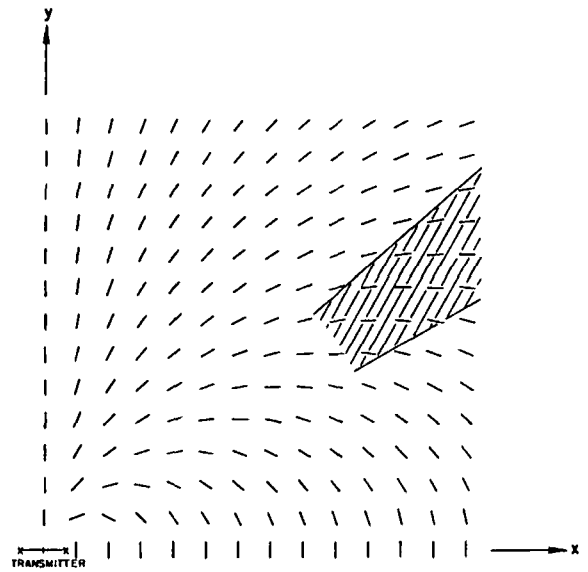

FIG. 3. Orientations of the major axes of the magnetic field polarization ellipses. The shaded area is the same as that in Figure 1.

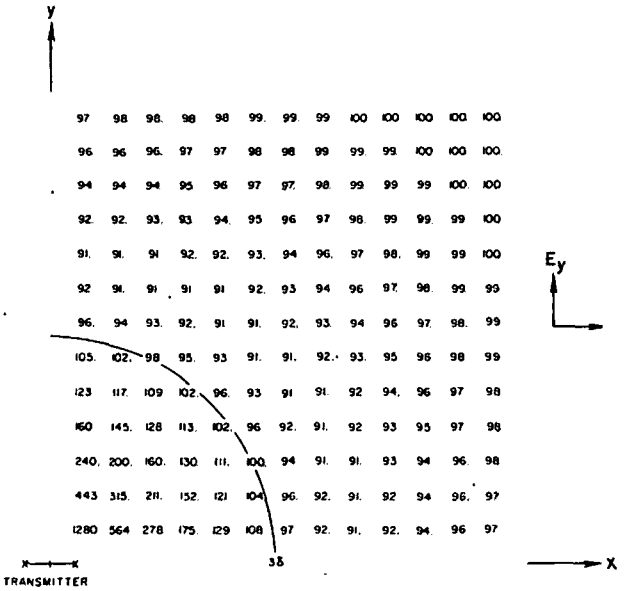

FIG. 4. Apparent resistivities calculated using E_y and H_x with the transmitter bipole parallel to the x-axis. Three skin depths distance from the center of the transmitter is shown.

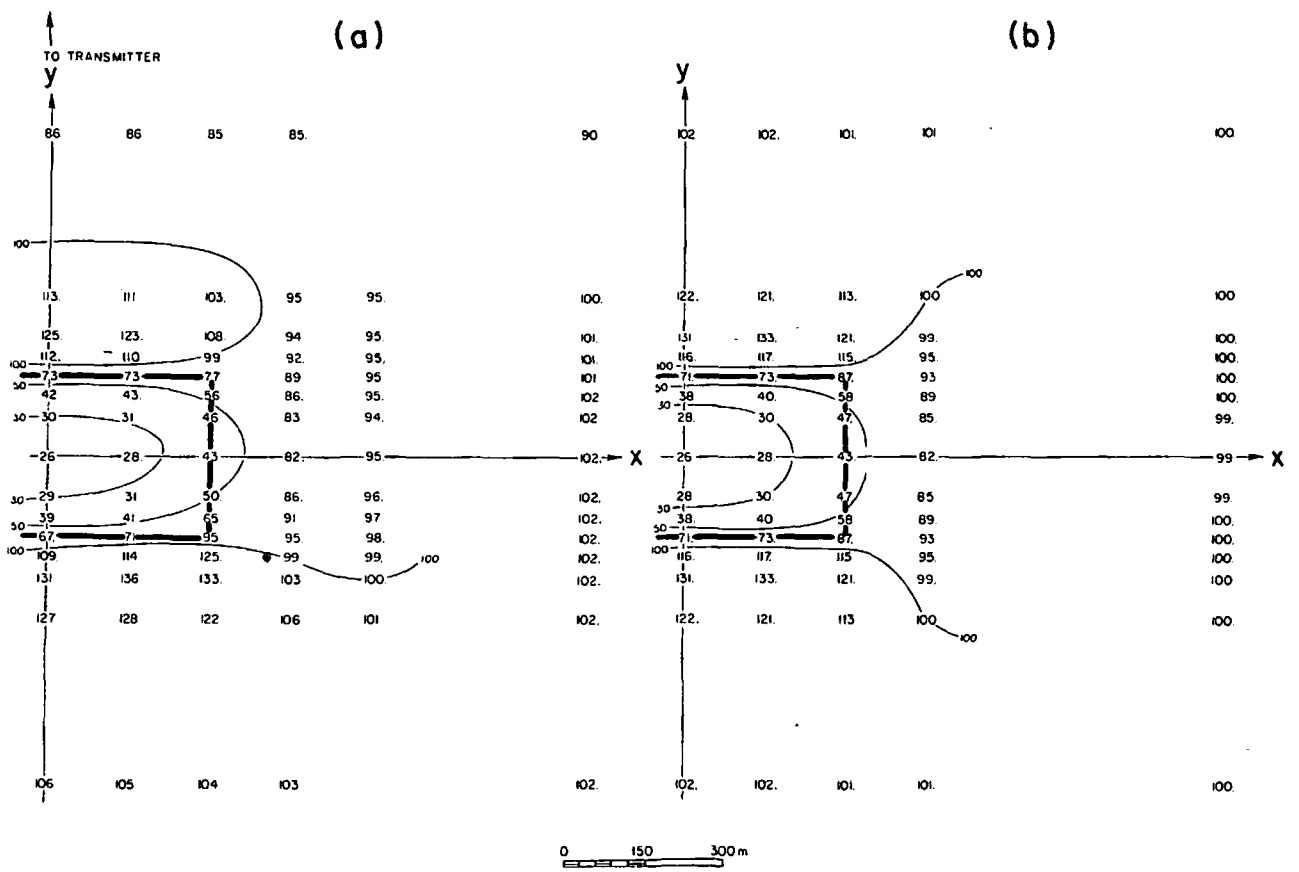

FIG. 5. Plan view of apparent resistivities over a buried 3-D prism calculated using E_y and H_x. Due to the symmetry, only half of the area is shown. Prism resistivity = 10 Ω-m, background half-space resistivity = 100 Ω-m, frequency = 100 Hz. (a) Transmitter bipole in collinear configuration centered at y = 2900 m. (b) Plane-wave source with the electric field polarized in the y-direction. A profile of data along y = 600 m has been added in (a) to constrain the apparent resistivity contours.

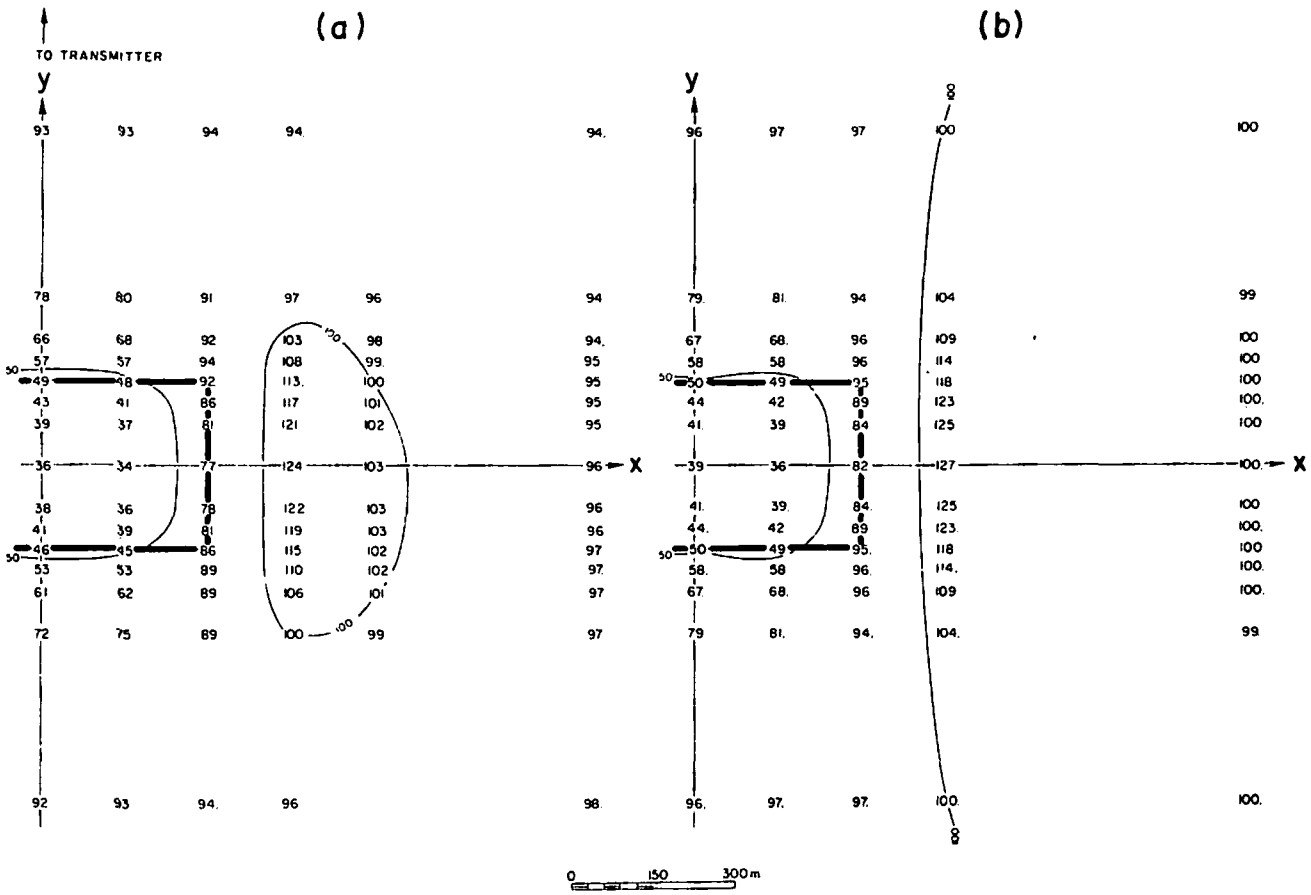

FIG. 6. Plan view of apparent resistivities over a buried 3-D prism calculated using E_x and H_y. (a) Transmitter bipole in broadside configuration centered at y = 2900 m. (b) Plane-wave source with the electric field polarized in the y-direction. A profile of data along y = 600 m has been added in (a) to constrain the apparent resistivity contours.

H_y for transmitter electrodes centered 2900 m from the origin in the y-direction (5.8 skin depths from the center of the prism) and parallel to the x-axis, i.e., the broadside configuration. For comparison, Figure 6b shows apparent resistivities for a plane-wave source with the electric field in the x-direction. There is good agreement, showing that the source is sufficiently far away that the plane-wave approximation is valid.

The effect of obtaining data too close to the transmitter was simulated by placing source electrodes on the y-axis 700 and 1300 m from the origin in Figure 7a. Electrodes 900 m from the origin in the y-direction and parallel to the x-axis represent the other incident field mode in Figure 7b. Both modes exhibit resistivity lows over the buried prism, but the apparent resistivities are far from the plane-wave values shown in Figures 5b and 6b. The incident field does not approximate a plane wave in this case, because the distance from the center of the transmitter to the center of the body is only 1.8 skin depths.

When applying CSAMT in highly resistive terrain, the required transmitter-receiver separation may be so large that obtaining data too close to the transmitter is necessary in order to receive the signal. Such data are not quantitatively interpretable with plane-wave MT modeling. Goldstein and Strangway (1975) presented curves for one-dimensional (1-D) interpretation of soundings taken too close to the transmitter.

ROOSEVELT HOT SPRINGS CSAMT SURVEY

We carried out a CSAMT survey at Roosevelt Hot Springs KGRA during August and September, 1979. The KGRA is located in Beaver County, in west central Utah on the western margin of the Mineral Mountains. Bedrock in the area is dominated by metamorphic rocks of Precambrian and Paleozoic age. The geothermal system is located within the granitic Mineral Mountains pluton of Tertiary age. There is evidence of recent igneous activity in rhyolite flows, domes, and pyroclastics of Pleistocene age.

The area has been studied in detail by the Dept. of Geology and Geophysics, University of Utah and by the Earth Science Laboratory, University of Utah Research Institute. A summary of the work can be found in Ward et al (1978). Because the area is so well documented, it is a good location for testing an exploration technique.

Roosevelt Hot Springs is a structurally controlled geothermal reservoir. Geothermal exploration targets are the faults and fractures which control the movement of fluids. Alteration products observed along these faults and fractures are associated with chemical reactions caused by the hydrothermal system. Due to the alteration minerals and the brine, the fault zones respond as low-resistivity anomalies in an otherwise moderate to high-resistivity background.

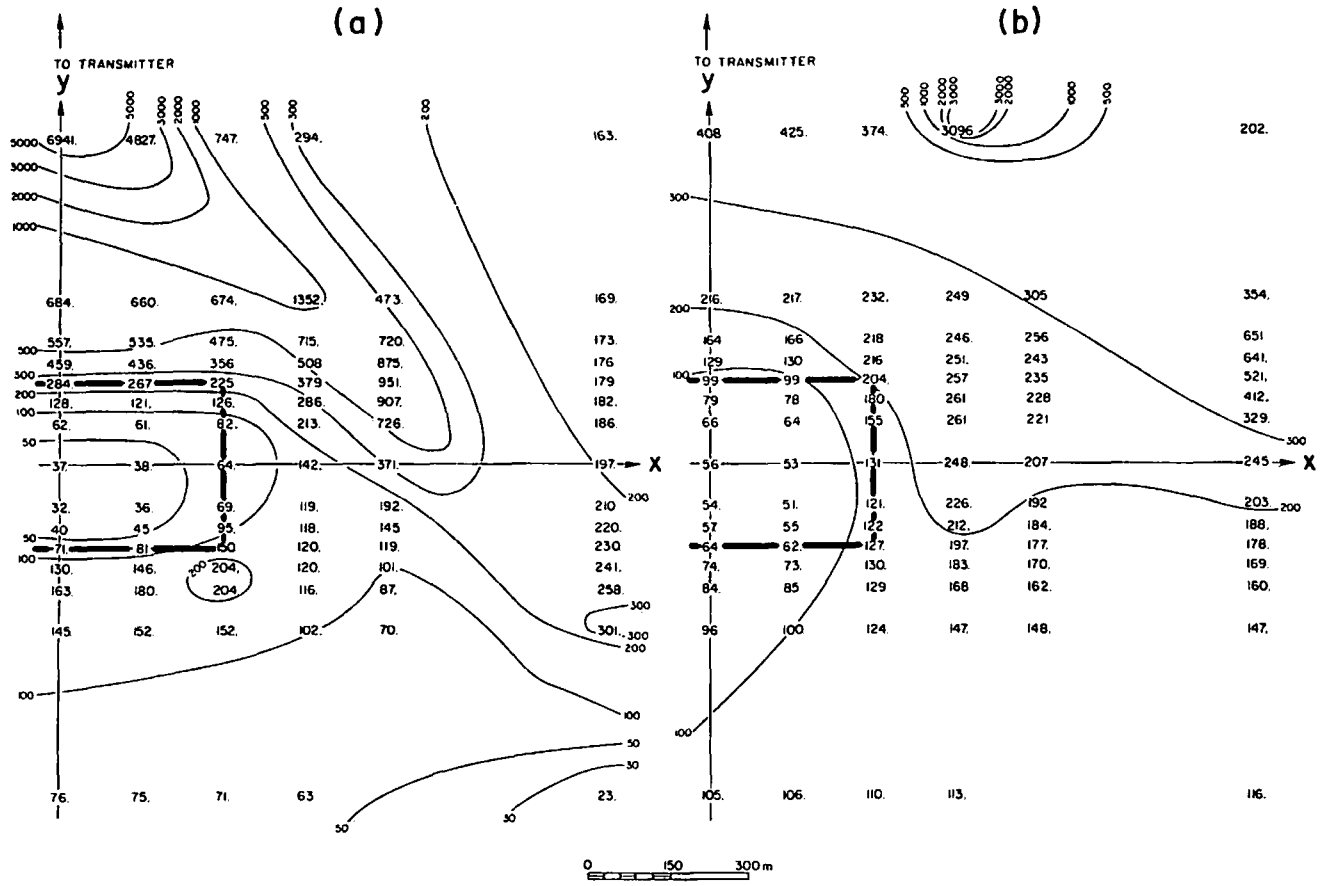

FIG. 7. (a) Same as Figure 5a except transmitter is centered at y = 1000 m. (b) Same as Figure 6a except transmitter is centered at y = 900 m.

The resistivity range expected is between one and a few hundred ohm-meters. Formation water resistivities are in the range 0.5 to 2 Ω-m (Glenn and Hulen, 1979). Laboratory measurements on core samples from the clay alteration zone (30–60 m) in drillhole 1A near the Opal Mound fault show resistivities as low as 3–5 Ω-m (Ward and Sill, 1976).

Previous resistivity work was done in the area by Ward and Sill (1976). A first separation (n = 1) 300-m dipole-dipole resistivity contour map from their work is shown in Figure 8. They used this map (along with dipole-dipole resistivity pseudo-sections, an aeromagnetic map, air photos, plus mapped and interpreted geology) to produce a fracture map of the Roosevelt Hot Springs KGRA. Resistivity contours were also used to support the possibility that brine is leaking out of the convective hydrothermal system to the north.

We carried out the CSAMT survey in two parts. First, a resistivity mapping study was completed to assess the method by comparing it with the dipole-dipole resistivity map (Figure 8). The second part of the survey consisted of two east-west profiles across the low-resistivity zone, with subsequent quantitative interpretation using a 2-D MT modeling program.

The transmitter used in the field work was a Geotronics model EMT-5000. The receiver was a Kennecott Minerals Co. scalar AMT unit consisting of a two-channel, tunable, high-gain, narrow band-pass analog instrument which measured the logarithmic ratio of the channel inputs. A reading consisted of an electric-to-magnetic field ratio with no phase information.

The depth of exploration usually given for AMT is one skin depth. However, actual depth of exploration is somewhat less, as discussed later in this paper. In our field work, the lowest frequency was 32 Hz, so in 10 Ω-m ground the depth of exploration is less than 280 m, while in 50 Ω-m ground, it is less than 628 m.

Resistivity mapping

The CSAMT procedure for resistivity mapping is based on our theoretical results. The assumption of a 1-D (layered) earth at each receiver site allows apparent resistivity calculations to be made by measuring the field in maximum coupling orientations. A transparent plot of electric field direction (Figure 2) over a half-space is constructed at the same scale as the field map. Overlaying the field direction plot helps to orient the receiver for maximum signal strength. The distance from the transmitter should be at least three skin depths, using the largest resistivity between receiver and transmitter and the lowest frequency of the sounding. Apparent resistivities are calculated for several frequencies at each station, and a contour map is constructed for each frequency to delineate the near-surface resistivity pattern.

Field work at Roosevelt Hot Springs KGRA resulted in 136 unique stations occupied, 47 of which were located on two pro-

files. For resistivity mapping, apparent resistivities were measured at four frequencies: 5208, 977, 98, and 32 Hz. Two transmitter sites were used for the reconnaissance survey, and three others were occupied for profiling. Apparent resistivity contour maps at each of the four frequencies are shown in Figures 9, 10, 11, and 12. The general contour trend and the positions of the low-resistivity zones compare well with the first separation dipole-dipole resistivity map in Figure 8.

The 5208 Hz map of Figure 9 exhibits two zones of low apparent resistivity. One is located around the early steam well. The other is just west of well 3-1 and trends northwest from there through well 82-33 and northeast toward well 12-35. The low resistivities coincide with mapped near-surface alteration and brines associated with the geothermal system. These low resistivities are bounded on the east by the more resistive unaltered granitic pluton, and on the west by unaltered alluvium west of the Opal Mound. Geothermal production wells lie within or just to the east of the low-resistivity zone, and nonproducing wells lie to the south and west. The 100 Ω-m contour north of well 82-33 is not due to noise in the data; high resistivities also occur here in 100-m dipole-dipole data.

The 977 Hz map of Figure 10 defines the same general resistivity trend. A station in the northwest part of the map has a low apparent resistivity of 15 Ω-m. This low-resistivity area

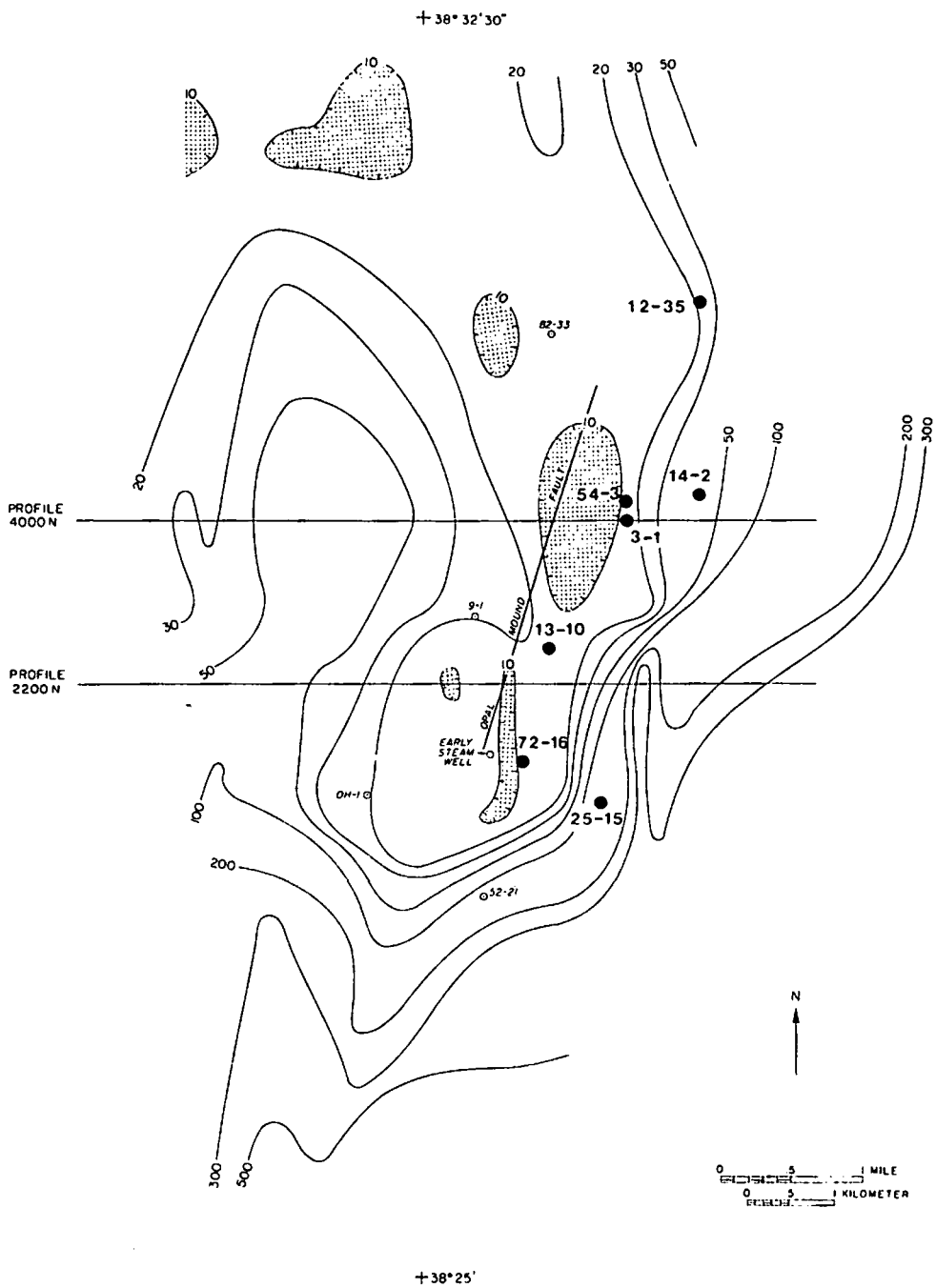

FIG. 8. First separation dipole-dipole resistivity map of the Roosevelt Hot Springs KGRA (a = 300 m). After Ward and Sill (1976). Areas less than 10 Ω-m are shaded. Solid circles denote producing geothermal wells, open circles indicate nonproducing wells.

broadens and becomes more defined in the maps of apparent resistivity for the lower frequencies. Prehistoric Lake Bonneville sediments in this area (Ward and Sill, 1976) explain the feature. The northern low-resistivity zone along the Opal Mound fault extends farther northwest at this frequency. This could indicate that the geothermal system is leaking or has leaked to the northwest.

The 97.7 Hz map of Figure 11 shows low-resistivity zones larger in area, with the northern zone extending due north. The conductive zone to the northwest is well defined.

The 32.02 Hz map of Figure 12 shows bedrock to the east and southeast indicated by the high apparent resistivity values. Conductive zones correspond to the geothermal areas as well as the Lake Bonneville sediments to the northwest. The conductive zone along 2200N at the Opal Mound fault is enlarged to the west at this frequency, possibly indicating westward brine leakage from the fault.

The absolute accuracy of the resistivities obtained by our equipment was checked by reoccupying an MT site obtained in an earlier survey. CSAMT data agree with the MT data within measurement error, indicating that our equipment was working properly and apparent resistivities are accurate.

In order to determine the reliability of the data obtained in the survey, we repeated several stations. The repeatability was usually within one decibel of the E/H ratio read from the receiver (one decibel greater corresponds to multiplying the apparent resistivity by 1.26, and one decibel less yields apparent resistivity divided by 1.26). Two receiver and coil sets were used; ratio differences

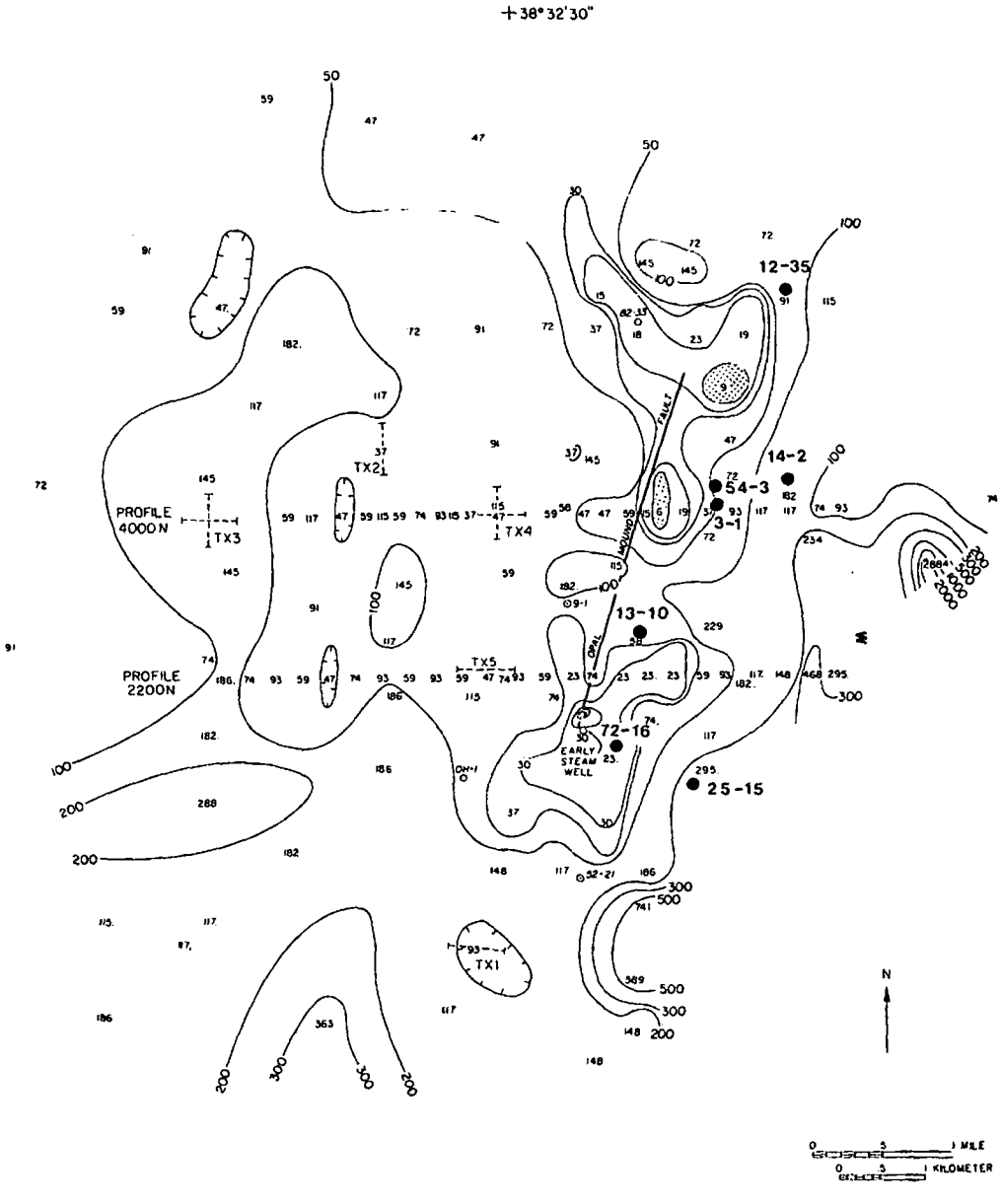

FIG. 9. CSAMT apparent resistivity map of Roosevelt Hot Springs KGRA. Frequency = 5208 Hz. Areas less than 10 Ω-m are shaded.

between the two different sets usually were within one decibel of each other. These accuracy and repeatability tests are explained in more detail in Sandberg (1980).

A CSAMT resistivity mapping survey appears to be more efficient than conventional dipole-dipole resistivity mapping. The CSAMT receiver only requires a 30-m wire for the electric field sensor and a portable coil for detecting the magnetic field, instead of several hundred meters of wire as in the dipole-dipole resistivity procedure. We found that a four-frequency CSAMT station could be read in about 15 minutes, including set-up. Also, since the technique does not need to be confined to profiles, as in the case of dipole-dipole resistivity, rapid areal coverage is possible using existing roads.

The similarity between the CSAMT maps and the first separation dipole-dipole resistivity map, along with the reoccupied MT site results and repeatability tests, indicate that these data are accurate enough for quantitative interpretation. We ran two profiles across the low-resistivity zone and modeled the results. The locations of the profiles are shown in Figure 9.

Profile 1

Profile 1 is an east-west traverse along dipole-dipole resistivity line 4000N (Figure 8). The CSAMT station spacing was 300 m, and two transmitter locations (labeled TX3 and TX4 in Figure 9) were used. The transmitter consisted of an orthogonal pair of 2000 ft (609.6 m) bipoles, allowing apparent resistivity measure-

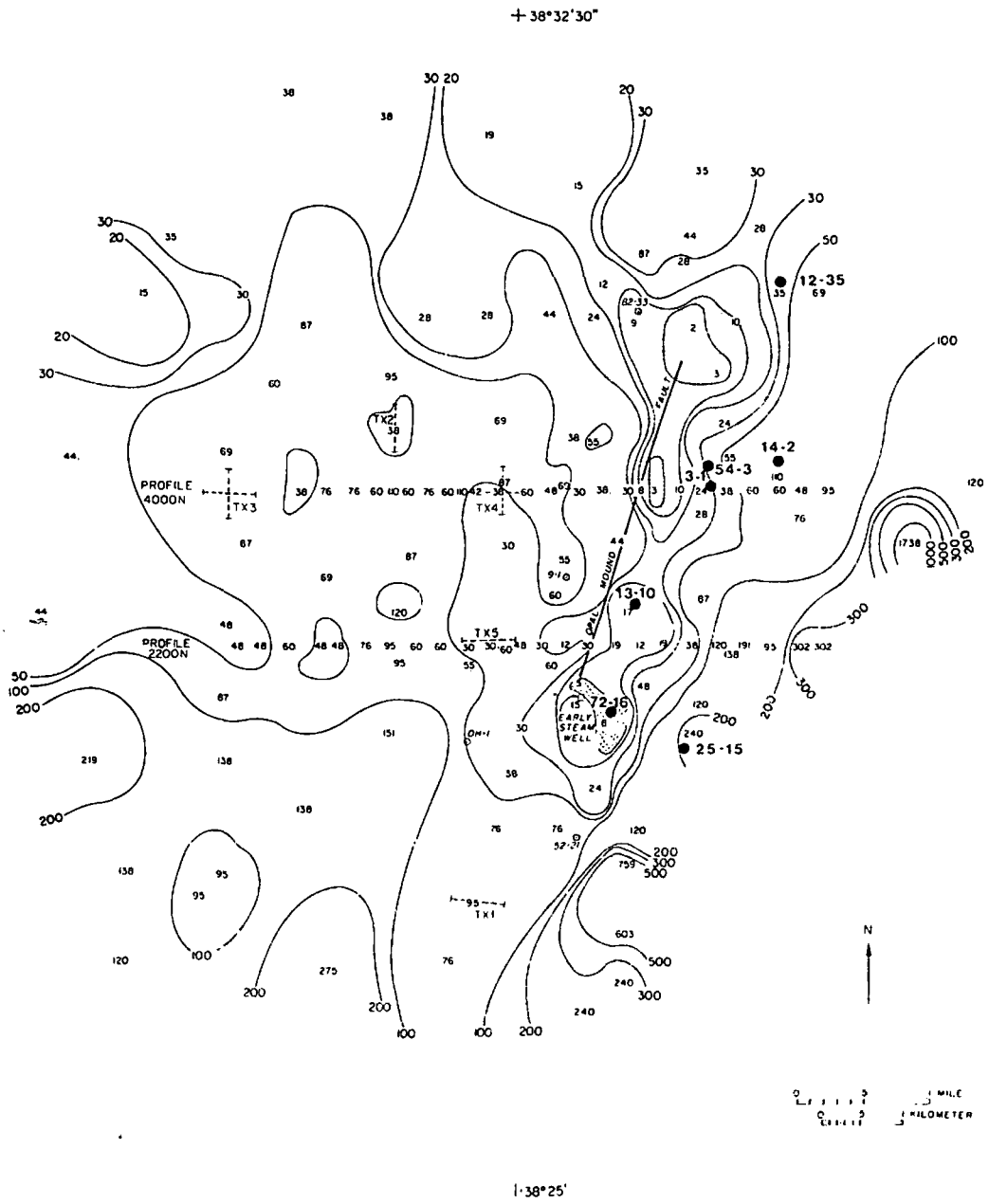

FIG. 10. CSAMT apparent resistivity map of Roosevelt Hot Springs KGRA. Frequency = 977 Hz. Areas less than 10 Ω-m are shaded.

ments with the electric field perpendicular and parallel to the traverse. Two sets of data were thereby obtained, corresponding to electric field orientations perpendicular (TM) and parallel (TE) to geologic strike. The two sets of data are plotted as pseudo-sections in Figures 13 and 14.

One-dimensional MT inversion of the TM mode data at each station along the profile resulted in an initial 2-D resistivity model for the line. This model was then refined by utilizing a 2-D MT finite-element forward computer program (Stodt, 1978) and adjusting the model to fit the TM mode field data. In a complex area such as this, 2-D interpretation is possible only for TM mode data (Wannamaker et al, 1980). The resulting model is shown in Figure 15 along with a 2-D resistivity model for the same line (Ross et al, 1981) derived from combined 100- and 300-m dipole-dipole ($n \leq 4$) data (Ward and Sill, 1976). Theoretical AMT pseudo-sections for the CSAMT and resistivity models are shown in Figures 16 and 17, respectively. These theoretical pseudo-sections can be compared with the field data in Figure 13. The resistivity model AMT response (Figure 17) does not fit the low-frequency data very well, and apparent resistivities in the conductive area are not low enough.

A 2-D finite-element dipole-dipole resistivity computer pro-

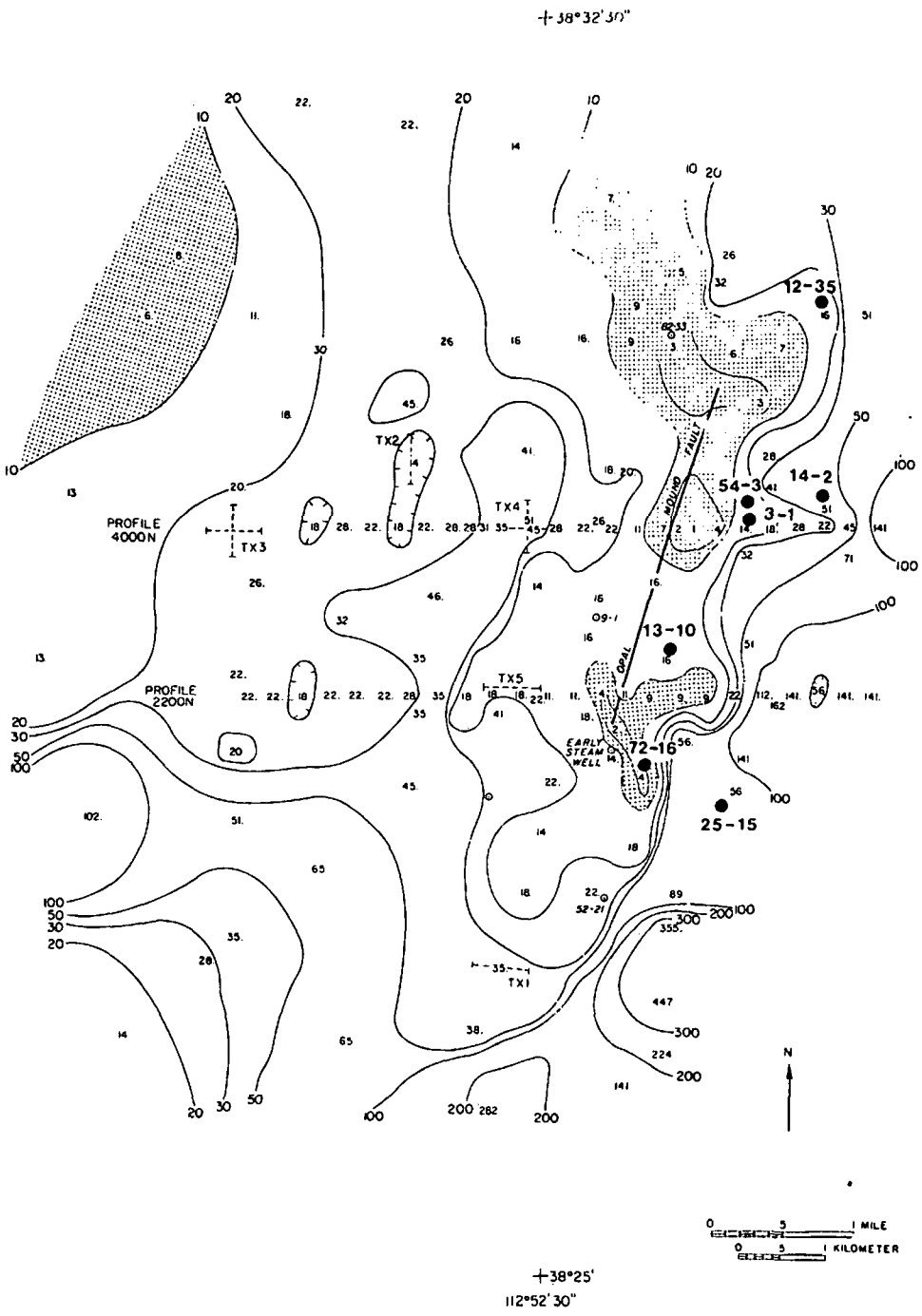

FIG. 11. CSAMT apparent resistivity map of Roosevelt Hot Springs KGRA. Frequency = 98 Hz. Areas less than 10 Ω-m are shaded.

gram (Killpack and Hohmann, 1979) was used to generate resistivity data from the CSAMT model. A comparison of this theoretical data and the resistivity field data is shown in Figure 18.

The dipole-dipole resistivity data in Figure 18 indicate a resistive overburden from CSAMT station 3900 on the west end of the profile. Lack of high-frequency data at stations 2100, 3000, 3300, 3600, and 3900 (Figure 13) along with probable noise at the high-frequency reading at station 2700 contribute to CSAMT's inability to detect this feature. The CSAMT model (Figure 15) was constructed to fit the field data, and therefore it does not show a resistive overburden.

One large disagreement between the resistivity and CSAMT interpretations is the depth to the conductive unit from stations 2400 to 3600 (Figure 15). This depth is modeled 300 m deep by resistivity and 150 m deep by CSAMT. Joint modeling of 300-m and 1-km dipole-dipole data by Ward and Sill (1976) on this line also indicated a resistive-to-conductive interface at 300 m. The similarity between TM and TE mode CSAMT data in this region (see Figures 13 and 14) suggests that 1-D inversion results should be meaningful. We inverted data from stations 2400 through 3600 to determine the depth to this conductive zone.

Inversion results indicate that the 150-m interface modeled by CSAMT is a shallow limit, and the 300-m interface modeled by resistivity is too deep. An inversion of Schlumberger resistivity sounding data (Tripp et al, 1978) obtained just west of station 3300 indicates a resistive-to-conductive interface at about 119 m with a range of 73 to 196 m. When EM sounding data (10.5 Hz to 86 kHz) in the same position were inverted (Tripp et al, 1978),

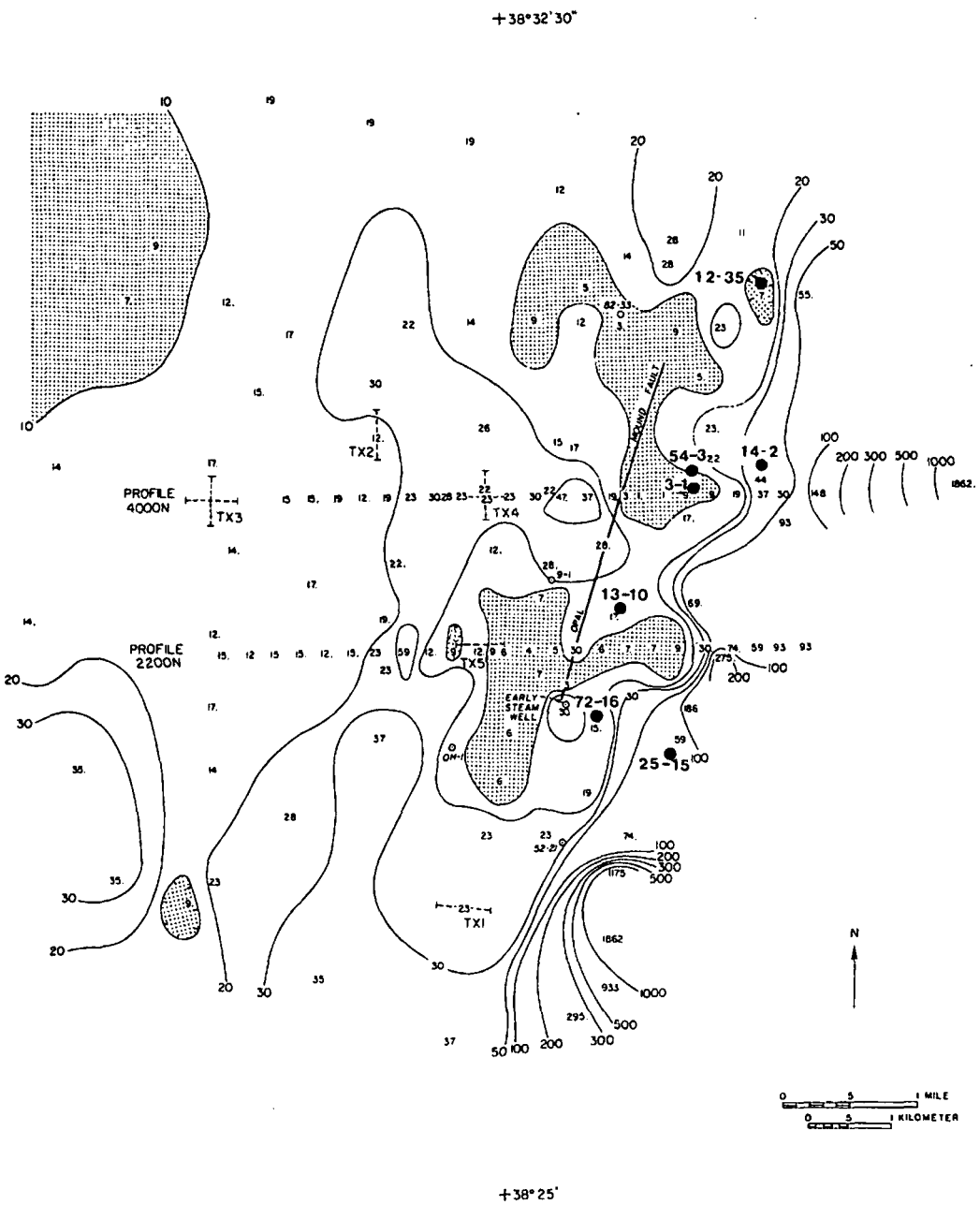

FIG. 12. CSAMT apparent resistivity map of Roosevelt Hot Springs KGRA. Frequency = 32 Hz. Areas less than 10 Ω-m are shaded.

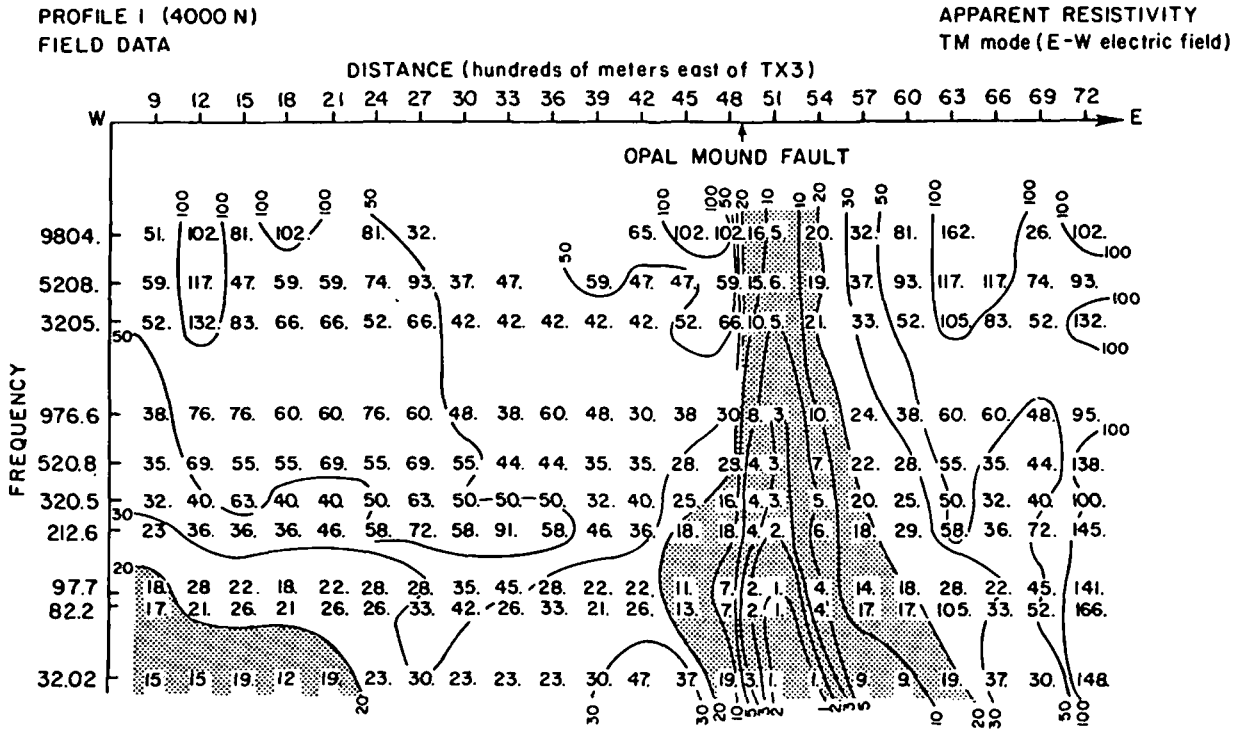

FIG. 13. TM mode field data pseudo-section from profile I (4000 N). Apparent resistivity less than 20 Ω-m is shaded.

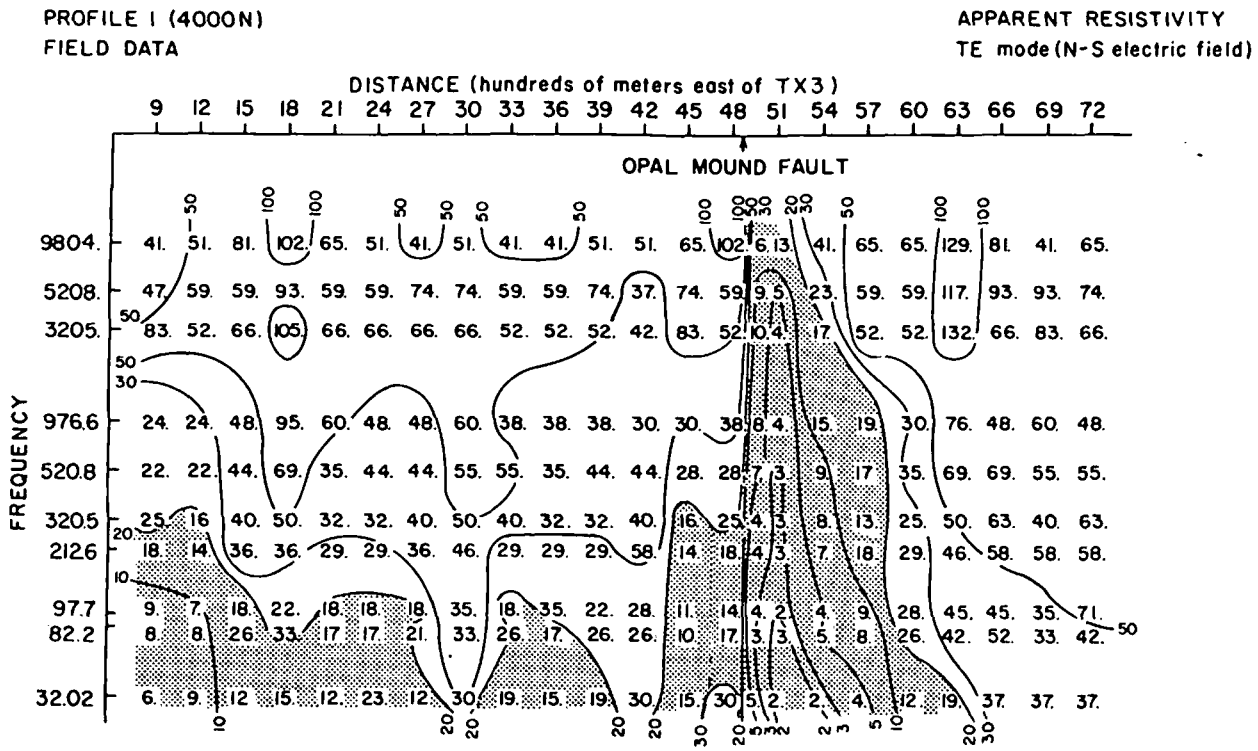

FIG. 14. TE mode field data pseudo-section from profile I (4000 N). Apparent resistivity less than 20 Ω-m is shaded.

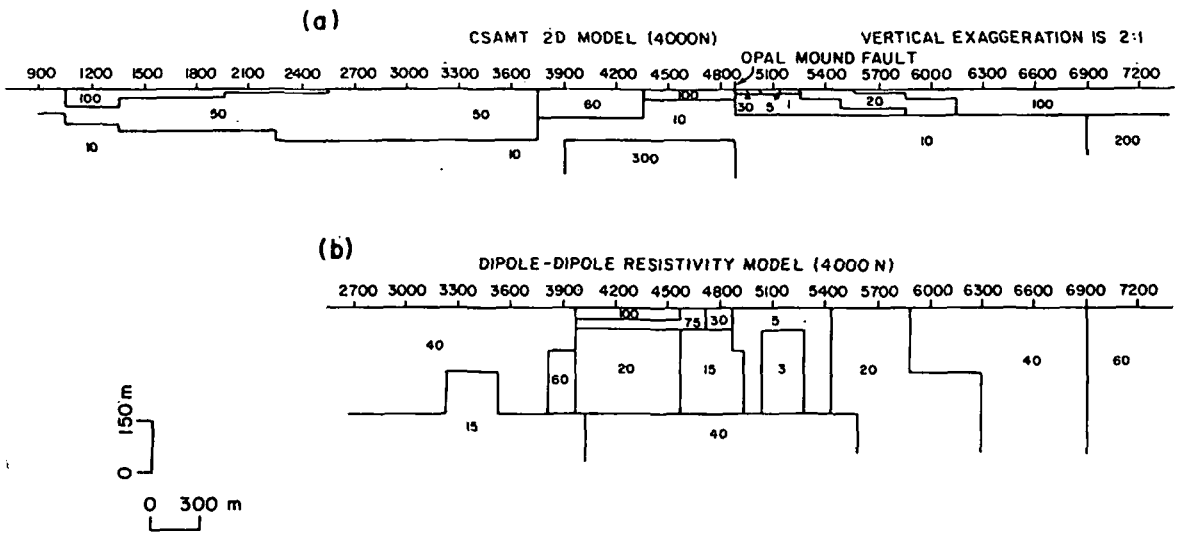

FIG. 15. (a) Two-dimensional CSAMT and (b) dipole-dipole resistivity (based on 100 m and 300 m dipoles) interpretations of profile 1 (4000 N).

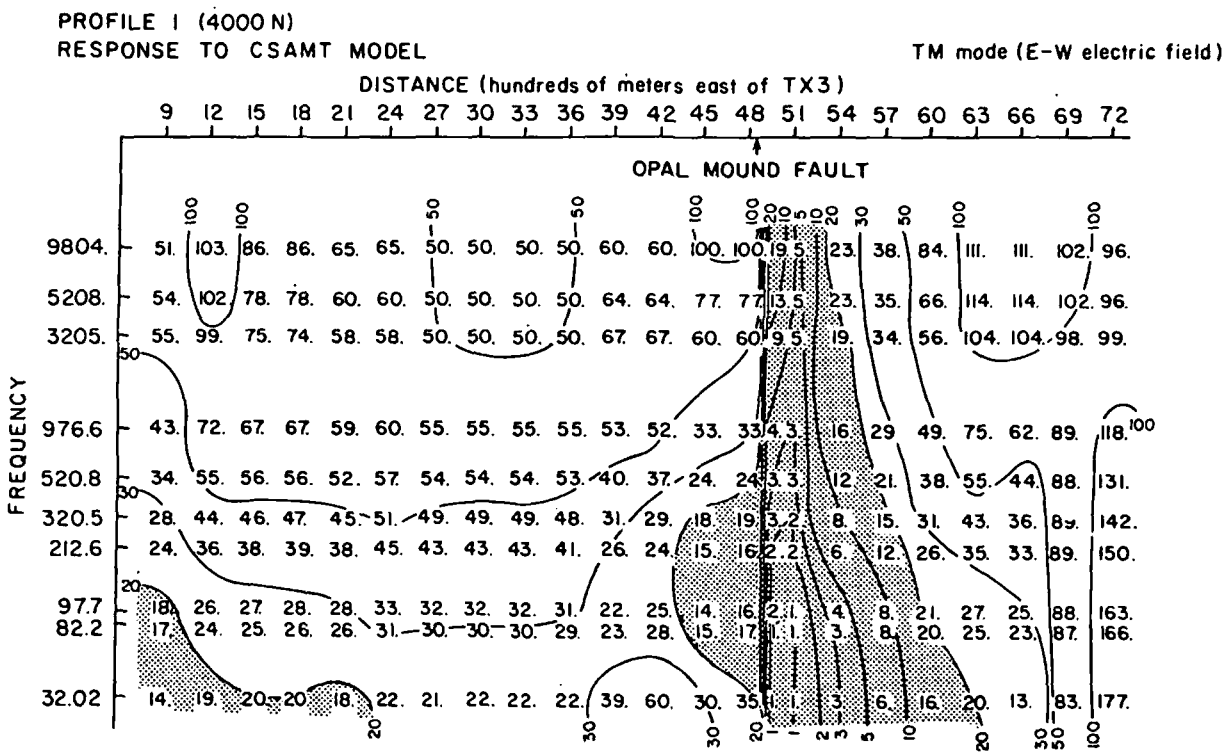

FIG. 16. Theoretical TM mode pseudo-section calculated from 2-D CSAMT model of profile 1 (4000 N). Apparent resistivity less than 20 Ω-m is shaded. Compare with field data in Figure 13.

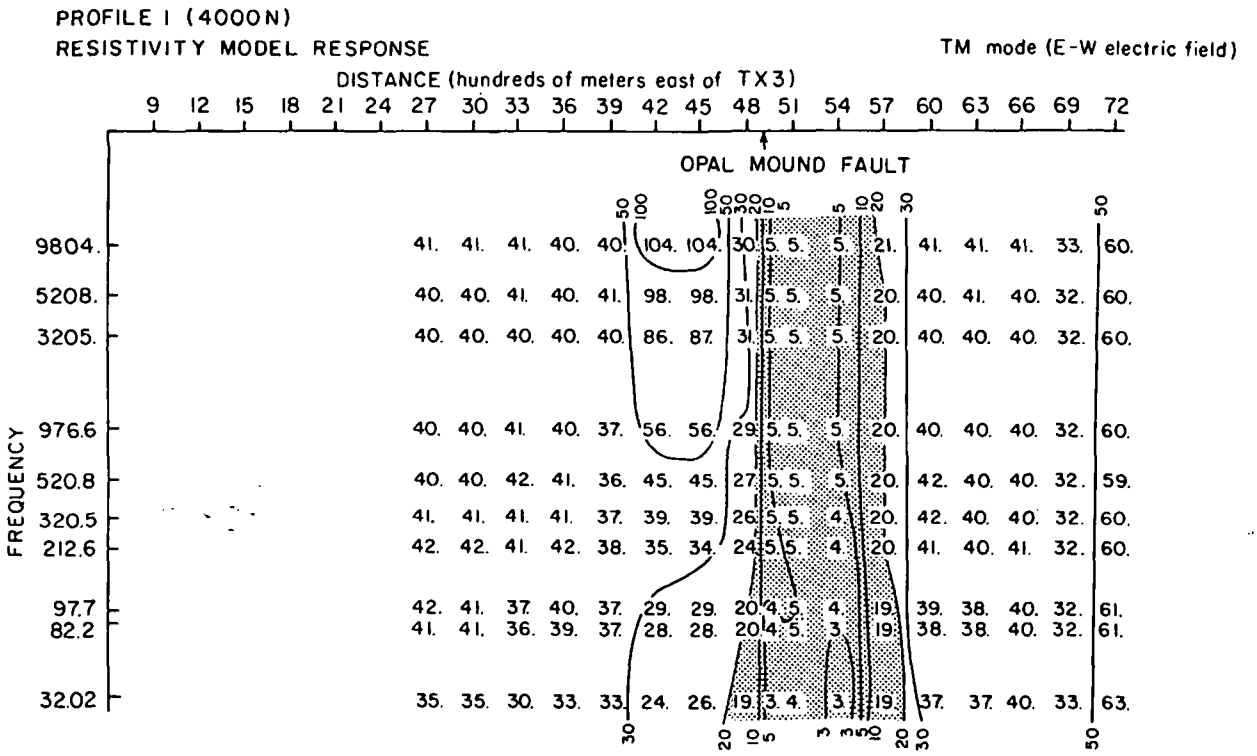

FIG. 17. Theoretical TM mode pseudo-section calculated from 2-D dipole-dipole resistivity model of profile 1 (4000 N). Apparent resistivity less than 20 Ω-m is shaded. Compare with field data in Figure 13.

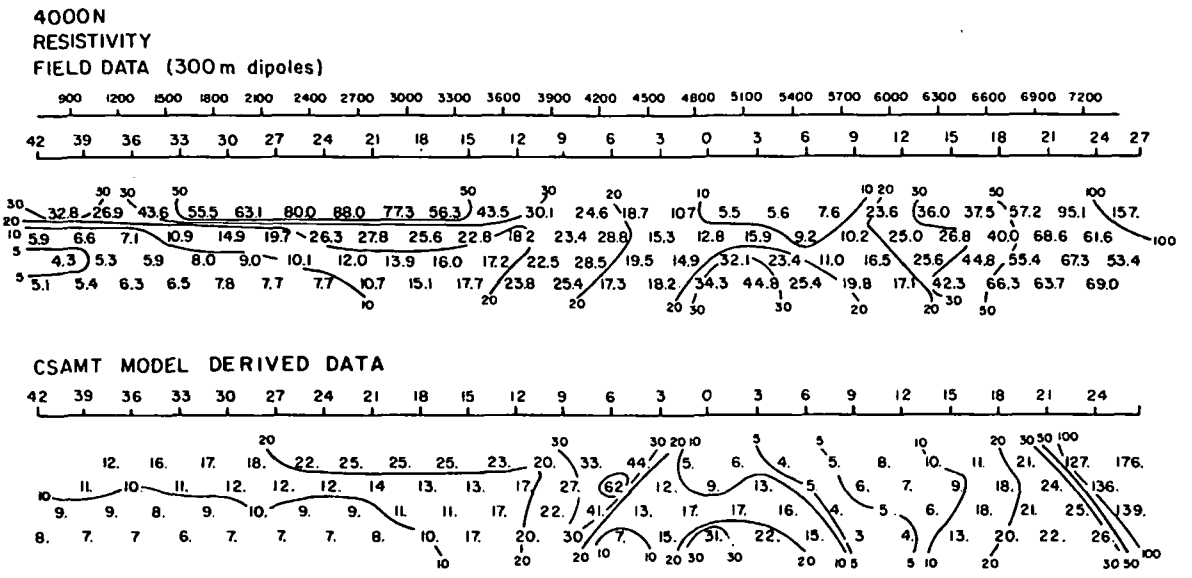

FIG. 18. Dipole-dipole (a = 300 m) resistivity field data compared with theoretical dipole-dipole data calculated from the CSAMT model of profile 1 (4000 N).

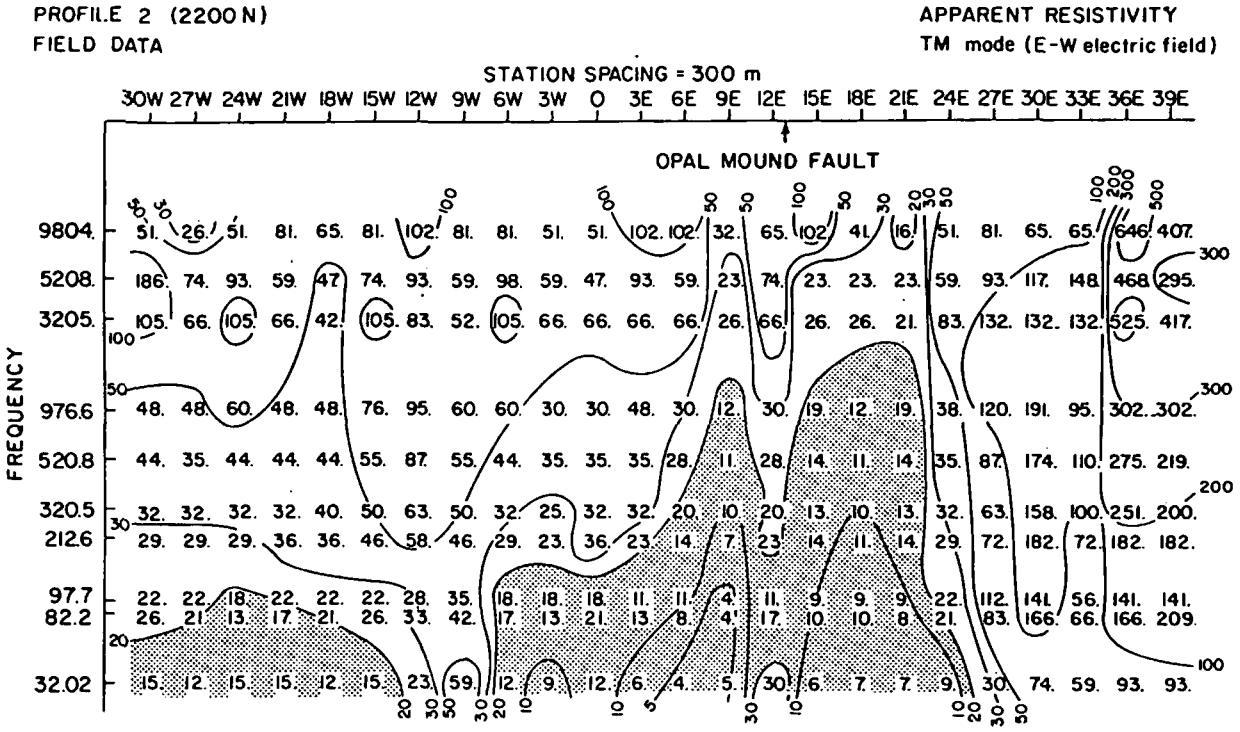

FIG. 19. Field data pseudo-section from profile 2 (2200 N). Apparent resistivity less than 20 Ω-m is shaded.

15 m of 119 Ω-m overburden underlain by 55 Ω-m material was interpreted. The EM sounding, although unable to penetrate to the resistive-conductive interface, gave a check on the resistivity of the upper layer. Based on this information, the upper layer resistivity for the CSAMT inversion was constrained at 50 Ω-m, eliminating high parameter correlations.

A 300 Ω-m resistive body corresponding to bedrock at depth is the main feature in the CSAMT section from 3900 to 4800. This body is modeled 150 m deep, but the depth is not well resolved. It is not shown in the interpretation of the dipole-dipole data (Figure 15b). The evidence for this resistive block occurs at the two lowest frequencies at stations 4200 and 4500, and the lowest frequency at stations 3900 and 4800. Two-dimensional Schlumberger modeling 500 m to the south of this line (Tripp et al, 1978) delineated a 300 Ω-m block at a similar depth. The joint 300-m and 1-km dipole-dipole model (Ward and Sill, 1976) indicates a 300 Ω-m substratum 600 m deep from station 3900 eastward.

The ability to resolve a narrow resistive structure at depth is related to the depth of exploration. The CSAMT technique, using the skin depth criterion, has a depth of exploration in 10 Ω-m material of 280 m (at 32 Hz). However, sensitivity tests indicate that the depth of exploration is less than a skin depth with our instrumentation due to apparent resistivities being repeatable only within a factor of 1.26. The dipole-dipole technique at $n = 4$ has depths of exploration of about 120, 360, and 1200 m for 100 m, 300 m, and 1 km dipoles, respectively (Roy and Apparao, 1971) for a plane interface. For tabular vertical structures, depths of exploration are less than for a plane interface. However, the 300-m dipole-dipole data should include information about the 300 Ω-m block. However, probably due to nonuniqueness of resistivity modeling, this block was not modeled (see Figure 15b).

Gravity modeling on this line (Crebs, 1976) shows bedrock 70 m deep below station 4800 increasing to about 140 m just west of station 4200. By adjusting the density contrast to a more reasonable value, Tripp (1977) suggested that the depth could compare quite reasonably with the 150 m modeled here. This resistive body is most likely unaltered Precambrian gneiss bedrock.

A thermal gradient hole was drilled a short distance from station 4800, intersecting the water table at 35 m. This depth coincides with the CSAMT model interface between 100 and 10 Ω-m material at 40 m depth.

Just east of station 4800 there is a sharp surface lateral resistivity contrast corresponding to the Opal Mound fault mapped by resistivity, heat flow, and geology. Inversion of EM sounding data shows 19 m of 24 Ω-m material underlain by 3.4 Ω-m material in this position (Tripp et al, 1978). This agrees well with the CSAMT model of 15 m of 30 Ω-m material underlain by 1 Ω-m material. The bottom of the 1 Ω-m block and the east edge of the 300 Ω-m block (see Figure 15) are not resolved because the near-surface region is so conductive that it is impossible to "see through" it at these frequencies. The eastern end of the 1 Ω-m unit is modeled as a staircase structure which implies a shallow, eastward dipping altered zone east of the Opal Mound fault.

A sensitivity study helped to explain the lack of fit in the theoretical dipole-dipole pseudo-section (Figure 18) from station 5100 eastward. An AMT 1-D study to simulate the resistivity section beneath station 5100 indicated that it was not possible to

determine the resistivity of anything below a 15 m layer of 5 Ω-m material overlying 60 m of 1 Ω-m material, even though a skin depth in 1 Ω-m material at 32 Hz is 89 m. When the errors in data measurement are considered, the thickness of the 1 Ω-m layer could be decreased to about 40 m and still shield information from below. Therefore, the exploration depth in this case is less than 0.6 skin depths.

A similar study simulating the resistivity section beneath station 5400 indicated no information could be derived about material below a 20 Ω-m layer 30 m thick overlying a 1 Ω-m layer 45 m thick. The depth of exploration is therefore less than .8 skin depths.

Based on the sensitivity tests, a model similar to the CSAMT model in Figure 15 was constructed which fit the 300 m dipole-dipole data out to station 6000. The modified model included thinning the 1 Ω-m layer and inserting 40 Ω-m material beneath it under stations 5100 to 5700. Lack of fit east of station 6000 is likely due to the fact that the area is not 2-D because of faulting parallel to the traverse 500 m to the north.

Profile 2

Profile 2 is an east-west traverse along resistivity line 2200N and is located 1800 m south of profile 1 (see Figure 9). The data are plotted in pseudo-section form in Figure 19. Five stations in the center of the line (6W, 3W, 0, 3E, and 6E) were obtained using transmitter TX4, and the rest were taken by working off both ends of transmitter TX5 [an east-west, 2000 ft (609.6 m) bipole]. Hence the data shown in Figure 19 are for the TM mode (i.e., east-west electric field).

Low-frequency data at station 9W erroneously indicate a resistive body at depth, because the station was too close to the transmitter. For a 50 Ω-m earth at 32 Hz, the distance from the center of the transmitter (at 0) to 9W is only 1.4 skin depths. Thus the low-frequency data at station 9W were not modeled.

As in the previous profile, 1-D MT inversion was used at individual stations to construct an initial 2-D model. Trial-and-error, 2-D, TM-mode MT modeling improved the data fit, resulting in the CSAMT interpretation model in Figure 20a. The data fit is illustrated by comparing the theoretical data in Figure 21 with the field data in Figure 19. Figure 20b shows a 2-D dipole-dipole resistivity model of the same line (Ross et al, 1981) for comparison. Again, a theoretical AMT pseudo-section derived from the resistivity model (not shown) does not fit the field data very well.

The resistivity and CSAMT models are similar. At 6W on the profile, the resistive-to-conductive interface depth is 90 m in the resistivity model compared to 70 m in the CSAMT model, although the resistivity values are somewhat different.

A gravity interpretation of this profile (Crebs, 1976) shows a 230-m wide bedrock horst below station 12E buried 30 m deep. The Opal Mound fault lies on the east flank of this horst. We modeled a resistive block 300 m wide, 155 m from the surface in the same position. A value of 300 Ω-m was chosen for the resistivity to coincide with a similar bedrock structure on profile 1. The model derived from dipole-dipole resistivity data indicates a similar resistive structure at station 1200E: a 100 Ω-m block 150 m wide and 300 m deep. This resistive structure, an extension of the one from profile 1, is most likely unaltered Precambrian gneiss bedrock.

Another similarity between the CSAMT and resistivity models is a contact between 24E and 27E. Resistivity increases to the east corresponding to the unaltered but weathered granitic Mineral Mountains pluton.

CONCLUSIONS

Controlled source AMT appears to be an effective method for rapidly mapping the near-surface expression of a geothermal system. CSAMT resistivity mapping at Roosevelt Hot Springs

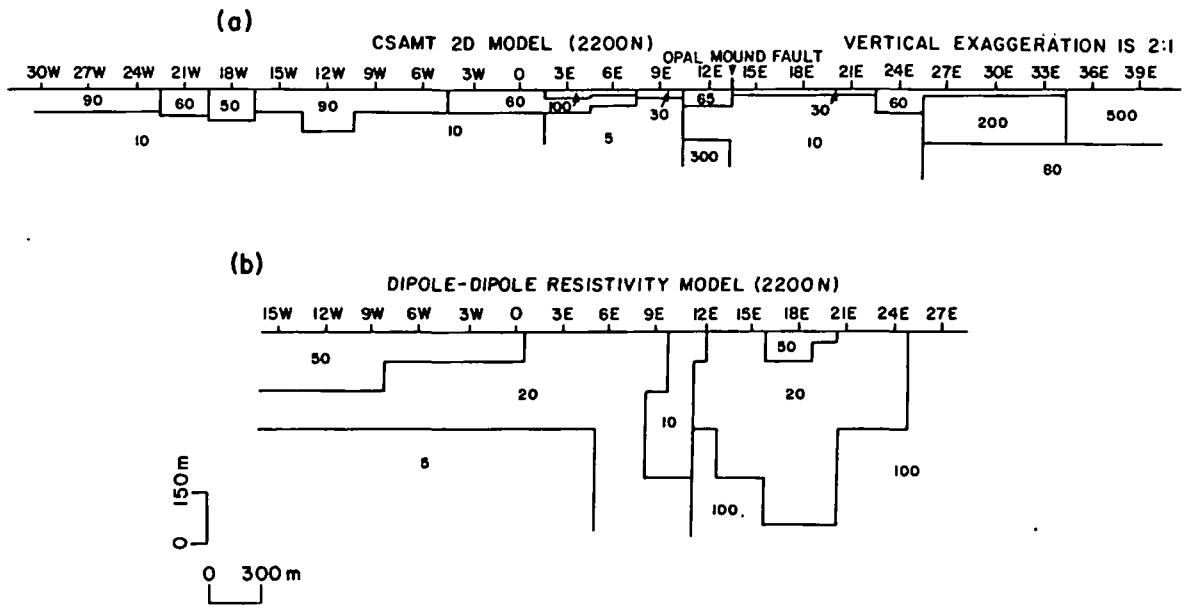

FIG. 20. (a) Two-dimensional CSAMT and (b) dipole-dipole resistivity (based on 100 m and 300 m dipoles) interpretations of profile 2 (2200 N).

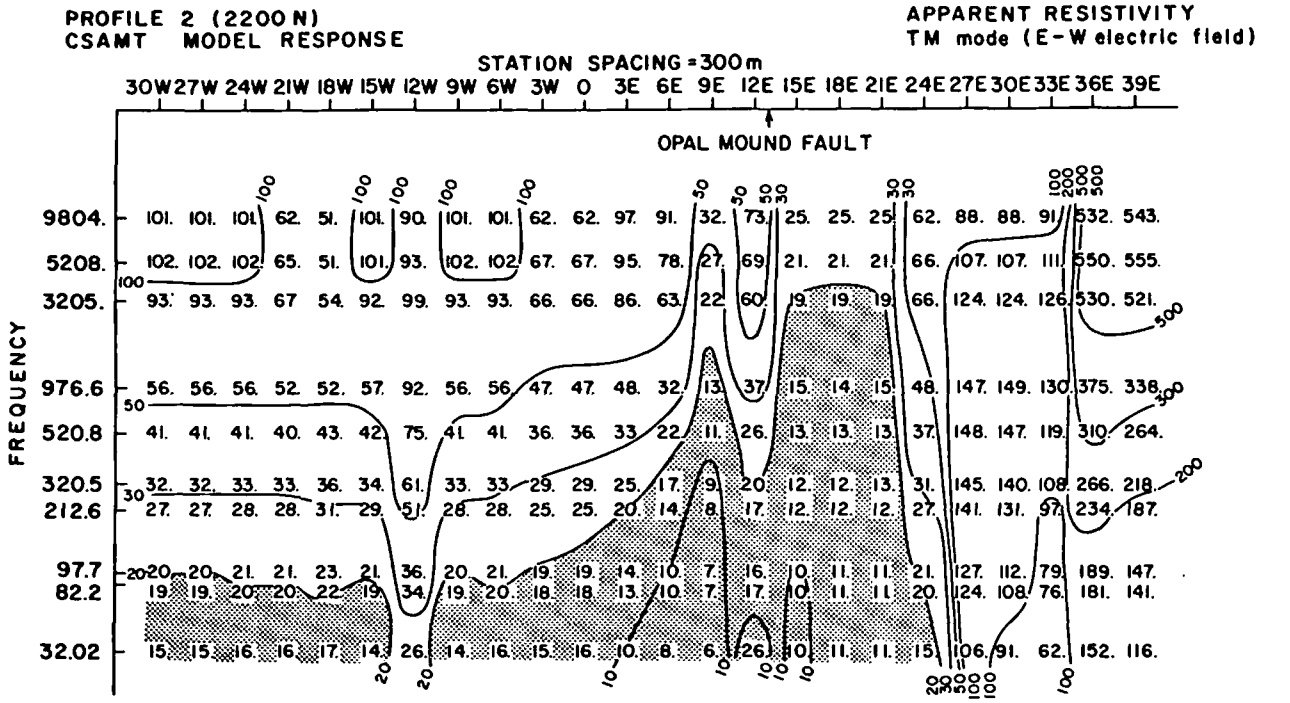

FIG. 21. Theoretical pseudo-section calculated from 2-D CSAMT interpretation of profile 2 (2200 N). Apparent resistivity less than 20 Ω-m is shaded. Compare with field data in Figure 19.

KGRA delineates the same low-resistivity zones as those shown on a first separation 300-m dipole-dipole resistivity map. However, the CSAMT data were collected more rapidly because stations were not constrained to lines, long wires were not necessary, and only two transmitter sites were required. While no cost study was made, we believe that CSAMT would be cost comparable, or more likely, more cost effective than dipole-dipole resistivity mapping in a geothermal environment.

Profiling with CSAMT using 10 frequencies and subsequent 2-D TM-mode modeling produced interpretations consistent with other geophysical and geologic evidence. Two-dimensional modeling of profile 1, supported by gravity data, indicates a resistive structure at depth probably corresponding to unaltered bedrock beneath stations 3900 to 4800. A shallow, eastward-dipping conductive zone, probably altered alluvium due to brine leakage from the Opal Mound fault, is indicated from stations 5100 to 5700. Profile 2 indicates a resistive structure at depth below station 12E in the same position as a bedrock horst modeled by gravity. Alteration and/or brine leakage is indicated on both east and west sides of the Opal Mound fault along profile 2.

A good initial guess for a 2D CSAMT model can be obtained by stitching together 1-D inversions for all stations. This appears to be an advantage over dipole-dipole 2-D modeling where an initial guess is not as easily obtained.

The ambiguity of electrode effects inherent in the dipole-dipole technique is not present in CSAMT since the receiver samples only the ground nearby which is independent of the transmitter. If the transmitter is far enough removed, the source field is approximately a plane wave yielding measurements which are source independent.

Skin depth considerations suggest that CSAMT mapped the electrical resistivity to 300 m depth in conductive areas. However, modeling and sensitivity tests confirmed the findings of Strangway et al (1973) that the technique has difficulty detecting structure beneath conductive overburden. Depth of exploration, given the accuracy of our measurements, was found to be considerably less than a skin depth in conductive areas.

ACKNOWLEDGMENTS

We wish to thank Kennecott Minerals Co. for providing the receiver used in the field work. Technical advice and assistance were gratefully received from W. SanFilipo, W. Petrick, P. Wannamaker, and J. Stodt. We also wish to thank S. H. Ward, C. M. Swift, Y. Shoham, and W. D. Stanley for critically reviewing the manuscript. This work was supported under DOE contract number DE-AC07-80ID12079.

REFERENCES

Crebs, T. L., 1976, Gravity and ground magnetic surveys of the central Mineral Mountains, Utah: M. S. thesis, Univ. of Utah.

Glenn, W. E., and Hulen, J. B., 1979, Interpretation of well log data from four drill holes at Roosevelt Hot Springs KGRA: Univ. of Utah Research Inst., Earth Science Lab. Rep. 28, DOE/DGE contract EG-78-C-07-1701.

Goldstein, M. A., and Strangway, D. W., 1975, Audio frequency magnetotellurics with a grounded electric dipole source: Geophysics, v. 40, p. 669–683.

Hohmann, G. W., 1975, Three-dimensional induced polarization and electromagnetic modeling: Geophysics, v. 40, p. 309–324.

Hoover, D. B., Frischknecht, F. C., and Tippens, C., 1976, Audio-magnetotelluric soundings as a reconnaissance exploration technique in Long Valley, Calif.: J. Geophys. Res., v. 81, p. 801–809.

Hoover, D. B., and Long, C. L., 1976, Audio-magnetotelluric methods in reconnaissance geothermal exploration: Proc. 2nd U.N. Symp. Dev. Geothermal Resources, p. 1059–1064.

Hoover, D. B., Long, C. L., and Senterfit, R. M., 1978, Some results

from audiomagnetotelluric investigations in geothermal areas: Geophysics, v. 43, p. 1501–1514.
Kan, T., and Clay, C. S., 1979, Hybrid-ray approximation in electromagnetic sounding: Geophysics, v. 44, p. 1846–1861.
Killpack, T. J., and Hohmann, G. W., 1979, Interactive dipole-dipole resistivity and IP modeling of arbitrary two-dimensional structures (IP2D users guide and documentation): Univ. of Utah Research Inst., Earth Science Lab. Rep. 15, DOE/DGE contract EG-78-C-07-1701.
Long, C. L., and Kaufman, H. E., 1980, Reconnaissance geophysics of a known geothermal resource area, Weiser, Idaho, and Vale, Oregon: Geophysics, v. 45, p. 312–322.
Ross, H. P., Nielson, D. L., Smith, C., Glenn, W. E., and Moore, J. N., 1981, An integrated case study of the Roosevelt Hot Springs Geothermal System, Utah: Submitted to AAPG Bull.
Roy, A., and Apparao, A., 1971, Depth of investigation in direct current methods: Geophysics, v. 36, p. 943–959.
Sandberg, S. K., 1980, Controlled-source audiomagnetotellurics in geothermal exploration: M.S. thesis, Univ. of Utah.
Stodt, J. A., 1978, Documentation of a finite-element program for solution of geophysical problems governed by the inhomogeneous 2-D scalar Helmholtz equation: NSF grant AER-11155, U. of Utah, 66 p.
Strangway, D. W., Swift, C. M., and Holmer, R. C., 1973, The application of audio-frequency magnetotellurics (AMT) to mineral exploration: Geophysics, v. 38, p. 1159–1175.
Ting, S. C., and Hohmann, G. W., 1981, Integral equation modeling of three-dimensional magnetotelluric response: Geophysics, v. 46, p. 182–197.
Tripp, A. C., 1977, Electro-magnetic and Schlumberger resistivity sounding in the Roosevelt Hot Springs known geothermal resource area: M.S. thesis, Univ. of Utah.
Tripp, A. C., Ward S. H., Sill, W. R., Swift, C. M., Jr., and Petrick, W. R., 1978, Electromagnetic and Schlumberger resistivity sounding in the Roosevelt Hot Springs KGRA: Geophysics, v. 43, p. 1450–1469.
Wannamaker, P. E., Ward, S. H., Hohmann, G. W., and Sill, W. R., 1980, Magnetotelluric models of the Roosevelt Hot Springs thermal area, Utah: Univ. of Utah Dept. Geol. and Geophys. rep. DOE/ET/27002-8, 213 p.
Ward, S. H., and Sill, W. R., 1976, Dipole-dipole resistivity surveys, Roosevelt Hot Springs KGRA: NSF final rep., v. 2, grant GI-43741, Univ. of Utah, 29 p.
Ward, S. H., Parry, W. T., Nash, W. P., Sill, W. R., Cook, K. L., Smith, R. B., Chapman, D. S., Brown, F. H., Whelan, J. A., and Bowman, J. R., 1978, A summary of the geology, geochemistry, and geophysics of the Roosevelt Hot Springs thermal area, Utah: Geophysics, v. 43, p. 1515–1542.

Geothermal Resources Council, TRANSACTIONS Vol. 4, September 1980

marginal use

GEOPHYSICAL STUDIES OF THE LASSEN KGRA, CALIFORNIA

Karen R. Christopherson

U.S. Geological Survey
Denver, CO 80225

ABSTRACT

During the summer of 1979, the U.S. Geological Survey conducted a geophysical study of the Lassen Known Geothermal Resource Area (KGRA) in northern California.

The only data available before this study were a regional geological map and gravity surveys of the Susanville 2° sheet. As part of the USGS work, audio-magnetotelluric (AMT) and magnetotelluric (MT) soundings were made in this area, along with E-field ratio telluric and self-potential traverses.

Data obtained with the four techniques used correlated quite well and delineated two major areas of low resistivities within the KGRA.

INTRODUCTION

The U.S. Geological Survey conducted a geophysical study of the Lassen KGRA in 1979. Data already available included a regional gravity survey of the Susanville 2° sheet (Griscom and Oliver, 1980) and regional geologic mapping of the 2° sheet (Lydon et al, 1960). A detailed magnetic survey was flown in the spring of 1980 by Oregon State University, but results are not yet available.

As part of the USGS study, audio-magnetotelluric (AMT) and magnetotelluric (MT) surveys were made in the area, along with self-potential and E-field ratio telluric traverses.

LOCATION AND GEOLOGY

The Lassen KGRA covers approximately 324 square kilometers (125 square miles) immediately south of Lassen Volcanic National Park and about 50 kilometers (31 miles) west of Susanville in northern California. Elevations in the KGRA range from about 1400 to 2300 meters. The KGRA lies at the southern edge of the Cascade Mountains section. Mesozoic and Paleozoic rocks of the Sierra Nevada section extend to within about 10 kilometers southeast of the area.

Lassen Peak, lying about 7 kilometers north of the KGRA in Lassen National Park, is the southernmost volcano in the Cascade Range. It was last active in 1914-1917 when explosions and lava flows occurred at the peak. Numerous hot springs, hot pools, and steam vents lie just north of the KGRA boundary in Lassen Park and are most prominent in the Sulphur Works and Terminal Geyser areas. Thermal manifestations (hot springs, and mud pots) are present in the western part of the KGRA at Morgan and Growler Hot Springs.

Almost all of the exposed rock units in the KGRA are Cenozoic volcanics. The oldest rocks are small exposures of Miocene pyroclastics. Most of the area is covered by Pliocene and Pleistocene rhyolites, andesites, basalts, and pyroclastics. Several Pleistocene dacite domes are exposed in the western half of the KGRA. There are minor exposures of Holocene basalt, Pleistocene fanglomerate, and Quaternary glacial deposits. Quaternary alluvium exists as valley fill. Post-Pleistocene faulting occurred mostly in the eastern part of the KGRA and to the north with a west to northwest trend.

GRAVITY

Regional gravity coverage is available from the Bouguer gravity map of the Susanville 2° sheet (Griscom and Oliver, 1980).

A regional gravity gradient, caused by isostatic compensation (thicker crust under higher topographic areas), was removed from the complete Bouguer anomaly map to obtain a better look at local gravity features, which otherwise may have been obscured by sharp gradients on the Bouguer map. This adjustment was made by subtracting a value of 0.9 mgal/10 meters of elevation over a smoothed topographic map from the complete Bouguer map. The resulting gravity map (fig. 1) shows residual gravity anomalies ranging from +25 to -35 mgals. The borders of Lassen KGRA and Lassen Volcanic National Park are located approximately on the map.

The broad, northwesterly trending high (0 to +25 mgals) in the southwest part of the sheet and the more circular high in the middle of the sheet (-10 to +20 mgals) are believed to represent an extension of the Sierra Nevada composed of metasediments and metavolcanics (Griscom and Oliver, 1980). The highs are separated from the Lassen area by steep gravity gradients (apparent on both maps), which perhaps result from faulting or lithology change (as the volcanics thicken and become prominent near Lassen and to the north).

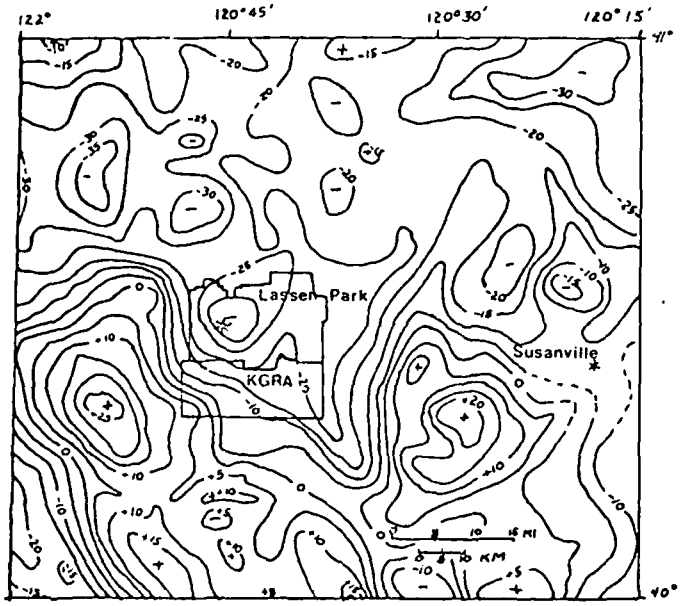

Fig. 1. Residual Gravity Map, Lassen KGRA vicinity California. 5 mgal contours.

The volcanics of the Lassen area and those to the north are characterized by residual gravity contours of -15 to -30 mgals. The low values are due, in part, to the lower density of the volcanics compared to the metamorphics of the Sierra Nevada.

In the area of Lassen Peak, the residual anomaly is -30 mgals, about -10 mgals different from the average for the volcanic region. The most recent interpretation (Griscom and Oliver, 1980) attributes the low to local subsidence of 1000 meters or more near Lassen Peak or to a possible intrusion of lower density rocks beneath the park.

The regional gravity contours in the KGRA show no detailed structure but do indicate a subtle northeast trend through the middle of the area which coincides with some trends of electrical data. No detailed gravity data are available for the Lassen area, but would probably be useful.

AUDIOMAGNETOTELLURIC SURVEY

Sixty-eight audio-magnetotelluric (AMT) soundings were made in and near the Lassen KGRA at nine frequencies between 7.5 hertz and 18,600 hertz (Christopherson et al, 1980). The 7.5 hertz data were log-averaged for the two E-line orientations and are plotted in fig. 2.

The skin depth (approximate depth of penetration) of electromagnetic waves at 7.5 hertz ranges from about 600 meters in 10 ohm-meter material to about 2000 meters in 100 ohm-meter rock. In volcanic rocks, low resistivity values can result from alteration or from the presence of geothermal or saline waters. In the Lassen area, low values can perhaps denote older volcanics in which more fracturing and alteration has occurred or regions of more extensive geothermal activity and alteration.

The 7.5-hertz map (fig. 2) provides the deepest information. It is complex, yet it points to some interesting results. The two areas of modern geothermal activity included in the survey, Sulphur Works and Terminal Geyser, are designated by low (less than 18 ohm-meter) apparent resistivity values. The other geothermally active area, Morgan and Growler Hot Springs, was inaccessible.

There are seven other areas of relatively low apparent resistivity compared to background values of 40 to 100 ohm-meters in the KGRA and greater than 100 ohm-meters near the KGRA and park borders. These low values range from 14.40 ohm-meters (near Wilson Lake) to about 11.0 ohm-meters south of Willow Lake. Most of these low resistivity stations lie in the middle of the KGRA, to the south and southwest of Willow Lake extending to the south and east of Childs Meadows. The resistivity differences seem unrelated to topography or surficial lithology. The low values occur mostly in areas with surface exposures of Pleistocene and Pliocene andesites and basalts, within which the apparent resistivity values can vary by more than one order of magnitude. This area also coincides with magnetotelluric soundings of low to intermediate resistivity (James O'Donnell, written commun., 1980).

A northeast-trending low-resistivity zone through Childs Meadows and Terminal Geyser is apparent on all AMT maps, but is more obvious at 7.5 hertz. Although the cause of this zone is unknown, it does coincide with a gravity trend and is probably quite important.

One of the more interesting areas is southwest of Willow Lake, where the log-averaged 7.5-hertz resistivity values at two stations are 20.0 and 21.0 ohm-meters. A magnetotelluric sounding in this area shows decreasing resistivity to a depth of investigation of about 10 kilometers. Seven other magnetotelluric soundings in the KGRA show increasing resistivity at depth with the lowest values centered at about 7.5 hertz.

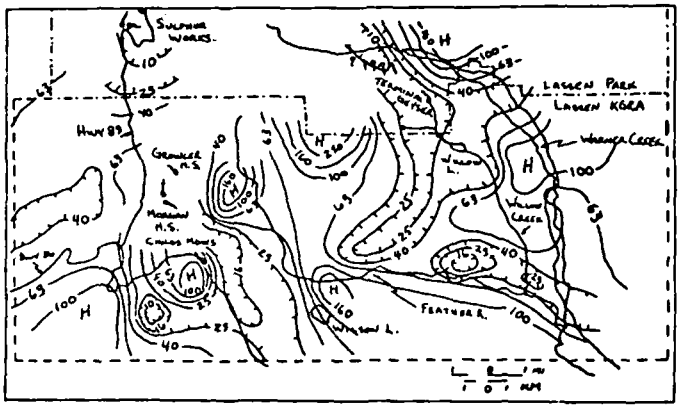

Fig. 2. Audio-magnetotelluric (AMT) Apparent Resistivity Map at 7.5 hertz (log-averaged). Logarithms contours in ohm-meters.

TELLURIC AND SELF-POTENTIAL SURVEYS

Two E-field ratio telluric and self-potential traverses were made in the Lassen KGRA (fig. 3), one near Childs Meadows and one southeast of Terminal Geyser (Christopherson et al, 1980).

Traverse 1 (fig. 4) was run east-west from southern Mill Creek Valley to the eastern flank of Wild Cattle Mountain. The large increase in self-potential voltage between stations 4 west and 3 west occurs where the traverse moves from the southern end of Morgan Mountain into Mill Creek Valley and can probably be explained by the drop in elevation and by changes in ground-water content or lithology. The self-potential voltage

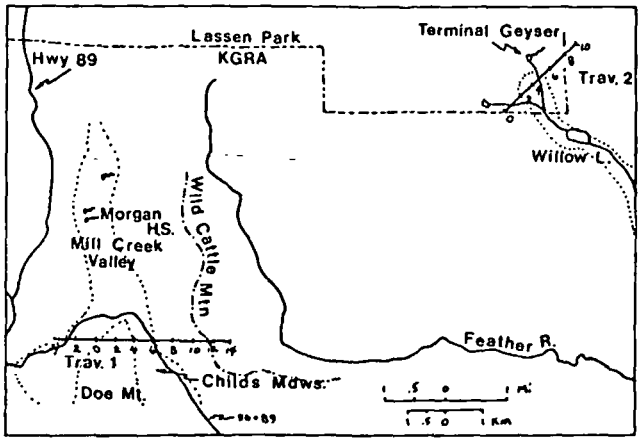

Fig. 3. Telluric and Self-Potential Profiles Location Map.

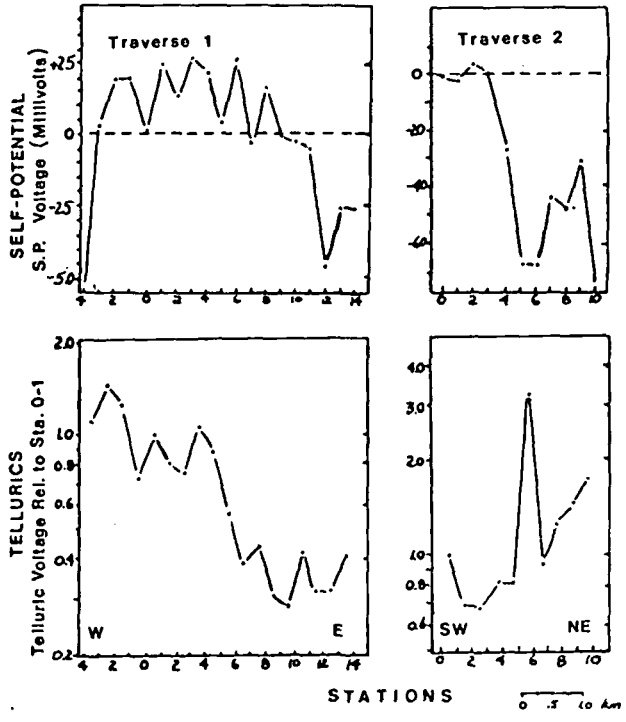

Fig. 4. Telluric and Self-Potential Profiles.

then varies from station 3 west to 7 east due to more subtle geologic changes. The decrease in potential from stations 7 to 12 (with the lowest value occurring on the ridge of Wild Cattle Mountain) probably is the result of a self-potential gradient caused by elevation increase.

The telluric voltage drops east of station 2 west where the profile crosses Mill Creek Valley, possibly indicating faulting. The voltage then increases slightly as the traverse moves onto Doe Mountain (station 0 to 1 east). The telluric response is varied between 1 east and 4 east. Between stations 4 east and 7 east the resistivity (proportional to the voltage squared) drops sharply when the traverse crosses Childs Meadows and starts up Wild Cattle Mountain. The telluric voltage remains at a relatively low level as the traverse crosses over Wild Cattle Mountain, signifying a major resistivity contrast between the western and eastern halves of the profile. This low coincides with an AMT low, suggesting that the low-resistivity zone is continuous from a fairly shallow depth to several kilometers; rough one-dimensional modelling substantiates this continuity.

Traverse 2 (fig. 4) was run from southwest to northeast near Terminal Geyser in the northern part of the KGRA. The most significant change in both self-potential and telluric voltages occurs near stations 5 and 6; the self-potential voltage drops nearly 70 millivolts between stations 3 and 5 and then increases by 25 millivolts between stations 6 and 7. The telluric voltage quadruples between stations 5 and 6 (relative to its value between stations 4 and 5) and then drops to approximately its previous level.

This peak reveals a narrow, highly resistive zone, less than one-half mile southwest of Terminal Geyser, that could be indicative of an intrusive (ring dike?) trending to the northwest. No such structure was detected by the other geophysical methods, probably because of low station density, but the traverse lies within a low-resistivity (less than 40 ohm-meter) AMT region.

MAGNETOTELLURICS

Eight magnetotelluric (MT) soundings were made in the Lassen KGRA at frequencies ranging from .01 to 10 hertz (James O'Donnell, written commun., 1980). The soundings were done at or near previous AMT stations, and their locations are shown in figure 5. The MT data were combined with the AMT data at each station and plotted as frequency vs. resistivity. A smoothed curve was fit to the data, and the data were then inverted (Bostick, 1977) to obtain resistivity vs. depth; the resistivities from the inversion curves for depths of 1, 5, and 10 kilometers are listed in fig. 5. For sounding 1, three sets of curves were generated (for both the field data and inversions), because a split between the two modes resulted in one curve for each mode and an intermediate curve.

The lowest resistivity values trend east-northeast between stations 1 and 5. Stations 6, 7, and 8 have relatively higher resistivities (indicative of fresher, unaltered rock) to a depth of 10 kilometers. The lowest value, 6 ohm-meters at a depth of 5 kilometers at station 3, is probably quite significant as this is very low resistivity for volcanic rock, even with severe alteration. Stations 2, 4, and 5 are of moderate resistivity at all depths, probably signifying a fair amount of alteration. The split in the curves at station 1, some being low and some moderate, indicates that station 1 is located near a pronounced lateral change in resistivity.

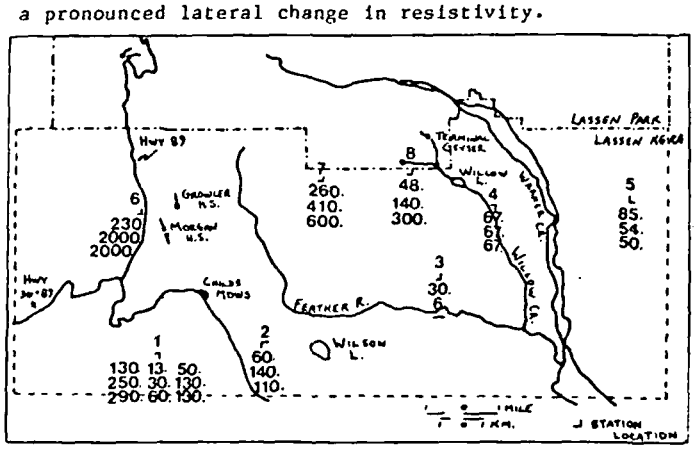

Fig. 5. Magnetotelluric Station Location Map. Station number (above station) and resistivity in ohm-meters at depths of 1, 5, and 10 km (below station).

CONCLUSION

The Lassen KGRA is identified by a complex geophysical signature reflecting lithologic contrasts within the volcanic province associated with complicated changes in alteration, porosity, permeability, and other factors affecting the electrical conductivity of the volcanics. The KGRA lies just south of Bouguer and residual gravity lows, the implications of which are not fully understood. It is inferred from these lows of that a deficiency of mass exists at depth, although the cause of it is still debatable. The other geophysical methods seem to correlate well in mapping areas of low resistivity in the KGRA.

The AMT results point to two major areas of low resistivity within the KGRA; one near Childs Meadows and one south and north of Willow Lake, both covering at least 50 square kilometers. These low-resistivity areas coincide with low relative voltages on the telluric traverses and low to intermediate MT resistivity values. The low values do not coincide with changes in topography or lithology; the AMT resistivity values within one rock type can vary by more than one order of magnitude. Both of the main low-resistivity zones seem prospective and worthy of further study. The area near Childs Meadows lies south of Growler and Morgan Hot Springs (the only surface geothermal manifestations within the KGRA). The AMT resistivity contours at Childs Meadows appear to trend toward the Growler and Morgan Springs area, indicating perhaps the same geologic environment. This trend appears to follow the edge of a major andesite body along Wild Cattle Mountain.

The low south of Willow Lake is very interesting, as it is unmarked by surface indications of any geothermal activity and yet shows very low MT resistivity at 5 kilometers depth (6 ohm-meters at station 3). It is also worth noting that, in the area of this MT station, resistivity decreases with depth from more than 40 ohm-meters at 7.5 hertz (AMT) to 30 ohm-meters at 1 kilometer (MT) and is along a subtle northeast trend seen in all geophysical data.

This area also lies south of the postulated ring dike located near Terminal Geyser (shown by telluric traverse #2). The dike appears to follow a geologic trend northwest-southeast. Considering the clustering of low resistivities in the middle of the KGRA, this trend could be indicative of a large, older volcanic collapse structure bounded roughly by Willow or Warner Creek on the east and Highway 89 on the west.

REFERENCES

Bostick, F. X., Jr., 1977, "A Simple Almost Exact Method of MT Analysis," in Workshop on Electrical Methods in Geothermal Exploration, Proceedings, Univ. of Utah, Dept. of Geology and Geophysics (USGS Contract 14-08-0001-G-359).

Christopherson, K. R., D. B. Hoover, V. Lewis, B. Radke, and R. M. Senterfit, 1980, "Lassen Known Geothermal Resource Area, California: Audio-magnetotelluric, Telluric Profiling, and Self-Potential Studies", USGS Open-File Report 80-313.

Griscom, A., and H. W. Oliver, 1980, "Interpretation of the Bouguer Gravity Map of the Susanville Sheet, California," in Bouguer Gravity Map of the Susanville Sheet, California, Calif. Div. Mines and Geology (in press).

Lydon, P. A., T. E. Gay, and C. W. Jennings (compilers), 1960, Geologic Map of California, Westwood Sheet (Susanville), Scale 1:250,000; California Div. of Mines and Geology.

Geothermal Resources Council, TRANSACTIONS Vol. 4, September 1980

ELECTRICAL RESISTIVITY SURVEY OF THE PILGRIM SPRINGS GEOTHERMAL AREA, ALASKA

Eugene Wescott, Richard Sydora, Jerry Peace, and Andrew Lockhart

Geophysical Institute
University of Alaska
Fairbanks, Alaska 99701

ABSTRACT

Pilgrim Springs is located on the Seward Peninsula about 50 miles north of Nome, Alaska. This paper presents a case history of the use of electrical resistivity to delineate a geothermal reservoir and for drilling recommendations. Pilgrim Springs water, being saline, has an electrical resistivity value of 1 Ω-m, providing an ideal contrast for resistivity definition of the reservoir. In 1979 several deep Schlumberger and co-linear dipole-dipole surveys were run in and near the 1.5 km^2 thaw window. The results suggest that there is a pancake-shaped reservoir near the surface, approximately 50 m thick, which has the shape of the thaw window but is thicker and deeper to the north under the Pilgrim river. The conduit is suspected to be a small feature which is difficult to find under the near-surface, low-resistivity reservoir.

INTRODUCTION

The high salinity of the Pilgrim Springs water (15 gm/l) and its temperature (80°C) result in an electrical resistivity of 1 Ω-m. Thus we would expect resistivities of a few Ω-m to be characteristic of porous reservoir sediments and rocks containing this hot, saline connate water. On the other hand, sediments and rocks of the Pilgrim valley and the metamorphic rocks of the basement complex with fresh cold connate waters have much higher resistivities. This situation is ideal for use of electrical methods to delineate the reservoir characteristics.

Some preliminary resistivity work had been done earlier by Harding Lawson Associates. They had run an east-west Schlumberger depth profile, and then converted to equatorial dipole arrays to the north and south. Their data suggested an east-west trending fault down-dropped to the north with an offset of 150 m. They suggested that this proposed fault acted as the conduit for the hot water.

By use of two-dimensional computer modelling we found that a co-linear, dipole-dipole survey line run north-south would be very sensitive to the sort of fault model proposed. So such a survey as well as some Schlumberger arrays were planned to determine the structure.

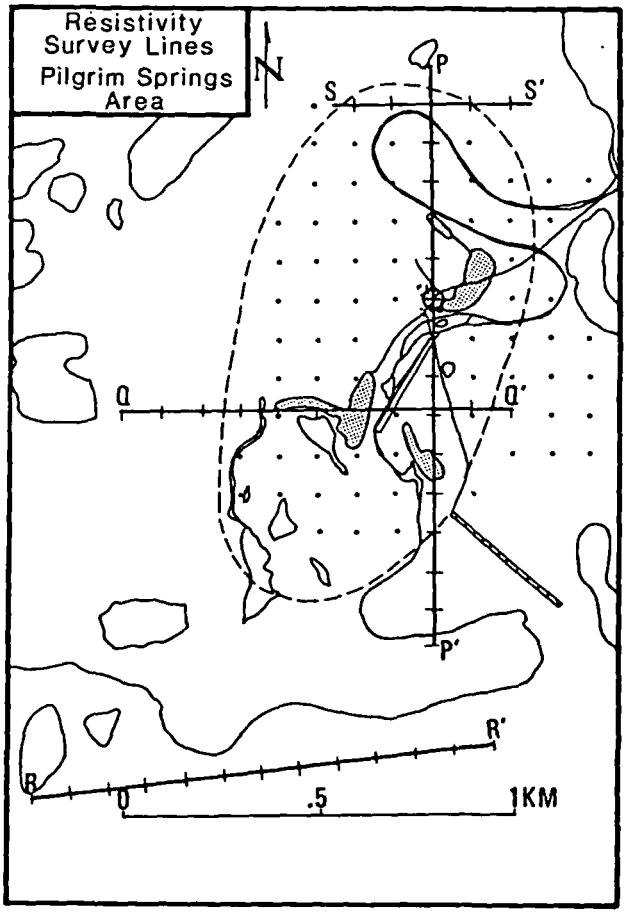

Figure 1. Location of resistivity survey lines. Stippled areas indicate agricultural fields. Origin of grid is at the circle.

1979 Resistivity Surveys

Figure 1 shows the location of the resistivity lines which were run in 1979. A Zonge Engineering and Research Organization GDP-12 receiver was used in conjunction with a Geotronics 4-ampere transmitter at 1/4 Hz. Two Schlumberger depth sounding profiles were run within the Pilgrim thaw ellipse: SS' (to half current electrode spacing, 1/2 AB =

256 m) and QQ' (to 1/2 AB = 512 m). Figure 2 shows the SS' profile. We interpret the data to show a 6.3 Ω-m layer 54 m thick below shallow surface layers and underlain by higher resistivity layers. Figure 3 shows the QQ' profile centered

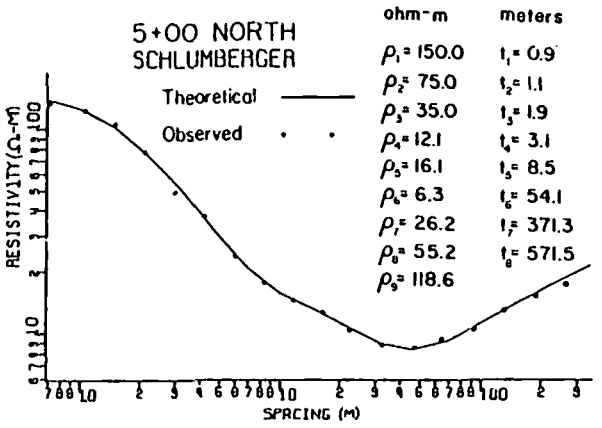

Figure 2. East-west Schlumberger depth sounding at a station 5N (500 m north of origin). The model resistivities and bed thicknesses are shown.

near the area found to have the highest soil temperatures at 4.5 m depth. The interpretation shows a 3.5 Ω-m layer 40 m thick beneath shallow surface layers and underlain by layers of higher resistivity. Computer model curves were run for

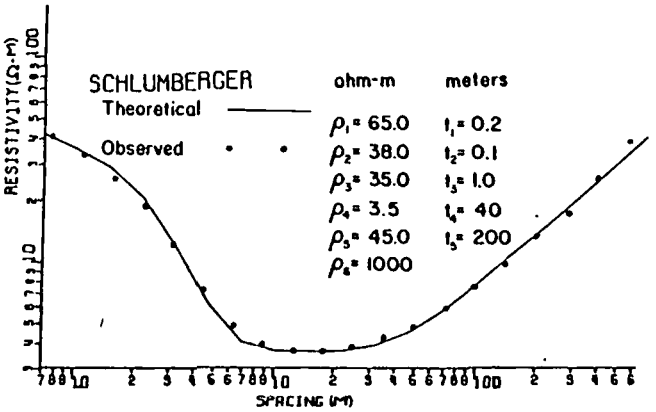

Figure 3. Field data points and calculated model curve of a Schlumberger depth profile run east-west and centered on the ground temperature anomaly at 290 m S, 290 mW of origin.

QQ' putting in thin layers of low resistivity at depth to see what would be detectable, and we found that a 25 m thick layer of 1 Ω-m would have a profound effect if it were at a depth of a few hundred meters.

The co-linear, dipole-dipole line was run using 100 m dipoles, and spreads to n = 5. To interpret the dipole-dipole data, we used a two-dimensional computer code developed by Dey and Morrison (1975) using a mesh of discrete resistivity values. The model has a 25 x 25 m minimum size for resistivity features. Work towards three-dimensional modelling of the data is under way at this time.

Figure 4a shows the pseudo-section plot of the measured apparent resistivity values. Two n = 1 resistivity values were 2.5 and 2.6 Ω-m respectively. In general, we apparently found the reservoir edge on the right or south side, but not on the north or left side. Figure 4b shows the basic model calculations, with 25 m thick, 3 Ω-m plate, underlain by a 25 m thick, 1 Ω-m plate, on a 200 Ω-m infinite substratum. We ran a large number of other models including the proposed fault model, a plume model, and various thicknesses of reservoir which gave poor fits to the data. The models, however, are insensitive to the inclusion of low-resistivity layers at depth. For instance Figure 4c shows the model pseudo-section when a 50 m thick layer of 1 Ω-m is included at a depth of 150 m. We must point out that these are two-dimensional models, when clearly the thaw anomaly is roughly circular.

A dipole-dipole resistivity profile RR' confirmed an N-S trending fault which runs by the west side of the thaw anomaly, but which did not seem to be a conduit for hot water, at least south of the thaw anomaly. Another dipole-dipole survey over a small thaw window about 4.5 km NE of Pilgrim Springs showed resistivities of about 30 Ω-m at a depth of a few tens of meters.

SUMMARY OF RESULTS

The interpretation of the resistivity profiles suggests a reservoir of hot saline water approximately 50 m thick in an elliptical area 1.5 km^2 aligned NE. Analysis of the data rules out the sort of fault model proposed earlier. The conduit system was not discovered, and it is probably small and fault controlled. The basement complex was not found, and it is probably at a depth greater than 250 meters. The data are consistent with heat flow evidence that most of the hot water discharge flows at depth to the north under the Pilgrim River. Two shallow (50 m) exploratory wells confirmed the reservoir, but did not reach the predicted bottom.

ACKNOWLEDGEMENTS

This work was supported by cooperative agreement DE-FC07-79ET27034 with the U.S. Department of Energy and the State of Alaska, Division of Energy and Power, Contract 79-580.

REFERENCES

Dey A., and H. F. Morrison, Resistivity modelling for arbitrarily shaped two-dimensional structures, Engineering Geoscience and Lawrence Berkeley Laboratory, University of California, 1975.

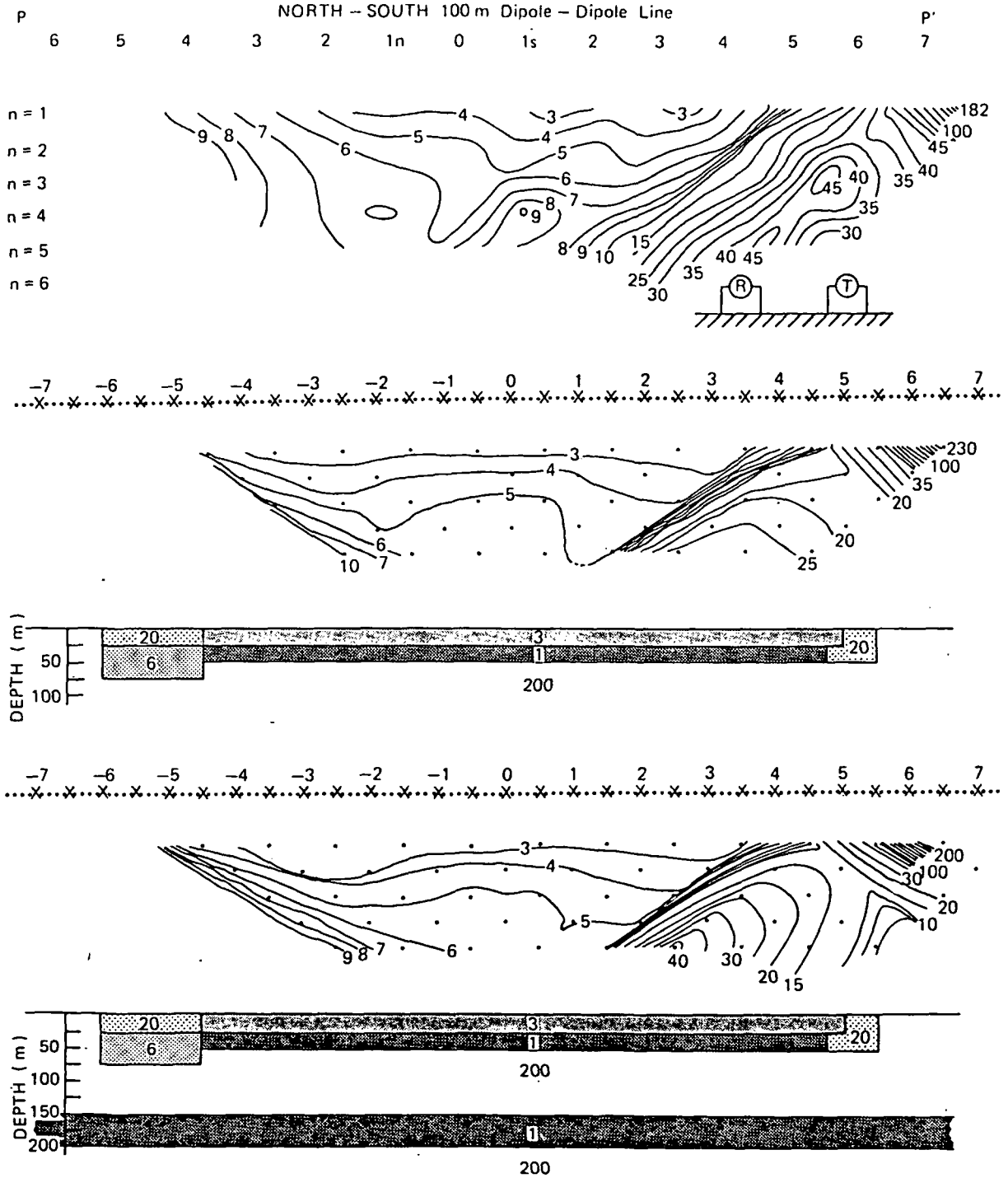

Figure 4a. Field Data, N-S 100 m dipole-dipole pseudosection. Station numbers in hundreds of meters (e.g., 1S = 100 m south of origin).

Figure 4b. Two-dimensional computer model of the basic shallow reservoir structure underlain by rocks of greater resistivity. All values in Ω-m.

Figure 4c. Two-dimensional computer model with a second, deeper hot brine layer at 150 m depth. All values in Ω-m.

interesting and useful electrical

Detection of Buried Zones of Fissured Rock in Geothermal Fields Using Resistivity Anisotropy Measurements

GEORGE F. RISK

Geophysics Division, Department of Scientific and Industrial Research, P.O. Box 8005, Wellington, New Zealand

ABSTRACT

If the rock of a geothermal hot-water reservoir has a regular set of parallel plane fissures filled with conductive hot water, its resistivity is likely to be strongly anisotropic. An attempt has been made to use this effect to locate buried fracture zones in a region 1.6 km^2 in area within the Broadlands geothermal field, New Zealand. Using current electrodes outside the region of study, current was passed through the region in six different directions and the resulting electric field strengths were measured at 58 receiver sites. Over the thickest part of a buried rhyolite dome beneath the study area, isotropic apparent resistivities of about 15 ohm·m were obtained; but over the flanks of the dome the apparent resistivities were strongly anisotropic, varying with direction from about 3 to 15 ohm·m. Schlumberger resistivity soundings display a similar pattern and suggest that the anisotropic rocks lie beneath the rhyolite at depths greater than 200 m. Of 15 wells in the study area, some of the most productive ones were drilled into the anisotropic zone. A possible explanation for the anisotropy is that stresses imposed during the eruption of the rhyolite have caused radial fracturing of the rock around the eruptive vent.

INTRODUCTION

Geothermal wells to be used for electricity generation must be capable of producing very large flows of high temperature water and steam. To achieve this, they must be drilled into permeable formations in the hot-water reservoir. The problem of locating underground permeable zones, prior to drilling, has not been satisfactorily solved. Wells have sometimes been sited along faults (Grindley, 1965) in the hope that they will intercept permeable rocks in the fault zone, but many wells sited in this way have proved to be unproductive. In areas where there are no faults, or where the existence of faults is doubtful, the method cannot be applied.

This paper examines the possibility of detecting, by geophysical means, buried zones which have been fractured by sets of parallel plane fissures. Such zones should have enhanced permeability, because the fissures would provide easy paths for fluid movement. Since the geothermal water filling the fissures is likely to be an order of magnitude more conductive than the unfractured parts of the rock, the resistivities of such fissured zones may be sufficiently anisotropic to be detectable by surface measurements.

RESISTIVITY ANISOTROPY

Set of Parallel Fissures

Figure 1a shows a section through a rock transected by a set of parallel fissures. Only the two-dimensional case, in which the fissures are perpendicular to the plane of the diagram, is considered. The unfissured parts of the rock are of thickness d_1 and resistivity ρ_1, while the fissures are of thickness d_2 and are filled with material (hot water, in the case being discussed) of resistivity ρ_2. The resistivity of the material in bulk is not a simple scalar quantity but a second rank tensor (Nye, 1957). The electric field strength vector **E** and the current density vector **J** are parallel to each other only when they lie parallel or perpendicular to the plane of the fissures.

E and J parallel to the fissures. In this case (Fig. 1b) the constraints imposed by the boundary conditions applying to current flow (Smythe, 1968) make the electric field strength E the same magnitude in each material. From Ohm's law, the current densities in materials 1 and 2 are, respectively, E/ρ_1 and E/ρ_2; and the average current density is $(d_1E/\rho_1 + d_2E/\rho_2)/(d_1 + d_2)$. Hence, the average resistivity $\rho_\parallel$ parallel to the fissures is

$$\rho_\parallel = (d_1 + d_2)/(d_1/\rho_1 + d_2/\rho_2). \quad (1)$$

E and J perpendicular to the fissures. Here (Fig. 1c) the current density J is the same in each material and the electric field strengths in materials 1 and 2 are, respectively, $\rho_1 J$ and $\rho_2 J$. Hence, the average electric field strength is $(d_1\rho_1 J + d_2\rho_2 J)/(d_1 + d_2)$ and the average resistivity $\rho_\perp$ perpendicular to the fissures is

$$\rho_\perp = (d_1\rho_1 + d_2\rho_2)/(d_1 + d_2). \quad (2)$$

If d_1/d_2 is large, $\rho_\perp$ will be almost the same as ρ_1, for a large range of ρ_1/ρ_2.

E and J nonparallel and oblique to the fissures. This case is illustrated in Figure 1d. Within each of the materials, **E** and **J** are parallel and obey Ohm's law; but the vectors undergo discontinuities of direction at the boundaries. As shown by Nye (1957), the vectors for the material in bulk obey the tensor relation

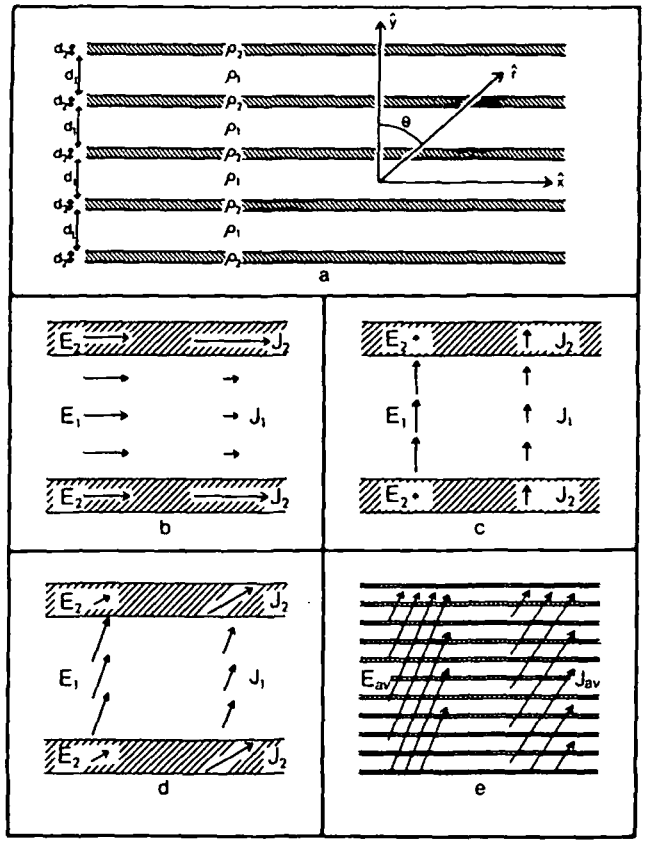

Figure 1. Illustration of current flow in a material consisting of a parallel set of fissures: (*a*) details of the fissuring and coordinate system, (*b*) flow parallel to the fissures, (*c*) flow perpendicular to the fissures, (*d*) and (*e*) flow oblique to the fissures.

$$\begin{bmatrix} E_x \\ E_y \end{bmatrix} = \begin{bmatrix} \rho_{\parallel} & 0 \\ 0 & \rho_{\perp} \end{bmatrix} \begin{bmatrix} J_x \\ J_y \end{bmatrix} \tag{3}$$

where $\rho_{\parallel}$ and $\rho_{\perp}$ are the principal values of the resistivity tensor (referred to its principal axes); and their magnitudes are defined by Equations (1) and (2). E_x, E_y and J_x, J_y are components of electric field strength and current density referred to the *x*-*y* coordinate system (the principal axes of resistivity) shown in Figure 1a.

For the material in bulk, the average directions of **E** and **J** are nonparallel as is illustrated in Figure 1e. It can be shown from Equations (1) and (2) that, for all possible combinations of ρ_1/ρ_2 and d_1/d_2, $\rho_{\parallel} \leq \rho_{\perp}$. Hence **J** is always aligned closer to the direction of the fissures than is **E**.

Resistivity tensor as an ellipse. The second rank tensor shown in Equation (3) can be represented as an ellipse whose major and minor axes have lengths of $\rho_{\perp}$ and $\rho_{\parallel}$, respectively. Nye (1957) refers to this ellipse as the magnitude ellipse to distinguish it from other elliptical representations of anisotropy. He shows, theoretically, that from hypothetical measurements of **E** and **J**, the magnitude ellipse can be constructed by plotting $\mathbf{E}/|\mathbf{J}|$ for a number of measurements in different directions.

Plots of $\mathbf{J}/|\mathbf{E}|$ form a conductivity magnitude ellipse. However, plots of $|\mathbf{E}|/|\mathbf{J}|$ in the direction of **J** or of $|\mathbf{J}|/|\mathbf{E}|$ in the direction of **E** are not ellipses.

Amount of anisotropy. The ratio $\rho_{\perp}/\rho_{\parallel}$ is a convenient measure of the amount of anisotropy. It is unity for isotropic material and its value increases as the anisotropy becomes more pronounced.

An idea of the range of values that the ratio might take can be judged from the following theoretical examples. In the example illustrated in Figure 1, $\rho_1/\rho_2 = 5$ and $d_1/d_2 = 3.6$; hence, the ratio $\rho_{\perp}/\rho_{\parallel} = 1.54$. It will be shown later in this paper that the resistivity of rock in deeper parts of the Broadlands reservoir is about 15 ohm·m. From the laboratory measurements of Quist and Marshall (1968) it can be deduced that the water in the Broadlands reservoir (of chloride concentration 2000 mg/kg and temperature 250°C) has a resistivity of about 0.5 ohm·m. Thus, for fissured parts of the reservoir where the fissures are filled with hot water, ρ_1/ρ_2 is likely to be about 30. It is not possible to assign typical values for d_1 and d_2 in a regularly fissured region. However, if ρ_1/ρ_2 is taken as 30 and d_1/d_2 is set at 10, then $\rho_{\perp}/\rho_{\parallel}$ will be 3.3. Alternatively, for the same ρ_1/ρ_2, but with $d_1/d_2 = 100$, the ratio $\rho_{\perp}/\rho_{\parallel}$ is only 1.3.

Several Sets of Fissures

Expressions for resistivity anisotropy in rocks containing sets of perpendicular fissures have been given by Nechai (1964). For such fissuring in two dimensions, the anisotropy can be described by a magnitude ellipse. However, it would be difficult to distinguish anisotropy due to a single set of fissures from that due to several sets of fissures. For the case of identical sets of perpendicular fissures, the resistivity is isotropic and would therefore be difficult to distinguish from unfissured rock.

For the case of a single set of fissures containing hot geothermal water, it is possible that the walls of the fissures may have become hydrothermally altered and have changed in resistivity. In bulk, the rock would then consist of layers having three different resistivity values. Theoretical expressions for $\rho_{\parallel}$ and $\rho_{\perp}$ can be derived easily.

MEASUREMENT OF RESISTIVITY ANISOTROPY

Variation of Direction of Current Flow

The measurements made in this survey were aimed at detecting resistivity anisotropy in the production zone of the geothermal field at depths of the order of 300 to 1000 m. Hence, it was necessary to pass current through the region to be studied (study region) to depths of the order of 1 km in several different directions. Of the many possible ways in which this can be done, the method chosen is shown schematically in Figure 2. Four current electrodes, A, B, C and D, are sited about the study region, which is represented by the hatching. By connecting the current electrodes two at a time to a current generator, there are six combinations, AB, AC, AD, BC, BD, and CD, for which the current will flow through the study region in different directions; however, only three of the combinations are independent. Provided the electrodes are separated by several kilometers, a significant amount of current will pass to depths of 1 km or more beneath the study region.

Broadlands Field

Figure 3 shows some of the features of the Broadlands geothermal field, including the sites of the deep bores, the

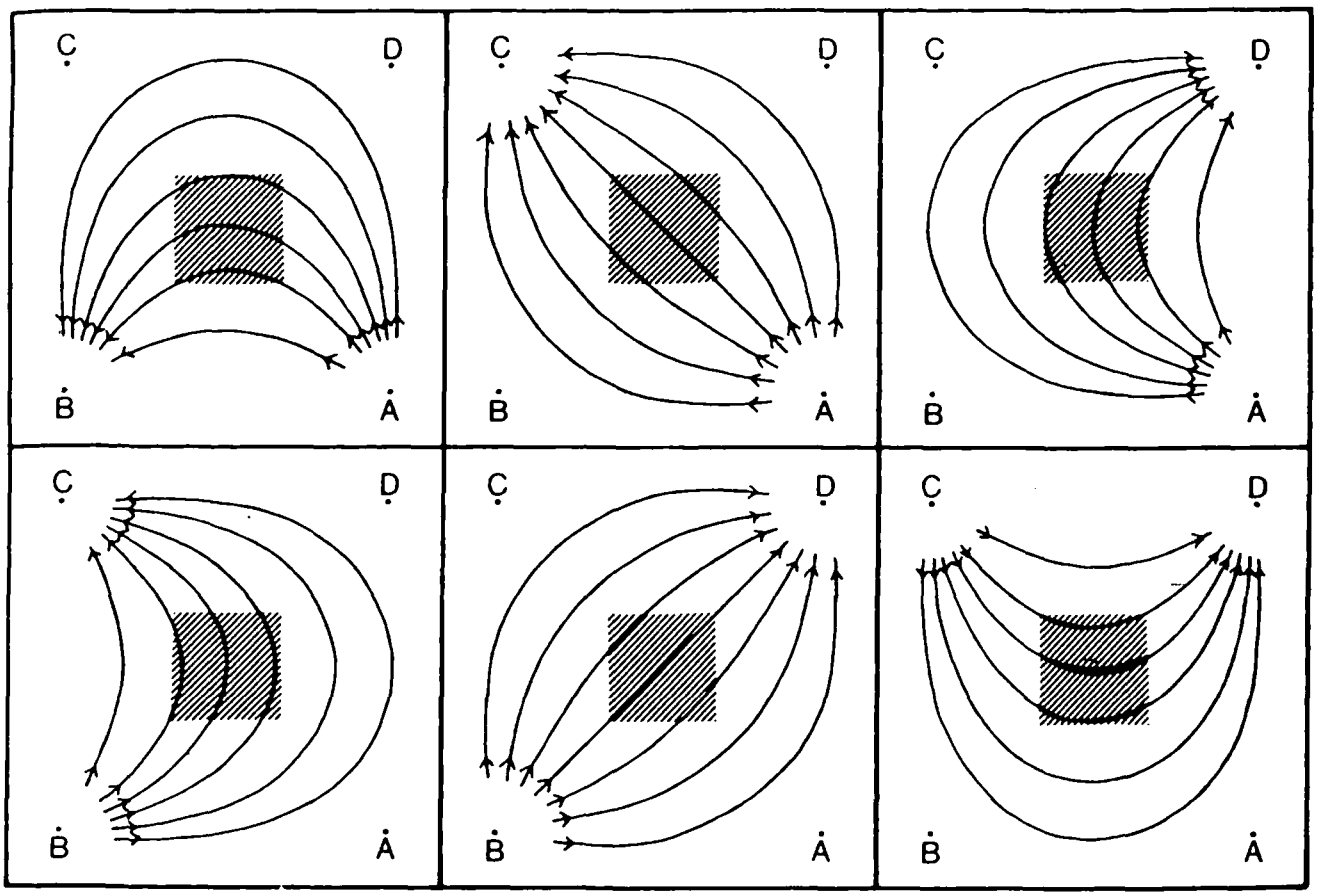

Figure 2. Schematic illustration showing how four electrodes can be connected, two at a time, to pass current in six different directions through the hatched area which represents the study region.

location of the boundary of the field as determined by Risk, Macdonald, and Dawson (1970) from resistivity surveys, and contours of thickness of a buried rhyolite dome. It was decided to make measurements of resistivity anisotropy in the area around the thickest part of the rhyolite dome because a large number of bores had been drilled there and many of them had encountered highly permeable formations. In 1970 when these measurements were made, people working on the Broadlands project debated whether the permeable zones were invariably associated with faults, or whether some of the permeable zones had other origins unrelated to faulting, such as fissuring caused by the extrusion of the rhyolite.

Measurements of Apparent Resistivity

Using current electrodes at the positions of the stars in Figure 3, current was passed through the study region (the outlined area in Figure 3) in six directions. For each direction of current flow, the magnitude and direction of the electric field strength was measured at 58 sites in the study region, using an array of electrodes consisting of two perpendicular dipoles, each 30 m in length.

From these data, the measured currents, and the locations of the current electrodes, apparent resistivities were calculated for each of the six current combinations, using the theory and method described by Bibby and Risk (1973) and Risk, Macdonald, and Dawson (1970). The definition of apparent resistivity ρ_a for this type of array (six-electrode) is not identical with that usually used for four-electrode arrays and can be defined as

$$\rho_a = |\mathbf{E}_{meas}| / |\mathbf{J}_{unif}| \quad (4)$$

where $\mathbf{E}_{meas}$ is the measured electric field strength vector and $\mathbf{J}_{unif}$ is the current density that would be measured at the site of the receiver array, if the half-space consisted of uniform isotropic material.

Figure 4 is an enlargement of the study region, in which the results are given as plots of apparent resistivity versus observed direction of electric field strength (that is, plots of $\mathbf{E}_{meas}/|\mathbf{J}_{unif}|$). Figure 5 gives more detailed drawings of four of the figures, showing how they were constructed from the apparent resistivity measurements. In the figures, the length of a diameter in a particular direction is proportional to the apparent resistivity in that direction. This way of displaying the data was chosen because the figures might be expected to resemble the theoretical magnitude ellipses discussed earlier in the paper. However, the assumed values used for $|\mathbf{J}_{unif}|$ in Equation (4) will, presumably, sometimes have been quite different from the true current densities in the ground. Hence, figures exactly elliptical in shape cannot be expected. Only a small part of the irregularities in shape will have been caused by measurement error.

Two principal types of resistivity figures can be distinguished in Figure 4. Within a few hundred meters of Bore 17 (that is, over the thickest part of the rhyolite dome), the figures are nearly circular in shape. This indicates that

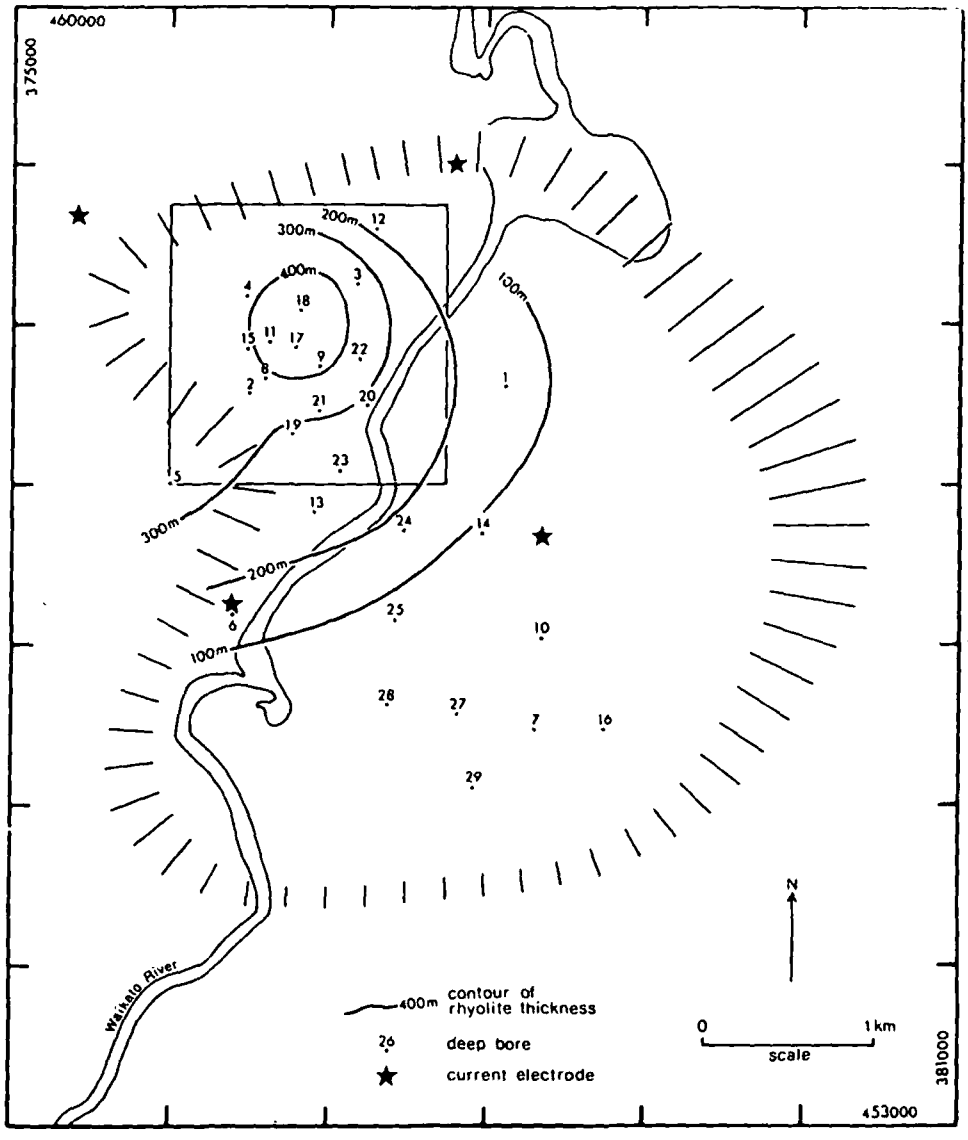

Figure 3. The Broadlands geothermal field. The hatched annulus represents the boundary of the field determined by Risk, Macdonald, and Dawson (1970) from resistivity surveys. The outlined area is shown at an enlarged scale in Figure 4.

the rocks beneath this region are reasonably isotropic and have resistivities of 8 to 15 ohm·m at depths of about 400 to 1000 m. The measurements provide no evidence for extensive fissuring around the center of the rhyolite dome.

In the vicinity of Bores 2, 19, 20, and 3, very elongated figures were obtained. For several of the figures, the ratio of maximum to minimum apparent resistivity is greater than 6:1, which indicates that the rocks are strongly anisotropic. These figures, and others with less pronounced anisotropy, lie in a zone around the rhyolite dome, about 500 m from its center. The directions of minimum apparent resistivity are parallel to lines radiating from the center of the dome. This suggests that if the anisotropy is due to sets of parallel fissures, then the fissures themselves must be aligned in these radial directions.

In other parts of the study region, figures with a variety of shapes were obtained. In some areas, particularly in the northeast of Figure 4, adjacent figures have shapes with similar irregularities. It is difficult to tell whether the elongation of these irregular figures is due to anisotropy or to other causes.

Possible Causes of Elongated Resistivity Figures

It can be seen from Figure 3 that the boundary of the field is close to the study region. To test whether this closeness could have caused elongation of the figures, some theoretical apparent resistivities were calculated using the hemispheroidal model of a geothermal field discussed by Bibby and Risk (1973). The positions of the current electrodes relative to the boundary were chosen to match, as closely as possible, the positions in Figure 3. The ratio of maximum to minimum apparent resistivity obtained for the theoretical figures was always less than 2:1, and the pattern of shapes obtained did not match that in Figure 4. Hence, it was concluded that the presence of the boundary would cause some irregularities in the shapes of the figures, but it cannot be the cause of the pronounced elongation of the most anisotropic figures.

It is possible that some of the anisotropy might have been caused by the effect on the measurements of a relatively resistant layer with a resistivity of about 15 ohm·m which has been revealed by the resistivity sounding results shown in Figure 6 (discussed in more detail below). Due to the

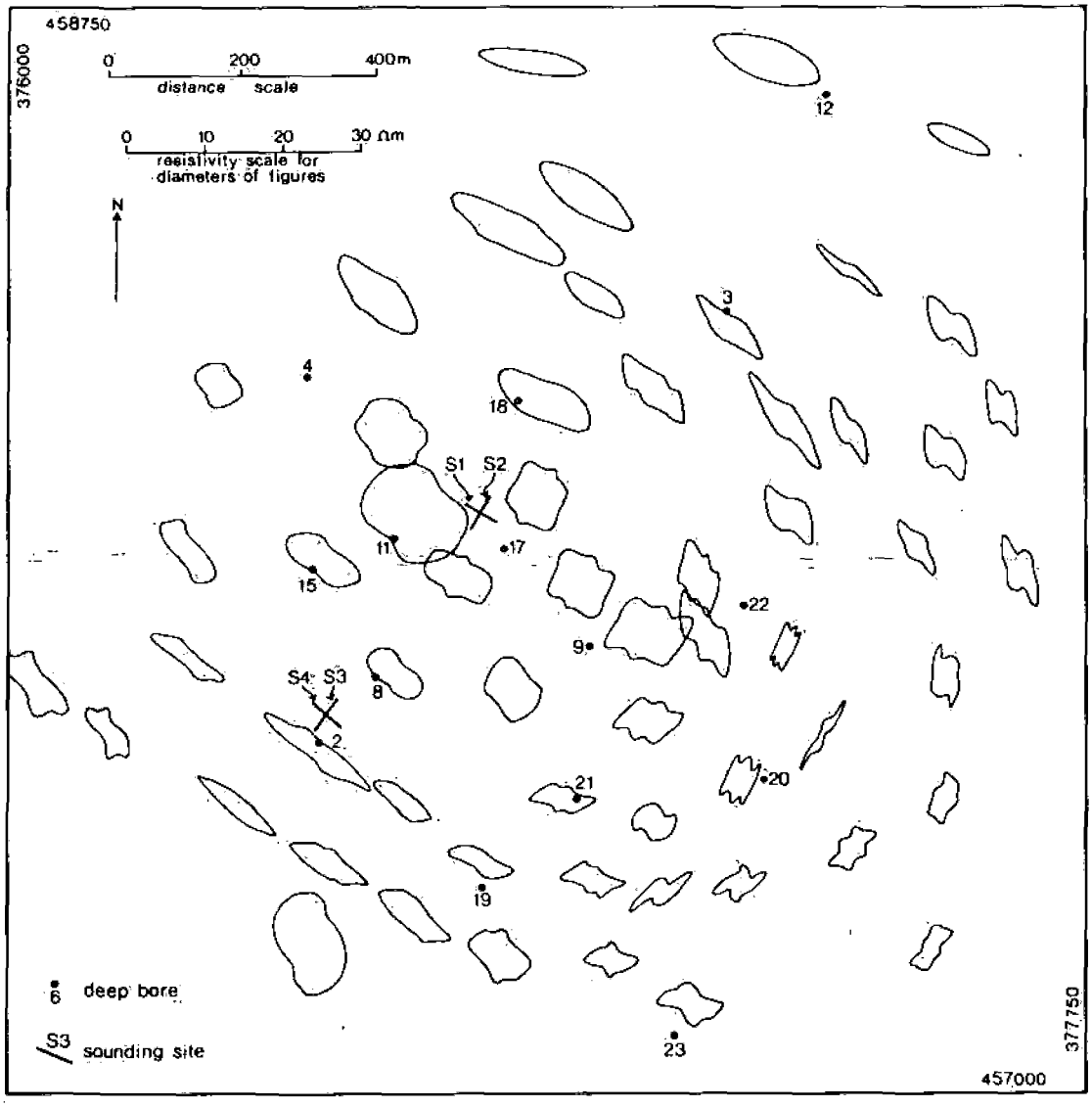

Figure 4. Enlargement of the outlined area in Figure 3, showing figures of apparent resistivity versus direction of electric field strength. The sites of the deep bores and resistivity soundings are shown.

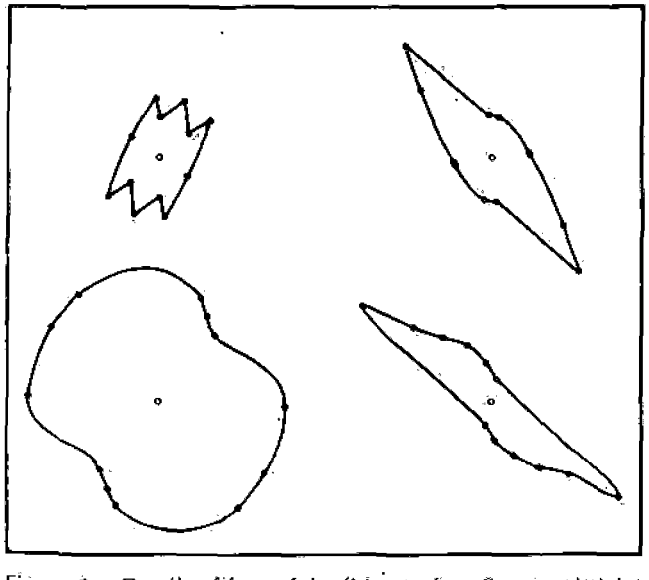

Figure 5. Details of four of the figures of apparent resistivity versus direction of E shown in Figure 4. The dots represent apparent resistivity measurements. An arbitrary scale has been used.

resistant basement, it would be expected that measurements for which the current passed deep into ground would give larger apparent resistivities than those for which the current passed only to shallow depths. A geometric probing depth (defined by Risk, Macdonald, and Dawson, 1970) was calculated for each measurement and used to estimate theoretically the amount of anisotropy which would result.

In the area enclosed by Bores 3, 20, 19, 2, and 4, ratios of maximum to minimum apparent resistivity of up to 2:1 could be attributed to this effect. Hence, the basement effect cannot explain the observed ratios of 6:1 or more. However, around the edge of the study region the effect would have caused a larger amount of anisotropy. In particular, the regular ellipse-like shape of the figures measured near bore 12 may have been caused almost entirely by this effect. To avoid this kind of disturbance in future surveys, a smaller study region should be chosen or a more suitable arrangement of electrodes used.

Any anisotropy due to interference effects from pipes, drains, wires, and other conductive objects in the bore field appears to be negligible because no relationship between the positions of the objects and the shapes of the figures could be found.

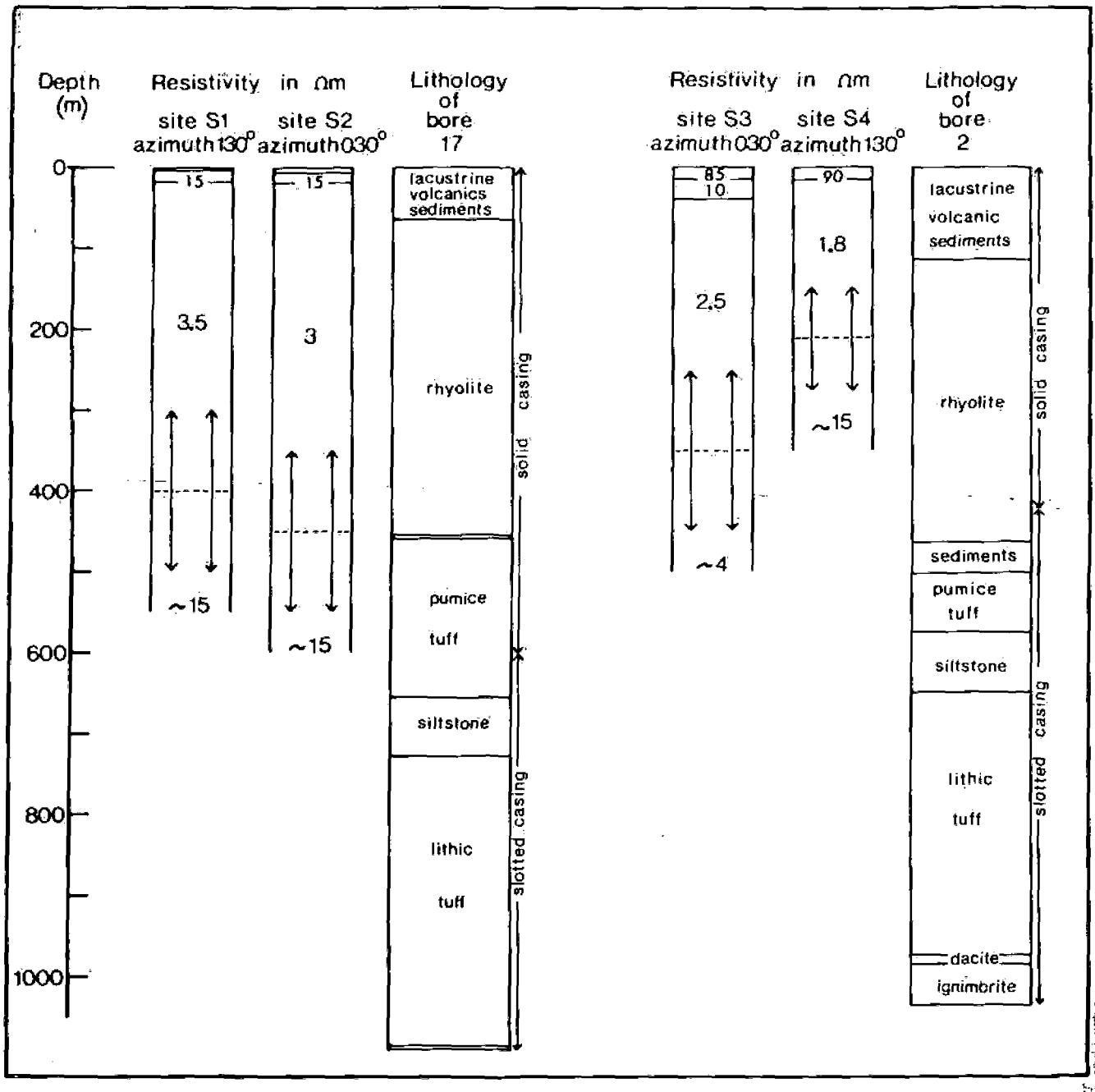

Figure 6. Resistivity sections interpreted from soundings made at the sites shown in Figure 4 and the lithology of nearby wells (from Browne, 1971).

An effect, known as the "paradox of anisotropy" (Kunetz, 1966; Maillet and Doll, 1933), predicts theoretically that large corrections are required in the interpretation of apparent resistivities made with arrays of point electrodes in a half-space which is everywhere uniformly anisotropic. The effect appears to be caused by the curved nature of the current flow and does not exist for uniform parallel flow. Referring to Figure 2, a small anisotropic zone within the hatched study area is similar to a small anisotropic zone in an otherwise uniform field. Since, for the latter case, the paradox of anisotropy effect requires that only minor corrections be made, its neglect during the interpretation of data from this survey will have caused negligible errors.

Resistivity Soundings

To confirm that resistivities at depth beneath the center of the rhyolite dome are isotropic while those beneath the highly elongated resistivity figures are anisotropic, resistivity soundings were made in two directions, using the Schlumberger method, at the sites shown in Figure 4. Since the necessary assumption in analyzing the results—that the ground is composed of a series of isotropic horizontal layers—is only approximately met, only the gross features of the interpreted resistivity sections are meaningful. These sections are shown in Figure 6 alongside the geological logs (from Browne, 1971) of the nearby wells.

Near the center of the rhyolite dome, the resistivities measured in the two perpendicular directions agree well, which substantiates the conclusion made earlier that underground resistivities are isotropic there. The rhyolite has a resistivity of about 3 to 3.5 ohm·m. The deeper layers have a resistivity of about 15 ohm·m in reasonable agreement with the measurements shown in Figure 4.

Soundings near Bore 2, made parallel and perpendicular

to the direction of elongation of the apparent resistivity figure measured there, yielded values of 4 and 15 ohm·m for the deepest layer. They agree reasonably well with those of 2.5 and 17 ohm·m, respectively, for the minimum and maximum apparent resistivities of the nearest figure to the sounding sites. Hence, the existence of strong anisotropy near Bore 2 at depths of a few hundred meters is confirmed.

Other Evidence for Resistivity Anisotropy

Measurements of apparent resistivity in three directions at about 20 sites in the study region were made as part of an earlier dipole-dipole resistivity survey of the Broadlands field (Risk, Macdonald, and Dawson, 1970). The measurements were seriously disturbed by the boundary of the field, but a plot of the data as apparent resistivity figures shows a distribution of figures with many similarities to that in Figure 4.

Comparison with Discharge Rates of Bores

The relationship between resistivity anisotropy and underground permeability has been investigated by plotting, in Figure 7, the ratio of maximum to minimum apparent resistivity measured (or interpolated from several measurements) at the bore sites against the rate of flow of water and steam from the bores measured with approximately the same wellhead pressures (9 to 14 bar). The rates of flow (from Bolton, unpub. data, 1973) were taken as a rough measure of the permeability of the open parts of the hole. No corrections were made for variations of the depths of the wells or of the lengths of open hole.

If the data (in Figure 7) from all the bores are considered, there is no clear correlation between the parameters; but if Bores 11, 12, and 20 are excluded as anomalous, the points show a rising trend. The large anisotropy parameter measured near Bore 12 may be due to the effect of the resistant basement, and the high permeabilities apparent in Bores 11 and 20 may not be caused by parallel fissuring. Bore 2 gives the best association between the parameters related to anisotropy and permeability.

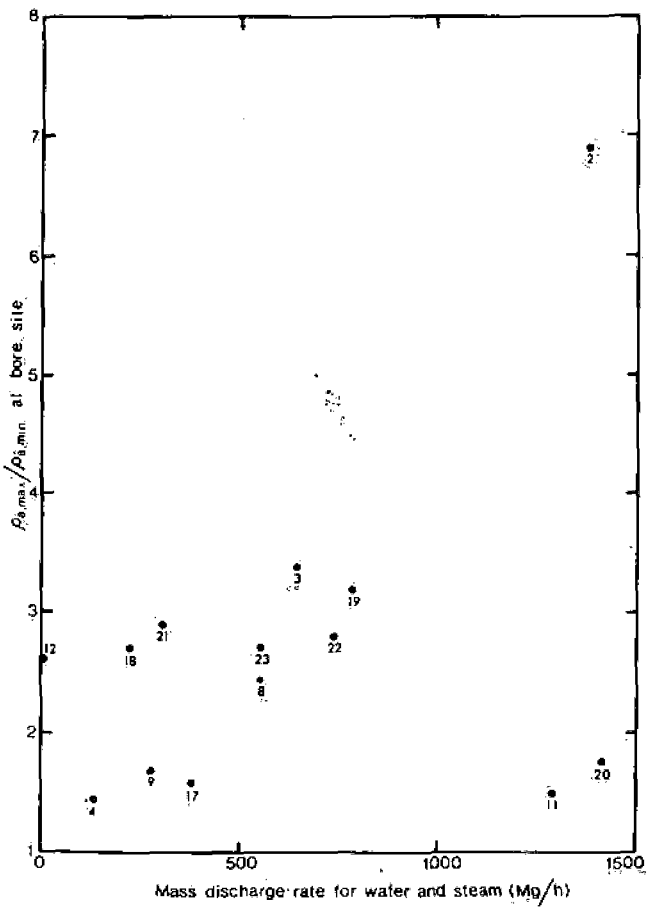

Figure 7. Graph of the ratio of maximum to minimum apparent resistivity at each bore site versus the mass-discharge rate of the bores.

Association of Anisotropy with the Rhyolite Dome

The coincidence of the isotropic region with the center of the rhyolite dome and the symmetry of the strongly anisotropic region about it suggests that the anisotropy may have been caused by the extrusion of the rhyolite. Stresses imposed during the extrusion process may have caused radial fractures in the country rock around the vent.

Processes similar to this would appear to have been the origin of radial dyke swarms which are observed about ancient igneous bodies in several parts of the world (see Hills, 1965). Ode (1957) gives a possible theoretical explanation for the radial pattern of dykes at Spanish Peaks, Colorado. An essential part of his mechanism is that dykes grow in length because of the wedging action of the very high pressure molten magma. Under the rhyolite dome at Broadlands, there is no evidence from the drill-hole information to suggest that rhyolite dykes exist. To the contrary, the observation of resistivity anisotropy suggests that fissures exist which are filled with hot water and not rhyolite. Hence the dyke analogy may not be relevant.

An alternative explanation is that the rhyolite flow itself is anisotropic. This is supported by the results of resistivity sounding S4 (in Figure 6) which indicate that the lower half of the rhyolite flow at that site is anisotropic, although the depth at which anisotropy begins has not been determined accurately. However, this possibility disagrees with inferences from the observations of Cole (1970) concerning rhyolite domes on Mount Tarawera. He claims that fissures in rhyolites are predominantly in the directions of concentric rings around the centers of the domes, which would produce elongations in the apparent resistivity figures perpendicular to those of the observed figures shown in Figure 4. Since in Bore 2 (Fig. 6) the solid casing extends almost to the bottom of the rhyolite, the fractured zone causing the high flows must be at greater depth. Resistivity soundings S1, S2, and S3 all show that the resistivity of the rhyolite is 2.5 to 3.5 ohm·m. A similar value would be expected from sounding S4, which suggests that the depth to the anisotropic layer has been grossly underestimated in the interpretation of sounding S4. Hence, the anisotropic region must be beneath the rhyolite.

CONCLUSION

The results presented here show that there is some likelihood that the resistivity anisotropy method can be refined to the point where it will be useful for locating zones of enhanced permeability in geothermal fields. Experiments with other electrode arrays should be tried and other geothermal fields should be investigated. However, before the method can be considered proven, it will be necessary

to verify by drilling that some permeable zones, predicted by resistivity anisotropy data, actually exist.

ACKNOWLEDGMENTS

I am grateful to C. A. Y. Hewson for assembling the power supply used in this work and to G. B. Dawson, H. H. Rayner, B. McGregor, and others for assisting with the field work. Discussions with many other people, including H. M. Bibby, W. J. P. Macdonald, M. Broadbent, W. I. Reilly, J. W. Cole, P. R. L. Browne, J. Healy, and B. N. Thompson are gratefully acknowledged.

REFERENCES CITED

Bibby, H. M., and Risk, G. F., 1973, Interpretation of dipole-dipole resistivity surveys using a hemispheroidal model: Geophysics, v. 38, p. 719.

Browne, P. R. L., 1971, Petrological logs of drillholes, Broadlands geothermal field: New Zealand Dept. Sci. and Indus. Research, New Zealand Geol. Survey Rept. 52, 87 p.

Cole, J. W., 1970, Structure and eruptive history of the Tarawera volcanic complex: New Zealand Jour. Geology and Geophysics, v. 13, p. 879.

Grindley, G. W., 1965, The geology, structure, and exploitation of the Wairakei geothermal field, Taupo, New Zealand: New Zealand Geol. Survey Bull. n.s. 75, 131 p.

Hills, E. S. 1965, Elements of structural geology: London, Methuen, 483 p.

Kunetz, G., 1966, Principles of direct current resistivity prospecting: Berlin, Gebrueder Borntraeger, 103 p.

Maillet, R., and Doll, H. G., 1933, Sur un théorème relatif aux milieux électriquement anisotropes et ses applications à la prospection électrique en courant continu: Beit. zur Angewardten Geophysik, v. 3, p. 109.

Nechai, A. M., 1964, The problem of quantitative calculation of secondary porosity of jointed oil and gas reservoirs (in Russian): Prikladnaya Geofizika, no. 38, p. 201.

Nye, J. F., 1957, Physical properties of crystals: Oxford, Oxford Univ. Press, 322 p.

Ode, H., 1957, Mechanical analysis of dike pattern at Spanish Peaks area, Colorado: Geol. Soc. America Bull., v. 68, p. 567.

Quist, A. S., and Marshall, W. L., 1968, Electrical conductances in aqueous sodium chloride solutions, from 0 to 800° and at pressures to 4000 bars: Jour. Phys. Chemistry, v. 72, p. 684.

Risk, G. F., Macdonald, W. J. P., and Dawson, G. B., 1970, D.C. resistivity surveys of the Broadlands geothermal region, New Zealand: UN Symposium on the Development and Utilization of Geothermal Resources, Pisa, Proceedings (Geothermics, Spec. Iss. 2), v. 2, pt. 1, p. 287.

Smythe, W. R., 1968, Static and dynamic electricity: New York, McGraw-Hill, 3d ed., 623 p.

GEOPHYSICS, VOL. 47, NO. 1 (JANUARY 1982); P. 100-116, 21 FIGS.

Controlled-source audiomagnetotellurics in geothermal exploration

Stewart K. Sandberg* and Gerald W. Hohmann‡

ABSTRACT

Theoretical and field tests indicate that the controlled-source audiomagnetotelluric (CSAMT) method provides an efficient means of delineating the shallow resistivity pattern above a hydrothermal system. Utilizing a transmitter overcomes the main limitation of conventional audiomagnetotellurics—variable and unreliable natural source fields. Reliable CSAMT measurements can be made with a simple scalar receiver. Our calculations for a half-space show that the plane-wave assumption is valid when the transmitter is more than 3 skin depths away in the broadside configuration and more than 5 skin depths away in the collinear configuration. Three-dimensional (3-D) numerical modeling results for a bipole source 5 skin depths away compare well with those for a plane-wave source, showing that the method is valid.

A CSAMT survey at the Roosevelt Hot Springs geothermal area in Utah produced apparent resistivity contour maps at four frequencies: 32, 98, 977, and 5208 Hz. These maps show the same features as those of a dipole-dipole resistivity map. We also collected detailed CSAMT data at 10 frequencies on two profiles. Two-dimensional (2-D) plane-wave modeling (transverse magnetic mode) of the resulting pseudo-sections yields models similar to those derived by modeling the dipole-dipole resistivity data. However, CSAMT resolved details not shown by the resistivity modeling. Thus, high resolution along with an efficient field procedure make CSAMT an attractive tool for geothermal exploration.

INTRODUCTION

Dipole-dipole resistivity and scalar audiomagnetotelluric (AMT) surveys frequently are conducted to delineate the shallow resistivity pattern above a hydrothermal system. The former method is slow and expensive, while the latter is not dependable. Natural fields in the AMT band ($10-10^4$ Hz) are due to thunderstorm energy propagating in the earth-ionosphere cavity; therefore, the source fields at certain times of the day or in certain seasons may be so weak that it is impossible to obtain reliable data. Furthermore, tensor measurements are required, because the source field direction varies with time. These limitations can be overcome by utilizing a controlled source, i.e., a grounded wire driven at one or several frequencies and located far enough away that the incident field at the receiver approximates a plane wave.

Strangway et al (1973) discussed the application of natural-field AMT in mineral exploration. Hoover et al (1976), Hoover and Long (1976), Hoover et al (1978), and Long and Kaufman (1980) described reconnaissance natural-field AMT investigations with station spacings of several kilometers in geothermal areas. However, in geothermal exploration AMT may be most useful for detailed mapping of near-surface low-resistivity zones due to rock alteration and saline pore fluids.

Goldstein and Strangway (1975) introduced the use of a controlled source for AMT surveys and discussed applications in mineral exploration. If the source is located several skin depths from the observation point, the electromagnetic (EM) field behaves as a plane wave, and the conventional magnetotelluric (MT) formula for apparent resistivity can be used to reduce the data.

We investigate the validity of the plane-wave approximation for half-space and three-dimensional (3-D) models. Then we describe the results and interpretation of a controlled-source audiomagnetotelluric (CSAMT) survey at the Roosevelt Hot Springs KGRA (known geothermal resource area) in Utah.

PLANE-WAVE APPROXIMATION

Expressions for the magnetic and electric fields due to an infinitesimal grounded electric dipole on a half-space were presented by Goldstein and Strangway (1975). We integrated the infinitesimal dipole solution numerically over a finite length source to simulate a field situation. Solutions were calculated over a 3¼ × 3¼ mile (5.23 × 5.23 km) grid for a 2000 ft (609.6 m) transmitter, a half-space resistivity of 100 Ω-m, and a frequency of 32.02 Hz.

AMT scalar apparent resistivities are calculated according to the relation

$$\rho_a = \frac{1}{\mu\omega}\frac{|E|^2}{|H|^2},$$

where E and H are perpendicular horizontal electric and magnetic field components, respectively. For our half-space model, the transmitter bipole is oriented along the x-axis.

Figure 1 shows apparent resistivities calculated using the component of the electric field parallel to the transmitter. For

Presented at the 50th Annual International SEG Meeting, November 18, 1980 in Houston. Manuscript received by the Editor September 2, 1980; revised manuscript received April 30, 1981.
*Amoco Minerals Co., 333 West Hampden, Englewood, CO 80110.
‡Dept. of Geology and Geophysics, University of Utah, Salt Lake City, UT 84112.

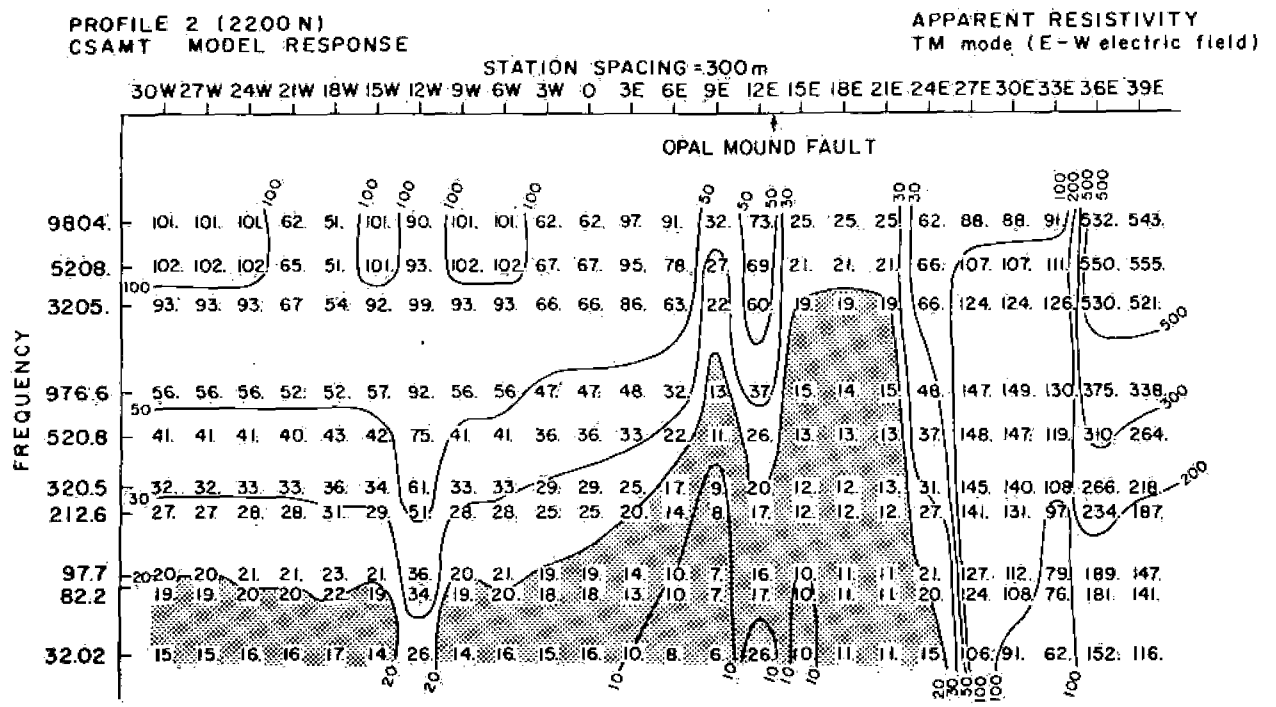

FIG. 21. Theoretical pseudo-section calculated from 2-D CSAMT interpretation of profile 2 (2200 N). Apparent resistivity less than 20 Ω-m is shaded. Compare with field data in Figure 19.

KGRA delineates the same low-resistivity zones as those shown on a first separation 300-m dipole-dipole resistivity map. However, the CSAMT data were collected more rapidly because stations were not constrained to lines, long wires were not necessary, and only two transmitter sites were required. While no cost study was made, we believe that CSAMT would be cost comparable, or more likely, more cost effective than dipole-dipole resistivity mapping in a geothermal environment.

Profiling with CSAMT using 10 frequencies and subsequent 2-D TM-mode modeling produced interpretations consistent with other geophysical and geologic evidence. Two-dimensional modeling of profile 1, supported by gravity data, indicates a resistive structure at depth probably corresponding to unaltered bedrock beneath stations 3900 to 4800. A shallow, eastward-dipping conductive zone, probably altered alluvium due to brine leakage from the Opal Mound fault, is indicated from stations 5100 to 5700. Profile 2 indicates a resistive structure at depth below station 12E in the same position as a bedrock horst modeled by gravity. Alteration and/or brine leakage is indicated on both east and west sides of the Opal Mound fault along profile 2.

A good initial guess for a 2D CSAMT model can be obtained by stitching together 1-D inversions for all stations. This appears to be an advantage over dipole-dipole 2-D modeling where an initial guess is not as easily obtained.

The ambiguity of electrode effects inherent in the dipole-dipole technique is not present in CSAMT since the receiver samples only the ground nearby which is independent of the transmitter. If the transmitter is far enough removed, the source field is approximately a plane wave yielding measurements which are source independent.

Skin depth considerations suggest that CSAMT mapped the electrical resistivity to 300 m depth in conductive areas. However, modeling and sensitivity tests confirmed the findings of Strangway et al (1973) that the technique has difficulty detecting structure beneath conductive overburden. Depth of exploration, given the accuracy of our measurements, was found to be considerably less than a skin depth in conductive areas.

ACKNOWLEDGMENTS

We wish to thank Kennecott Minerals Co. for providing the receiver used in the field work. Technical advice and assistance were gratefully received from W. SanFilipo, W. Petrick, P. Wannamaker, and J. Stodt. We also wish to thank S. H. Ward, C. M. Swift, Y. Shoham, and W. D. Stanley for critically reviewing the manuscript. This work was supported under DOE contract number DE-AC07-80ID12079.

REFERENCES

Crebs, T. L., 1976, Gravity and ground magnetic surveys of the central Mineral Mountains, Utah: M. S. thesis, Univ. of Utah.

Glenn, W. E., and Hulen, J. B., 1979, Interpretation of well log data from four drill holes at Roosevelt Hot Springs KGRA: Univ. of Utah Research Inst., Earth Science Lab. Rep. 28, DOE/DGE contract EG-78-C-07-1701.

Goldstein, M. A., and Strangway, D. W., 1975, Audio frequency magnetotellurics with a grounded electric dipole source: Geophysics, v. 40, p. 669–683.

Hohmann, G. W., 1975, Three-dimensional induced polarization and electromagnetic modeling: Geophysics, v. 40, p. 309–324.

Hoover, D. B., Frischknecht, F. C., and Tippens, C., 1976, Audio-magnetotelluric soundings as a reconnaissance exploration technique in Long Valley, Calif.: J. Geophys. Res., v. 81, p. 801–809.

Hoover, D. B., and Long, C. L., 1976, Audio-magnetotelluric methods in reconnaissance geothermal exploration: Proc. 2nd U.N. Symp. Dev. Geothermal Resources, p. 1059–1064.

Hoover, D. B., Long, C. L., and Senterfit, R. M., 1978, Some results

from audiomagnetotelluric investigations in geothermal areas: Geophysics, v. 43, p. 1501–1514.
Kan, T., and Clay, C. S., 1979, Hybrid-ray approximation in electromagnetic sounding: Geophysics, v. 44, p. 1846–1861.
Killpack, T. J., and Hohmann, G. W., 1979, Interactive dipole-dipole resistivity and IP modeling of arbitrary two-dimensional structures (IP2D users guide and documentation): Univ. of Utah Research Inst., Earth Science Lab. Rep. 15, DOE/DGE contract EG-78-C-07-1701.
Long, C. L., and Kaufman, H. E., 1980, Reconnaissance geophysics of a known geothermal resource area, Weiser, Idaho, and Vale, Oregon: Geophysics, v. 45, p. 312–322.
Ross, H. P., Nielson, D. L., Smith, C., Glenn, W. E., and Moore, J. N., 1981, An integrated case study of the Roosevelt Hot Springs Geothermal System, Utah: Submitted to AAPG Bull.
Roy, A., and Apparao, A., 1971, Depth of investigation in direct current methods: Geophysics, v. 36, p. 943–959.
Sandberg, S. K., 1980, Controlled-source audiomagnetotellurics in geothermal exploration: M.S. thesis, Univ. of Utah.
Stodt, J. A., 1978, Documentation of a finite-element program for solution of geophysical problems governed by the inhomogeneous 2-D scalar Helmholtz equation: NSF grant AER-11155, U. of Utah, 66 p.
Strangway, D. W., Swift, C. M., and Holmer, R. C., 1973, The application of audio-frequency magnetotellurics (AMT) to mineral exploration: Geophysics, v. 38, p. 1159–1175.
Ting, S. C., and Hohmann, G. W., 1981, Integral equation modeling of three-dimensional magnetotelluric response: Geophysics, v. 46, p. 182–197.
Tripp, A. C., 1977, Electro-magnetic and Schlumberger resistivity sounding in the Roosevelt Hot Springs known geothermal resource area: M.S. thesis, Univ. of Utah.
Tripp, A. C., Ward S. H., Sill, W. R., Swift, C. M., Jr., and Petrick, W. R., 1978, Electromagnetic and Schlumberger resistivity sounding in the Roosevelt Hot Springs KGRA: Geophysics, v. 43, p. 1450–1469.
Wannamaker, P. E., Ward, S. H., Hohmann, G. W., and Sill, W. R., 1980, Magnetotelluric models of the Roosevelt Hot Springs thermal area, Utah: Univ. of Utah Dept. Geol. and Geophys. rep. DOE/ET/27002-8, 213 p.
Ward, S. H., and Sill, W. R., 1976, Dipole-dipole resistivity surveys, Roosevelt Hot Springs KGRA: NSF final rep., v. 2, grant GI-43741, Univ. of Utah, 29 p.
Ward, S. H., Parry, W. T., Nash, W. P., Sill, W. R., Cook, K. L., Smith, R. B., Chapman, D. S., Brown, F. H., Whelan, J. A., and Bowman, J. R., 1978, A summary of the geology, geochemistry, and geophysics of the Roosevelt Hot Springs thermal area, Utah: Geophysics, v. 43, p. 1515–1542.